TECHNISCHE UNIVERSITÄT WIEN
Vienna University of Technology

DIPLOMARBEIT

Implementation and verification of Monte Carlo particle transport in electromagnetic fields in GATE

Ausgeführt am
Atominstitut
der Technischen Universität Wien

In Zusammenarbeit mit der
Universitätsklinik für Radioonkologie
der Medizinischen Universität Wien

unter der Anleitung von
Univ.-Prof. Dr. Dietmar Georg
Fatima Padilla Cabal, PhD
Hermann Fuchs, PhD

durch

David Haberl
Matrikelnummer: 01227245

Wien, am 24.03.2021 Unterschrift

Die approbierte gedruckte Originalversion dieser Diplomarbeit ist an der TU Wien Bibliothek verfügbar
The approved original version of this thesis is available in print at TU Wien Bibliothek.
TU Bibliothek Your knowledge hub WIEN

Die approbierte gedruckte Originalversion dieser Diplomarbeit ist an der TU Wien Bibliothek verfügbar
The approved original version of this thesis is available in print at TU Wien Bibliothek.

Abstract

Magnetic resonance guidance in proton therapy is currently being investigated by several research groups in radiation oncology. The first stage of research includes feasibility studies in silico to evaluate the impact of the magnetic field on the dose calculation, optimization and delivery. Moreover, dosimetric protocols in the presence of a strong magnetic field can be affected and the existing Code of Practices have to be reevaluated. These studies rely on accurate and validated Monte Carlo (MC) simulation frameworks. This project aimed to study particle transport in electromagnetic fields in the MC toolkit GATE. First, the accuracy of GATE for the transport of charged particles in electromagnetic fields was assessed. Afterwards, the accuracy of GATE for dosimetric applications within external magnetic fields was tested. More specifically, the relative deviation from the analytical solution of the Boltzmann transport equation is quantified based on the Fano theorem.

In a first step, GATE was extended to simulate particle transport in electromagnetic fields. The correctness of the implementation was benchmarked against an independently calculated numerical solution. Afterwards, a *Fano cavity test* for electrons and protons was implemented, also in the presence of a magnetic field. Mono-energetic electrons with energies between 0.05-20 MeV and protons with 1.5-250 MeV were spatially uniform and isotropically generated inside a plane parallel ionization chamber. The chamber was modelled as a cylinder with an energy-dependent radius and a 2 mm cavity inside it, ensuring the conditions of charged particle equilibrium and the Fano theorem. Uniform magnetic fields of $B = 0.35\text{-}3\,\mathrm{T}$ were applied along the central axis of the chamber. Different multiple scattering models (MSC) were employed to evaluate the performance in terms of accuracy and calculation time. Electromagnetic physics list *option 3* (*Urban* MSC) and *option 4* (*Goudsmit-Saunderson* for electrons and *WentzelVI* for protons) were primarily used. The relative difference between the simulated absorbed dose in the cavity and the theoretical calculated dose value (based on the Fano theorem) was determined to assess the accuracy of the MC transport algorithm.

Electrons with energies between 0.5-20 MeV showed deviations less than 0.3% ($B = 0\,\mathrm{T}$) and 0.6% ($B > 0\,\mathrm{T}$) for a maximum step size of 0.1 mm in the cavity (*option 4*). Comparable results with *option 3* could only be achieved with a maximum step size of 0.001 mm. The electron transport showed a lack of accuracy and stability in the low energy spectrum (0.05-0.1 MeV), even for different physics lists (e.g., single scattering) and smaller step sizes in the nanometer range. Differences up to 4.9% (*option 4*) and 5.8% (*option 3*) were obtained for $B \geq 0\,\mathrm{T}$. Protons with energies between 60-250 MeV showed relative differences less than 0.2% for $B = 0\,\mathrm{T}$ and 0.3% for $B > 0\,\mathrm{T}$ using a maximum step size of 0.1 mm (*option 4*). The relative deviation of protons in the energy range of 3-40 MeV was less than 0.6% for $B = 0\,\mathrm{T}$ and 0.01 mm. A maximum deviation

Die approbierte gedruckte Originalversion dieser Diplomarbeit ist an der TU Wien Bibliothek verfügbar
The approved original version of this thesis is available in print at TU Wien Bibliothek.
TU Bibliothek Your knowledge hub WIEN

of 7.7% was obtained for 1.5 MeV and could not be considerably improved by a single scattering model, different electromagnetic physics lists or smaller step sizes.

Deviations of up to 8% were observed within the transport algorithm, depending on the physics lists, step size and energy range. The simulation of low energy particles ($\leq$ 1.5 MeV) must be further investigated and improved since the results indicate considerable differences from the theoretical values. The results of this study pave the road towards the simulation of ionization chambers in magnetic fields. Moreover, the implemented extension in GATE, allows particle transport using custom and realistic electromagnetic field maps, as generated using finite element models from external software.

Die approbierte gedruckte Originalversion dieser Diplomarbeit ist an der TU Wien Bibliothek verfügbar
The approved original version of this thesis is available in print at TU Wien Bibliothek.
TU Bibliothek Your knowledge hub WIEN

Deutsche Kurzfassung

Die magnetresonanzgestützte Protonentherapie ist ein aktuelles Forschungsgebiet im Bereich der Radioonkologie. In der ersten Forschungsphase werden dabei zunächst computergestützte Machbarkeitsstudien durchgeführt, welche den Effekt des Magnetfeldes auf die Dosisberechnung, -optimierung und -abgabe untersuchen. Weiters werden möglicherweise Dosimetrie-Protokolle durch ein starkes Magnetfeld beeinflusst und existierende Leitfäden sollen neu evaluiert werden. All diese Studien benötigen akkurate und validierte Monte Carlo (MC) Simulationssysteme. Diese Arbeit untersucht den Teilchentransport in elektromagnetischen Feldern im MC toolkit GATE. Zunächst wird die Genauigkeit von GATE hinsichtlich des Transportes geladener Teilchen in elektromagnetischen Feldern bewertet. Anschließend wird die Genauigkeit von GATE in Bezug auf dosimetrische Anwendungen in externen Magnetfeldern getestet. Im Speziellen wird die relative Abweichung von der analytischen Lösung der Boltzmann Transportgleichung basierend auf dem Fano Theorem quantifiziert.

In einem ersten Schritt wurde GATE für den Transport von Teilchen in elektromagnetischen Feldern erweitert. Die korrekte Implementierung wurde mit einer unabhängig berechneten numerische Lösung verglichen. Anschließend wurde ein *Fano cavity test* für Elektronen und Protonen implementiert, sowohl im feldfreien Raum als auch für ein angelegtes Magnetfeld. Monoenergetische Elektronen mit einer Energie zwischen 0.05-20 MeV und Protonen mit 1.5-250 MeV wurden räumlich homogen und isotrop in einer planparallelen Ionisationskammer simuliert. Die Kammer wurde als Zylinder mit einem energieabhängigen Radius und einem darin befindlichen 2 mm Hohlraum modelliert. Dabei wurden die Bedingungen des Fano Theorems sichergestellt. Homogene Magnetfelder von $B = 0.35\text{-}3\,\mathrm{T}$ wurden entlang der zentralen Achse der Kammer angelegt. Verschiedene Modelle der Mehrfach-Coulombstreuung (MSC) wurden verwendet und hinsichtlich ihrer Genauigkeit und Rechenzeit evaluiert. Dabei wurden hauptsächlich die elektromagnetischen Physik-Listen *option 3* (*Urban MSC*) und *option 4* (*Goudsmit-Saunderson* für Elektronen und *WentzelVI* für Protonen) angewandt. Die relative Abweichung zwischen der simulierten absorbierten Dosis im Hohlraum und der auf der Grundlage des Fano Theorems theoretisch errechneten Dosis wurde verwendet, um die Genauigkeit des MC Transportalgorithmus zu bewerten.

Elektronen mit einer Energie zwischen 0.5-20 MeV wiesen Abweichungen kleiner als 0.3% ($B = 0\,\mathrm{T}$) und 0.6% ($B > 0\,\mathrm{T}$) mit einer maximalen Schrittlänge im Hohlraum von 0.1 mm auf (*option 4*). Vergleichbare Ergebnisse mit *option 3* konnten lediglich mit einer maximalen Schrittlänge von 0.001 mm erreicht werden. Der Transport von Elektronen zeigte höhere Ungenaugikeiten und Instabilitäten im Bereich niedriger Energien (0.05-0.1 MeV), auch für andere Physik-Listen (z.B. einem Modell der Einfachstreuung) und Schrittlängen im Nanometer-Bereich. Abweichungen bis zu 4.9% (*option 4*) und 5.8%

Die approbierte gedruckte Originalversion dieser Diplomarbeit ist an der TU Wien Bibliothek verfügbar
The approved original version of this thesis is available in print at TU Wien Bibliothek.
TU Bibliothek Your knowledge hub WIEN

(*option 3*) wurden für $B \geq 0\,\mathrm{T}$ gefunden. Protonen mit Energien zwischen 60-250 MeV wiesen relative Abweichungen kleiner als 0.2% für $B = 0\,\mathrm{T}$ und 0.3% für $B > 0\,\mathrm{T}$ bei einer maximialen Schrittlänge von 0.1 mm (*option 4*) auf. Die relative Abweichung von Protonen im niederenergetischen Bereich von 3-40 MeV war kleiner als 0.6% für $B = 0\,\mathrm{T}$ und 0.01 mm. Eine maximimale Abweichung von 7.7% wurde für 1.5 MeV beobachtet und konnte auch nicht durch die Verwendung anderer Physik-Listen und kleinerer Schrittlängen verbessert werden.

Es wurden Abweichungen bis zu 8% innerhalb des Transportalgorithmus festgestellt, welche im allgemeinen von der verwendeten Physik-Liste, Schrittlänge und dem Energiebereich abhingen. Die Simulation von niederenergetischen Teilchen ($\leq 1.5\,\mathrm{MeV}$) muss weiter untersucht und verbessert werden, da die Ergebnisse deutliche Unterschiede vom theoretisch errechneten Wert aufzeigen. Die Ergenisse dieser Arbeit dienen als Grundlage für die Simulation von Ionisationskammern in Magnetfeldern. Darüber hinaus erlaubt die Feld-Implementierung in GATE den Transport von Teilchen in benutzerdefinierten und realisitischen elektromagnetischen Feldern (homogen oder inhomogen), die durch externe Simulationssoftware basierend auf Finite-Elemente-Methoden genertiert werden können.

Die approbierte gedruckte Originalversion dieser Diplomarbeit ist an der TU Wien Bibliothek verfügbar
The approved original version of this thesis is available in print at TU Wien Bibliothek.
TU Bibliothek Your knowledge hub WIEN

Contents

Die approbierte gedruckte Originalversion dieser Diplomarbeit ist an der TU Wien Bibliothek verfügbar
The approved original version of this thesis is available in print at TU Wien Bibliothek.
TU Bibliothek Your knowledge hub WIEN

Die approbierte gedruckte Originalversion dieser Diplomarbeit ist an der TU Wien Bibliothek verfügbar
The approved original version of this thesis is available in print at TU Wien Bibliothek.

1 Motivation

1.1 Magnetic resonance imaging guided proton therapy

Image guidance is an essential concept in contemporary radiation therapy. It is used to visualize and quantify geometrical uncertainties arising from the treatment setup or the patient, e.g., due to breathing. Magnetic resonance imaging (MRI) has proved itself to be a promising device offering real-time imaging with high visual soft tissue contrast while adding no additional dose to the patient. Integrated hybrid MRI linear accelerators have been recently clinically implemented in external photon beam therapy.

Dedicated research is currently being conducted on feasibility concepts and design studies for MRI guidance in proton therapy. Major differences are expected due to the charged particle beam interactions with the magnetic fields of the MRI, resulting in significant beam deflections. Precise numerical calculations of the deflected particle beam in various materials are needed to account for this effect in treatment planning systems. Changes in the dose distribution of the target volume and at tissue interfaces have to be studied in great detail, and current dose calculation algorithms have to be extended. In addition, dosimetric validation measurements are affected by the magnetic fields [1] and fluence perturbation factors are needed for dosimetric applications. The performance of conventional detectors in magnetic field environments could be tested in advance. Existing Code of Practices in reference dosimetry have to be reconsidered and extended, taking into account magnetic-field-dependent changes in the detector response. For the determination of such perturbation factors, Monte Carlo (MC) simulations are a suitable alternative to measurements, which are particularly expensive in proton therapy due to the high equipment (e.g., synchrotron) and maintenance costs. Therefore, adequate MC models are indispensable to support particle dosimetry in magnetic field environments.

Apart from that, major differences are expected in the technical realization of such a hybrid system, not only because of the significantly different interaction rates of charged particles with matter. Magnetic resonance integrated proton therapy offers real-time imaging during the treatment and requires the operation in an environment exposed to transient electromagnetic fields originating from various hardware components, including the focussing magnets of the accelerator and the scanning magnets of the treatment nozzle [2].

The foundation of these studies is a reliable and accurate simulation framework to test those concepts at an early research stage in silico. Benchmarked MC transport codes are recognized as the standard simulation method in such conceptual studies. GATE is an open-source MC transport code used by the non-clinical research team of the Medical University of Vienna at the MedAustron Ion Therapy Center, Wiener Neustadt, Austria. It is used among others to support dose calculations, verification and

Die approbierte gedruckte Originalversion dieser Diplomarbeit ist an der TU Wien Bibliothek verfügbar
The approved original version of this thesis is available in print at TU Wien Bibliothek.
TU Bibliothek Your knowledge hub WIEN

QA measurements. Based on previous studies by the medical radiation research group at the Medical University of Vienna and an already established GATE environment, all MC simulations throughout this study were conducted using GATE.

1.2 Thesis outline

The aim of this project was primarily to design and implement a Fano cavity test in the presence of magnetic fields in the MC framework GATE. This test is recognized as a major requirement for MC simulations of particle transport, especially for dosimetric applications. It is based on the theoretical work from U. Fano and gives an analytical solution of the Boltzmann transport equation in media with varying density. The results of this project will later on form the basis of creating detailed simulations of ionization chambers to study their characteristics inside a magnetic field. Therefore, GATE was extended to simulate particle transport in custom electromagnetic fields. Since MC simulations are not designed for electromagnetic field modelling, the utilization of external simulation software, based on dedicated finite-element methods, will be necessary at a later research stage. Therefore, a key attribute of the field implementation was to employ external three-dimensional vector field maps.

A summary of the necessary steps along with their key objectives is presented below:

Agenda

- Implementation of particle transport within custom three-dimensional electromagnetic vector field maps in GATE.
- Design and implementation of a Fano cavity test in GATE, including also particle transport in electromagnetic fields environments.
- Verification of the implemented field model with (*i*) an independently calculated deterministic approach and (*ii*) a Fano cavity test.
- Study of MC particle transport with focus on ionization chamber dose response simulations.

Objectives

- Development of a robust and reliable model for particle transport inside an external electromagnetic field.
- High customizability of the implemented model: (*i*) allow transportation in static uniform and non-uniform fields utilizing external vector field maps and (*ii*) allow user defined settings by accessible transport parameters and numerical integration methods.

Die approbierte gedruckte Originalversion dieser Diplomarbeit ist an der TU Wien Bibliothek verfügbar
The approved original version of this thesis is available in print at TU Wien Bibliothek.
TU Bibliothek Your knowledge hub WIEN

- Perform a Fano cavity test for the first time, to the extend of our knowledge, in GATE.
- Use the outcome of the Fano test to provide a comprehensive insight in the simulation of ionization chambers inside magnetic fields.

Die approbierte gedruckte Originalversion dieser Diplomarbeit ist an der TU Wien Bibliothek verfügbar
The approved original version of this thesis is available in print at TU Wien Bibliothek.
TU Bibliothek Your knowledge hub WIEN

2 Introduction

2.1 Monte Carlo method

The Monte Carlo method encompasses a broad class of computational techniques that uses random sampling in order to solve generic problems numerically. These problems may or may not be deterministic in principle. In the following, the fundamental idea of the MC method in particle transport will be introduced based on reference [3]. Particle transport through a medium can be described in form of the integral

$$\langle o \rangle = \int_V p(x)\, o(x)\, dx \tag{2.1}$$

where the random variable x (for simplicity here in 1 dimension) defines a unique particle track through the medium, $p(x)$ is the probability distribution describing the occurrence of this particular track and $o(x)$ is an arbitrary observable, e.g. the energy deposition inside a detector volume V, along this track. The average energy deposition $\langle o \rangle$ is then the evaluation of this integral for each particle crossing the detector volume.

The fundamental idea of the MC method is to approximate this integral by evaluating it at N randomly sampled points x_i:

$$\overline{o} \approx \frac{1}{N} \sum_{i=1}^{N} o(x_i) \tag{2.2}$$

where x_i is randomly sampled according to $p(x)$ with $\int_V p(x)dx = 1$. The approximation $\overline{o}$ is the MC estimator of $\langle o \rangle$. In accordance with the central limit theorem, the approximation becomes exact for $N \to \infty$: $\overline{o} \to \langle o \rangle$. The MC estimator of the variance, $\sigma^2 = \text{var}$, is given by:

$$\sigma^2(o) = \frac{1}{N} \sum_{i=1}^{N} o^2(x_i) - \left[\frac{1}{N} \sum_{i=1}^{N} o(x_i) \right]^2 \tag{2.3}$$

Referring to the example before, a MC simulation can be thought of as a experiment where the experimenter repeats the experiment N independent times getting $\overline{o}$. This is performed by the computer using a random number generator with different seeds. This means, that the simulation of a single track provides a randomly sampled value x_i of x. The value $o(x_i)$, i.e., the energy deposition from this particular simulated track, is then scored and accumulated. After the simulation, the MC estimator in Eq. (2.2) is evaluated.

Die approbierte gedruckte Originalversion dieser Diplomarbeit ist an der TU Wien Bibliothek verfügbar
The approved original version of this thesis is available in print at TU Wien Bibliothek.
TU Bibliothek Your knowledge hub WIEN

In analogy to a normal experiment, the accuracy of the MC estimator is defined by the standard error of the mean:

$$\sigma(\overline{o}) = \frac{\sigma(o)}{\sqrt{N}} \tag{2.4}$$

The result can be expressed in the form $\overline{o} \pm n\,\sigma(\overline{o})$, which means that, e.g., for $n = 1$ the "true value" $\langle o \rangle$ lies within the error with a probability of 68%. It is worth mentioning, that the uncertainty is indirectly proportional to the number of simulated events N for large N, i.e., $\sigma(\overline{o}) \propto N^{-1/2} \propto t^{-1/2}$, and since the computation time t is roughly proportional to N, an increase of a factor of 10 in the uncertainty comes along with an increase of calculation time by a factor of 100.

2.2 Monte Carlo particle transport

Particle transport through a medium is governed by the linear Boltzmann transport equation (BTE). The BTE cannot be solved analytically as soon as one departs from neutral particles (e.g., photons) in a homogeneous medium. Even then, main contributing processes such as secondary electron transport and scattered radiation cannot be accounted for in a trivial way. Numerical methods for solving more complex scenarios can be divided into two groups: (*i*) deterministic BTE solvers which are based on various methods and approximations and (*ii*) MC methods which exploit the stochastic nature of the particle interactions using repeated random sampling as underlying concept.

MC approach The MC simulation is considered as the gold standard for calculating absorbed dose [4]. The true power of this method lies in the microscopic description of each individual particle traversing the medium. In a MC simulation, the particle's track through the medium is divided into small steps, by default typically of the length of the mean free path. In the absence of electromagnetic fields in vacuum, this is a straight line. In case of external fields, the path follows a curved trajectory. Fundamental physical processes are randomly sampled after each step from its corresponding set of interaction cross sections. Depending on the interaction, the particle undergoes among others energy loss, change in direction, spatial displacement, ionization or total energy deposition in the material. Then, a new step length is determined and another step is performed. The stepwise propagation of the particle is repeated until the particle's energy drops to zero or to a predefined cut off value. Secondary particles, generated by excitation processes, are tracked in the same way through matter. With increasing number of initial particles, macroscopic effects of particle beams such as energy deposition inside a target volume are simulated to a high level of accuracy. More specifically, the statistical uncertainty of a MC simulation decreases with an increasing number of simulated events. The microscopic approach also allows to incorporate rather complex phenomena (in terms of computational modeling) such as range straggling, which would be challenging for deterministic solvers due its stochastic nature. Furthermore, since fundamental interactions are directly modeled, there is no restriction in the transportation of particles through

Die approbierte gedruckte Originalversion dieser Diplomarbeit ist an der TU Wien Bibliothek verfügbar
The approved original version of this thesis is available in print at TU Wien Bibliothek.
TU Bibliothek Your knowledge hub WIEN

different materials, being homogeneous or heterogeneous, and geometries. In fact, this is one of the main advantages of MC simulations.

Reliability Several aspects have to be considered in the determination of the effectiveness of MC simulations. The accuracy of the cross sections are one of the key components in the outcome of a simulation. Cross sections are implemented either based on physical models (theories) or on tabulated experimental data. The quality of the employed cross sections often depends on the research domain for which the transport code was developed for, e.g., high or low energy physics applications. They are then inter-/extrapolated to cover the entire energy spectrum. The specific parametrization does not only apply to the cross sections. In general, there are different physical models available (e.g., for multiple scattering) which are typically optimized to a dedicated field of application.

Moreover, being a discrete numerical method, MC simulations are intrinsically limited by the choice of user parameters as for instance the step size and cut off values. Those transport parameters have to be carefully selected since they could considerably affect the outcome of a simulation. Conservative values, i.e., small step lengths and cut offs, result in remarkably high computation times (*accuracy vs. performance*). Further on, important concepts such as step limiting and boundary crossing algorithms are not exact and can be implemented differently.

The simulated particle interactions are natural stochastic processes. Hence, the uncertainty of a MC simulation heavily depends on the total number of particles simulated. This can be a problem in the simulation of small geometries. For example, the sensitive volume of an ionization chamber is very small ($\approx 2\,\mathrm{mm}$) compared to the surrounding walls, and so are the interaction probabilities. A high number of primary particles is necessary in order to reduce the statistical uncertainty. Variance reduction techniques (c.f. Subsec. 5.1.2 and 5.1.3) can be deployed but are not always applicable and difficult to implement.

Validation Due to the discussed considerations concerning the reliability of MC simulations, experimental validations of MC models are an essential part in dosimetry. Various transport codes (EGSnrc[1], FLUKA[2], Geant4[3], MCNP[4], PENELOPE[5]) have been developed focussing on different research fields. In addition, more user-friendly interfaces were extended for specific applications such as GATE[6] or TOPAS[7] in the field of medical physics. Besides experimental validation, it is common practice to benchmark MC codes either against each other or against other independent dose calculation methods. Furthermore, the self-consistency Fano test has become widely recognized to validate MC

[1] https://nrc-cnrc.github.io/EGSnrc/
[2] https://fluka.cern
[3] https://geant4.web.cern.ch
[4] https://mcnp.lanl.gov
[5] http://pypenelope.sourceforge.net/index.html
[6] http://www.opengatecollaboration.org
[7] http://www.topasmc.org/

Die approbierte gedruckte Originalversion dieser Diplomarbeit ist an der TU Wien Bibliothek verfügbar
The approved original version of this thesis is available in print at TU Wien Bibliothek.
TU Bibliothek Your knowledge hub WIEN

toolkits for the simulation of ionization chambers. Due to the importance of this method for the current study, more details will be presented in the upcoming Section 2.6.

2.3 Elastic scattering

Charged particles passing through matter undergo numerous elastic Coulomb scattering events with primarily atomic nuclei. Although the energy transfer is negligible due to the usually smaller masses of the incident particles, the scattering process causes a small angle deflection from the initial direction. The cumulative effect of these repeated small angle scattering events results in a net deflection of the incident particle. As elastic cross sections of charged particles are getting extensively large with decreasing particle energies, a vast amount of scattering events have to be simulated at the cost of high calculation times. This led to the development of different multiple scattering (MSC) simulation schemes which are a crucial component of any transportation code.

2.3.1 Simulation schemes

The simulation of multiple Coulomb scattering can be classified into three different classes: (*i*) *detailed*, (*ii*) *condensed* and (*iii*) *mixed* simulation.

Detailed MSC is based on the direct simulation of each individual scattering event. It can be considered as an exact method to the solution of the transport equation. However, this approach is only feasible for low energy particles ($\approx 100\,\text{keV}$ in case of electrons [3]) or specific geometries, such as thin foils or low density media (e.g., vacuum or gas). For kinetic energies larger than that, the average number of interactions is getting very large and the detailed simulation scheme becomes highly inefficient.

M. Berger [5] introduced an alternative approach specifically addressed to the simulation of particles with higher kinetic energies. Due to the large number of interactions ($\approx 10^4$ for an 1 MeV electron [6]), it is necessary to rely on approximations. In condensed-history (CH) MC simulations, interactions are grouped along a "macroscopic" step with constant cross sections, i.e., the step is assumed to be large enough to cover multiple collisions but simultaneously small enough so that the cross sections stay approximately constant along a step. Macroscopic effects such as the net energy loss (c.f. Sec. 2.4), displacement and angular deflection are then computed and can be partially sampled from MSC theories (c.f. Subsec. 2.3.3). However, the probability distribution of the spatial displacement after a given step length is the most challenging part since it is not well described by MSC theories [7]. This introduces a certain variability between different transport codes since the approximation of these quantities can be implemented differently. Furthermore, CH MC simulations have difficulties with boundary crossings, especially at interfaces with high density variations and in the low energy spectrum. For a reliable approximation, the step length should automatically reduce near boundaries so that the track segment ends inside the initial medium. Otherwise, it could be the case that particles cross the boundary although they would not be able to in a realistic scenario. Such artifacts are even more critical if the subsequent material has a considerably lower density, because the particle would then be propagated based on the mean free

Die approbierte gedruckte Originalversion dieser Diplomarbeit ist an der TU Wien Bibliothek verfügbar
The approved original version of this thesis is available in print at TU Wien Bibliothek.
TU Bibliothek Your knowledge hub WIEN

path of the low density medium. This is also a problem in the simulation of backscattering. The CH method is for obvious reasons not exact and the accuracy of the approach is restricted by the accuracy of the MSC approximations. Therefore, a dependence on various transport parameters such as the step size is introduced. These factors are the main contributors to the total uncertainty of a CH MC simulation.

The mixed simulation scheme [8] is a combination of the two latter methods and simulates soft collisions, i.e., those resulting in small angle deflections or energy losses, using MSC approximations and hard collisions, i.e., large angle scattering events, in a detailed manner. This turned out to be a suitable technique because most of the collisions experienced by a charged particle along a given step length are soft, while the number of hard collisions is moderately small. The calculation time of this method is usually higher compared to a pure CH approach but with a considerable gain in accuracy. According to the authors, this approach has numerous advantages, such as the application to any single scattering differential cross section, the utilization of correct spatial distributions and the circumvention of boundary crossing related problems and thereby a reduced dependence on transport parameters. A detailed explanation and the theoretical basis of the mixed simulation scheme is presented in reference [8].

2.3.2 Single scattering theory

In general, elastic scattering of charged particles in the Coulomb field of atomic nuclei is described by Rutherford scattering. The force between the incident particle with charge ze (for e^-: $z = 1$) and the positively charged nucleus Ze is the Coulomb force with $k = (4\pi\varepsilon_0)^{-1}$:

$$\boldsymbol{F} = k\frac{zZe^2}{r^2}\hat{\boldsymbol{r}} \tag{2.5}$$

Geant4 uses the single scattering model by Wentzel [9]. It is the quantum mechanical description of elastic scattering of charged particles using a simplified scattering potential:

$$V(r) = k\frac{zZe^2}{r}\exp(-r/R) \tag{2.6}$$

where an exponential function is used to account for electron screening. The screening radius is $R \simeq 0.885Z^{-1/3}a_0$ and estimated from the Thomas-Fermi model of the atom with Bohr radius a_0.

The resulting differential cross section differs from the classical Rutherford description only by an additional term, i.e., the screening parameter A_S. The analytical expression of the differential cross section (mass of target nucleus >> mass of incident particle) is given by:

$$\frac{d\sigma}{d\Omega} = \left(k\frac{zZe^2}{2p\beta c}\right)^2 \frac{1}{[A_S + \sin^2(\theta/2)]^2} \tag{2.7}$$

where $v = \beta c$ is the velocity, p the momentum and θ the deflection angle of the particle following reference [7].

Die approbierte gedruckte Originalversion dieser Diplomarbeit ist an der TU Wien Bibliothek verfügbar
The approved original version of this thesis is available in print at TU Wien Bibliothek.
TU Bibliothek Your knowledge hub WIEN

2.3.3 Multiple scattering theory

The fundamental idea behind MSC is that if the number n of small angle scatters is high enough ($n > 20$) compared with the number of hard scatters, then the multiple scattering net angular distribution becomes approximately Gaussian shaped at small angles while remaining Rutherford distributed at large angles (Fig. 2.1).

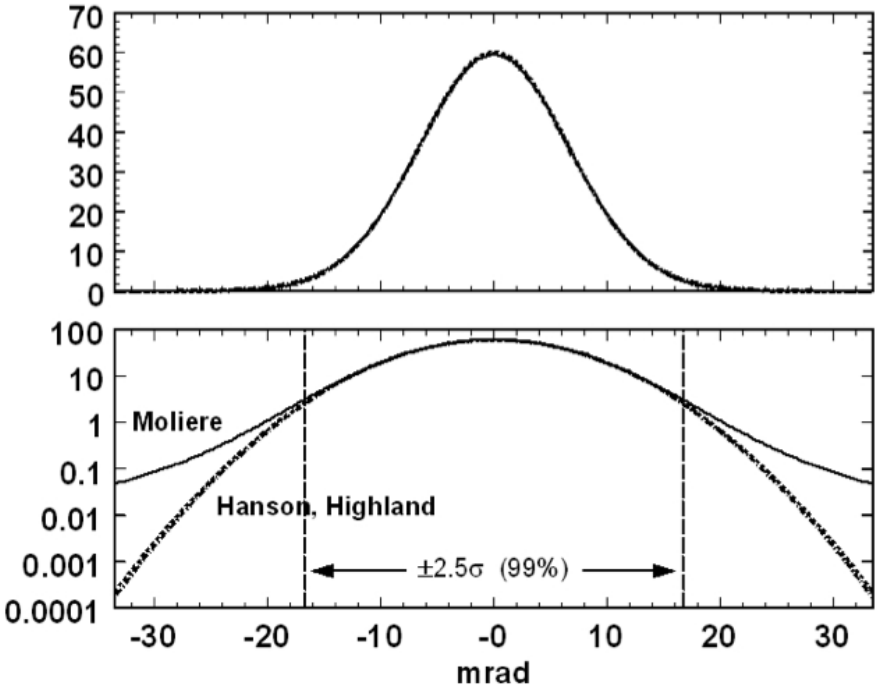

Figure 2.1: Angular distribution of a 156.8 MeV proton beam in water. The upper plot shows globally close agreement between the Molière distribution and the Hanson/Highland Gaussian approximation. However, on a logarithmic scale, differences up to a factor of 100 can be observed at 5σ. Figure taken from [10].

This was first described by Molière [11] and further improved by Bethe later on [12]. Hanson et al. [13] were the first presenting a formula for the best Gaussian fit based on the full theory of Molière. Later, Highland [14] found a more convenient way to obtain the best approximation of the characteristic angle by fitting the Molière/Bethe/Hanson distribution, circumventing the full calculation of Molière theory.

Although showing close agreement with experimental data, the Molière theory does not give any information about the spatial displacement of the scattered particle, which is a crucial component in the MSC approximation of transport codes.

Hence, Urban [15] proposed an implementation of MSC starting from Lewis theory [16], which is directly based on the transport equation of charged particles allowing one to obtain an analytical expression of the first moments of the spatial distribution. The

Die approbierte gedruckte Originalversion dieser Diplomarbeit ist an der TU Wien Bibliothek verfügbar
The approved original version of this thesis is available in print at TU Wien Bibliothek.
TU Bibliothek Your knowledge hub WIEN

basic idea is to use model functions, constrained by the Lewis theory, to sample the spatial and angular distributions after a step. It uses a separate parametrization of the central Gaussian part and the tails. The central part of the angular distribution $P(\theta)$ is approximated using a slightly modified Highland fit [17]:

$$P(\theta)\, d\Omega = \frac{1}{2\pi\theta_0^2} \exp\left(-\frac{\theta^2}{2\theta_0^2}\right) d\Omega \tag{2.8}$$

with

$$\theta_0 = \frac{13.6\,\mathrm{MeV}}{\beta cp} z \sqrt{\frac{x}{X_0}} \left[1 + 0.038 \ln\left(\frac{x}{X_0}\right)\right] \tag{2.9}$$

where x/X_0 is the true path length measured in radiation lengths X_0.

Another approach, the so called Goudsmit-Saunderson theory, also gives only the angular distribution after a step. However, in contrast to Molière theory, it does not assume any particular form of the single scattering differential cross section. Hence, the angular distribution is analytically exact [8].

In practice, it is important to differentiate between the underlying physical theory and the implemented numerical model. MSC models work best for a large number of interactions. The MSC formalism becomes invalid if the number of interactions between two steps is not high enough, i.e., for remarkably small step sizes. Thus, the special case of plural scattering ($2 \leq n \leq 20$) is very difficult to handle and might be considered in the model as well.

As pointed out by H. Bouchard et al. [18], in the presence of external electromagnetic fields, stochastic changes of the velocity due to scattering should be considered in the MSC model to accurately calculate the particle's trajectory.

2.4 Inelastic scattering and radiative losses

Besides elastic scattering, where almost no energy is transferred, charged particles lose energy due to inelastic scattering and radiative losses. The main contributing process (at intermediate energies) is inelastic scattering with atomic shell electrons resulting in ionization or excitation of the atom. In addition, electrons are deflected in the Coulomb field of atomic nuclei and lose energy. The energy loss is compensated by the generation of bremsstrahlung, thus satisfying the conservation of energy. Due to the higher mass of protons, this process is more likely for electrons. Apart from that, other electromagnetic processes occur, including Møller scattering, Bhabha scattering and electron-positron annihilation in case of electrons, and nuclear interactions and bremsstrahlung for heavier particles.

In the following, only the energy loss due to ionization and atomic excitation will be discussed, since it makes the biggest contribution to the total energy deposition in the medium.

Die approbierte gedruckte Originalversion dieser Diplomarbeit ist an der TU Wien Bibliothek verfügbar
The approved original version of this thesis is available in print at TU Wien Bibliothek.
TU Bibliothek Your knowledge hub WIEN

2.4.1 Notation

An overview of the notation used in Section 2.3 and 2.4 and important numerical values are shown in Table 2.1.

Symbol	Definition	Value or unit
ε_0	vacuum permittivity	$8.854 \cdot 10^{-12}$ F/m
e	elementary charge	$1.602 \cdot 10^{-19}$ C
a_0	Bohr radius	$5.29 \cdot 10^{-11}$ m
c	speed of light	299 792 458 m/s
K	$4\pi N_A r_e^2 m_e c^2$	0.307 075 MeV mol^{-1} cm^2
z	charge number of incident particle	
Z	atomic number of absorber	
A	atomic mass of absorber	g mol^{-1}
$m_e c^2$	electron mass $\times\, c^2$	511 keV
M	incident particle mass	MeV/c^2
I	mean excitation energy	eV
$\delta(\beta\gamma)$	density effect correction	

Table 2.1: Summary of the quantities.

2.4.2 Mean energy loss

Charged particles in the keV-MeV range lose only a small fraction of their energy (less than 100 eV for 90% of all collisions [19]) in a single ionization process and thus numerous of these interactions occur per unit path length.

The mean rate of *electronic* energy loss by protons (and other heavy charged particles) in the clinically relevant energy range (60-250 MeV) is described by the Beth-Bloch equation:

$$\left\langle -\frac{dE}{dx} \right\rangle = K z^2 \frac{Z}{A} \frac{1}{\beta^2} \left[\frac{1}{2} \ln \frac{2 m_e c^2 \beta^2 \gamma^2 W_{max}}{I^2} - \beta^2 - \frac{\delta(\beta\gamma)}{2} \right] \tag{2.10}$$

using the notation of the Particle Data Group in reference [19] and the Lorentz factor $\gamma = 1/\sqrt{(1-\beta^2)}$.

The maximum possible energy transfer to an electron in a single collision is

$$W_{max} = \frac{2 m_e c^2 \beta^2 \gamma^2}{1 + 2\gamma m_e / M + (m_e/M)^2} \tag{2.11}$$

Equation (2.10) is exactly the electronic *mass stopping power* [MeV g^{-1} cm^2], describing the average kinetic energy lost per unit distance and unit density due to ionization and atomic excitation. This is a useful definition, because it is *almost* independent of the material. As a consequence, it can be easily applied to different materials using the corresponding mass stopping power ratio. The last term in Eq. (2.10) is the density

Die approbierte gedruckte Originalversion dieser Diplomarbeit ist an der TU Wien Bibliothek verfügbar
The approved original version of this thesis is available in print at TU Wien Bibliothek.
TU Bibliothek Your knowledge hub WIEN

effect correction term by Fermi [20]. It is a pure relativistic correction and accounts for the polarization of the medium at high relativistic energies ($\geq$ GeV) because of the extended transversal electric field. The density correction term depends on the density of the material. Although this term can be omitted in the case of clinically protons, it must be considered for electrons (see Fig. 5.2). Further correction terms, e.g. the shell correction term at low energies and for heavy atoms, are known in the literature but will not be discussed here in detail.

The mean energy loss by electrons is slightly different from the stopping power of heavy charged particles. This is attributed to differences in (relativistic) kinematics, spin, charge and the quantum mechanical indistinguishability of the incident electron and the target electron.

The maximum energy transfer in a single collision should be the entire kinetic energy

$$W_{max} = \gamma m_e c^2 - m_e c^2 = m_e c^2(\gamma - 1) \tag{2.12}$$

but since the particles are identical, it is exactly half of W_{max}.

The analytical expressions for the mean rate of energy loss by electrons is given by [19]:

$$\begin{aligned}\left\langle -\frac{dE}{dx} \right\rangle = \frac{1}{2} K \frac{Z}{A} \frac{1}{\beta^2} \Bigg[\ln \frac{m_e c^2 \beta^2 \gamma^2 \{m_e c^2(\gamma - 1)/2\}}{I^2} + (1 - \beta^2) \\ - \frac{2\gamma - 1}{\gamma^2} \ln 2 + \frac{1}{8} \left(\frac{\gamma - 1}{\gamma} \right)^2 - \delta \Bigg]\end{aligned} \tag{2.13}$$

The similarity between Eq. (2.10) and Eq. (2.13) can be illustrated by comparing the logarithmic terms in both equations when substituting with $W_{max} = m_e c^2(\gamma - 1)/2$.

In analogy with the electronic stopping power for heavy particles, this is also known as *collision stopping power* referring to the loss only due to Coulomb collisions. The electronic and the collision stopping power is depicted in Figure 2.2a for electrons and protons, respectively.

Since the energy deposition increases with decreasing velocity, the particle loses progressively energy per unit path length while penetrating the material. The maximum energy loss is reached immediately before the particle is stopped, resulting in a sharp peak followed by a steep fall off, also referred to as the *Bragg-Peak* (see Fig. 2.2b).

This effect is beneficial in particle beam therapy because it allows to maximize the energy deposition in the target volume while sparing surrounding healthy tissue. The characteristics of the Bragg-Peak are different for different charged particles. For instance, carbon ions show a non negligible energy deposition behind the Bragg-Peak area caused by light nuclear fragments, which are produced by the initial beam and propagated through the medium. This *fragmentation tail* is even more distinct for heavier ions. In contrast, the electron Bragg-Peak is broader and superimposed by bremsstrahlung losses.

Die approbierte gedruckte Originalversion dieser Diplomarbeit ist an der TU Wien Bibliothek verfügbar
The approved original version of this thesis is available in print at TU Wien Bibliothek.
TU Bibliothek Your knowledge hub WIEN

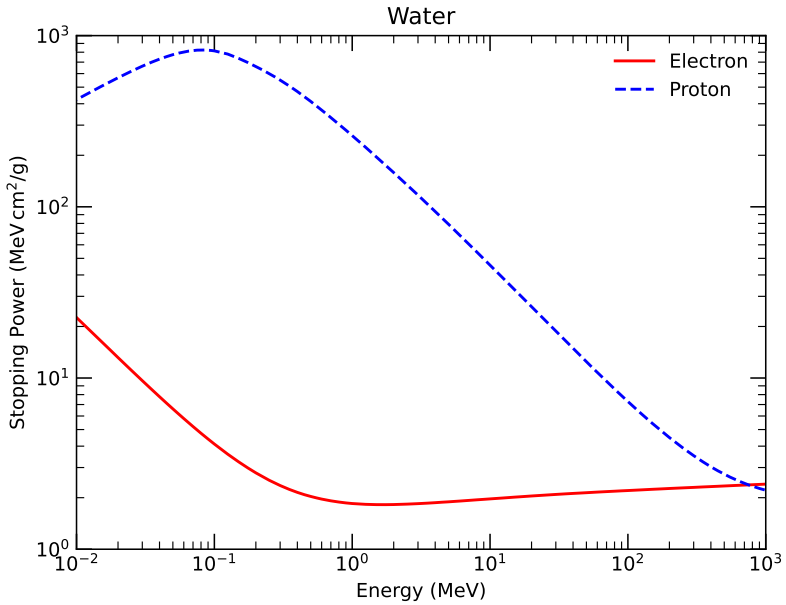

(a) Stopping power for different electron and proton energies in water. Numerical values were obtained from the NIST-(P)ESTAR database [21].

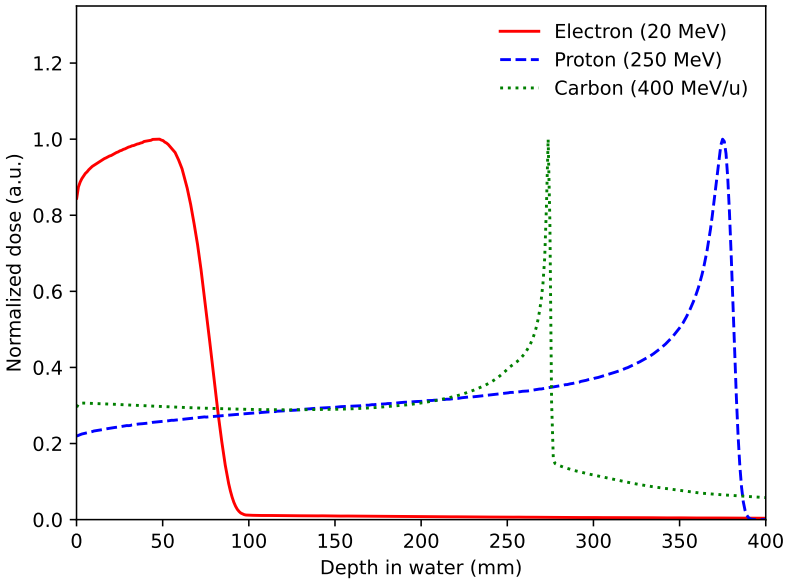

(b) MC calculation of the energy deposition per unit path length of an electron, a proton and carbon ion beam in water. The maximum energy loss is characterized by the Bragg-Peak.

Figure 2.2: (a) Stopping Power of electrons and protons and (b) Bragg peak in water.

Die approbierte gedruckte Originalversion dieser Diplomarbeit ist an der TU Wien Bibliothek verfügbar
The approved original version of this thesis is available in print at TU Wien Bibliothek.

2.4.3 Range

The range R of a charged particle which loses energy only by ionization and atomic excitation on a straight line (*continuous slowing-down approximation*; CSDA) can be obtained by integrating Eq. (2.10):

$$\langle R \rangle = \int_0^{E_0} \left(\frac{dE}{dx} \right)^{-1} dx \tag{2.14}$$

where E_0 is the initial kinetic energy of the particle. As denoted by the angular brackets, this quantity is an average value for a large number of particles (mean particle range) because the range of single particles vary slightly due to stochastic energy loss fluctuations. This is also known as range or energy straggling, which is mostly caused by small angle deflections of the particle while passing through matter. Since it based on random variations, it can be approximated by a Gaussian distribution if the number of events is large enough. Range straggling depends on the incident particle mass ($\propto 1/\sqrt{M}$) and energy [22]. Hence, the Bragg-Peak of heavier particles (e.g., carbon ions) is sharper compared to protons.

Even though charged particles do not traverse matter in straight lines due to MSC, the CSDA range is a sufficient approximation for many medical applications. Typical ranges of clinical electrons and protons in water are depicted in Figure 2.3.

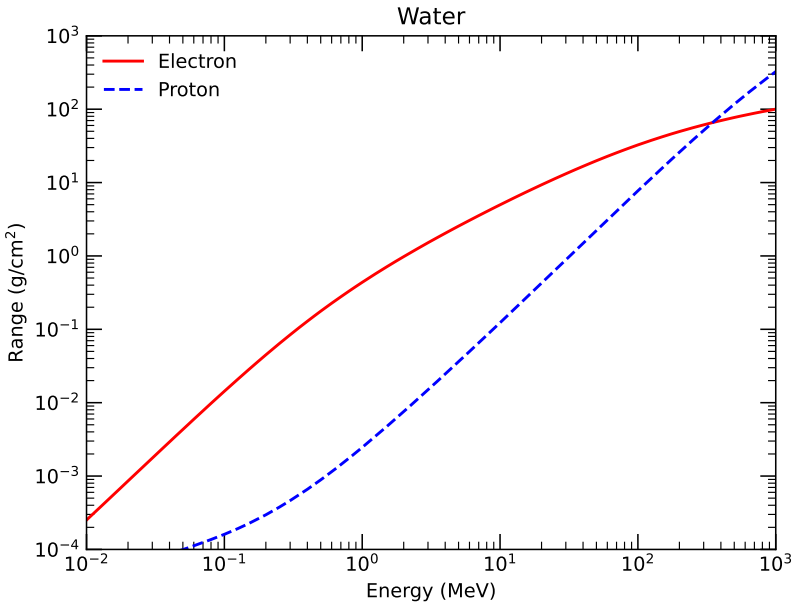

Figure 2.3: CSDA ranges for different electron and proton energies in water. Numerical values were obtained from the NIST-(P)ESTAR database [21].

Die approbierte gedruckte Originalversion dieser Diplomarbeit ist an der TU Wien Bibliothek verfügbar
The approved original version of this thesis is available in print at TU Wien Bibliothek.
TU Bibliothek Your knowledge hub WIEN

2.5 Boltzmann transport equation in external fields

In the context of radiotherapy, the (linear) Boltzmann transport equation (BTE) describes the conservation of particles during transport through a medium [23]. In the following, a brief derivation of the BTE in the presence of external electromagnetic fields will be given based on the theoretical framework proposed by H. Bouchard et al. [18]. This will help us to understand the upcoming section of this work.

Starting from the continuity equation, a transport equation for a given particle type can be written in the following form:

$$\frac{dn}{dt} = \rho(S + I) \tag{2.15}$$

where $n = n(\boldsymbol{r}, \boldsymbol{p}, t)$ is the spatial particle distribution and $\rho = \rho(\boldsymbol{r})$ the local mass density. The time derivative of the particle distribution depends on the net addition or loss of particles due to scattering events. The first term of the right-hand side of equation (2.15) is the source term $S = S(\boldsymbol{r}, \boldsymbol{p}, t)$ and represents the number of particles being produced by an external source. The second term is the collision or interaction term $I = I(\boldsymbol{r}, \boldsymbol{p}, t)$ and describes the number of particles generated by collisions. This term accounts for all electromagnetic processes of the given particle.

Decomposing the time derivative into multi-variable dependencies

$$\frac{dn(\boldsymbol{r}, \boldsymbol{p}, t)}{dt} = \frac{\partial n}{\partial t} + \sum_{i=1}^{3} \left(\frac{\partial n}{\partial x_i} \frac{dx_i}{dt} + \frac{\partial n}{\partial p_i} \frac{dp_i}{dt} \right) \tag{2.16}$$

$$= \left(\frac{\partial}{\partial t} + \frac{d\boldsymbol{r}}{dt} \cdot \nabla_{\boldsymbol{r}} + \frac{d\boldsymbol{p}}{dt} \cdot \nabla_{\boldsymbol{p}} \right) n \tag{2.17}$$

leads to the Boltzmann transport equation:

$$\left(\frac{\partial}{\partial t} + \frac{d\boldsymbol{r}}{dt} \cdot \nabla_{\boldsymbol{r}} + \frac{d\boldsymbol{p}}{dt} \cdot \nabla_{\boldsymbol{p}} \right) n = \rho \left(S + I \right) \tag{2.18}$$

The particle fluence Φ is given by

$$\Phi = n\beta c \tag{2.19}$$

and equation (2.18) can be rewritten as

$$\frac{1}{\beta c} \frac{\partial \Phi}{\partial t} + \boldsymbol{u} \cdot \nabla_{\boldsymbol{r}} \Phi + \frac{d\boldsymbol{p}}{dt} \cdot \left(\frac{1}{\beta c} \nabla_{\boldsymbol{p}} \Phi + \frac{\Phi}{c} \cdot \nabla_{\boldsymbol{p}} \frac{1}{\beta} \right) = \rho(S + I) \tag{2.20}$$

where $\frac{d\boldsymbol{r}}{dt} = \beta c \cdot \boldsymbol{u}$ is the velocity and $\boldsymbol{u} = \frac{\boldsymbol{p}}{|\boldsymbol{p}|}$ is the unit vector in the same direction as the momentum (and hence the velocity) of the particle. By using the expression of the relativistic momentum of a particle with rest mass m_0

$$p = \gamma \beta m_0 c \tag{2.21}$$

Die approbierte gedruckte Originalversion dieser Diplomarbeit ist an der TU Wien Bibliothek verfügbar
The approved original version of this thesis is available in print at TU Wien Bibliothek.
TU Bibliothek Your knowledge hub WIEN

one can write

$$\beta = \sqrt{\frac{(\frac{p}{m_0 c})^2}{1 + (\frac{p}{m_0 c})^2}} \tag{2.22}$$

and the derivative of β in equation (2.20) is found to be:

$$\nabla_{\boldsymbol{p}} \left(\frac{1}{\beta} \right) = \boldsymbol{u} \frac{\partial}{\partial p} \sqrt{\frac{1}{(\frac{p}{m_0 c})^2} + 1} \tag{2.23}$$

$$= -\frac{1}{\gamma^3 \beta^2 m_0 c} \boldsymbol{u} \tag{2.24}$$

The BTE in the absence of electromagnetic fields is therefore given by:

$$\frac{1}{\beta c} \frac{\partial \Phi}{\partial t} + \boldsymbol{u} \cdot \nabla_{\boldsymbol{r}} \Phi = \rho(S + I) - \frac{d\boldsymbol{p}}{dt} \cdot \left(\frac{1}{\beta c} \nabla_{\boldsymbol{p}} \Phi - \frac{1}{\gamma^3 \beta^2 m_0 c^2} \Phi \, \boldsymbol{u} \right) \tag{2.25}$$

The Lorentz force with charge q

$$\frac{d\boldsymbol{p}}{dt} = q(\boldsymbol{E} + \beta c \, \boldsymbol{u} \times \boldsymbol{B}) \tag{2.26}$$

acts on the charged particles and the BTE in the presence of external electromagnetic fields $\boldsymbol{E}, \boldsymbol{B}$ becomes:

$$\frac{1}{\beta c} \frac{\partial \Phi}{\partial t} + \boldsymbol{u} \cdot \nabla_{\boldsymbol{r}} \Phi = \rho(S + I) - q \left(\frac{\boldsymbol{E}}{\beta c} + \boldsymbol{u} \times \boldsymbol{B} \right) \cdot \nabla_{\boldsymbol{p}} \Phi + \frac{q}{\gamma^3 \beta^2 m_0 c^2} (\boldsymbol{E} \cdot \boldsymbol{u}) \Phi \tag{2.27}$$

because $(\beta c \, \boldsymbol{u} \times \boldsymbol{B}) \cdot \boldsymbol{u} = 0$. In general, the solution of the BTE under realistic conditions is non-trivial and numerous approximations and simplifications have to be done in order to obtain a numerical solution [23]. Analytical solutions are available only for very simplified scenarios. In the upcoming section, a theorem will be introduced which allows to obtain an exact solution of the BTE.

2.6 Fano theorem

The Fano theorem was formulated by U. Fano in 1954 [24] and states the following:

> *In a medium of given composition exposed to a uniform flux of primary radiation (such as X-rays or neutrons) the flux of secondary radiation is also uniform and independent of the density of the medium as well as of the density variations from point to point.*

Die approbierte gedruckte Originalversion dieser Diplomarbeit ist an der TU Wien Bibliothek verfügbar
The approved original version of this thesis is available in print at TU Wien Bibliothek.
TU Bibliothek Your knowledge hub WIEN

This theorem is essential in ionization chamber based dosimetry. It is the basis in the validation of cavity theories, which require charged particle equilibrium (CPE) as a fundamental condition. CPE is defined as:

$$\nabla\Phi = 0 \tag{2.28}$$

and exists in a certain volume if the charged particle fluence Φ is constant. This means that each charged particle leaving the volume is replaced by an identical particle of the same energy entering. Two conditions can be formulated in order to achieve CPE:

1. The medium has to have a uniform atomic composition and atomic interaction properties, i.e., differential cross sections.

2. The medium has to have a uniform source scaled with the local mass density.

Under compliance with these conditions, the energy- and angular-dependent particle fluence is uniform. As a consequence, regardless of local mass density variations and differential cross sections, the absorbed dose is uniform too.

Under the condition of CPE, i.e., constant particle fluence, the BTE in Eq. (2.25) reduces to:

$$\rho(S + I) = 0 \tag{2.29}$$

because $\boldsymbol{u}\cdot\nabla\Phi = 0$ and $d\Phi/dt = d\boldsymbol{p}/dt = 0$. Since both, the source and the interaction term, are proportional to the density, it may be cancelled out and the solution of the BTE is therefore independent of the mass density.

Although Fano's theorem validates cavity theories and allows an analytical dose expression (c.f. Subsec. 5.1.6), the conditions of CPE can hardly be met in real-life experiments and fluence perturbation correction factors are introduced. However, Smyth [6] proposed to use the Fano theorem as a benchmark test for (condensed history) MC particle transport codes since the conditions can be exactly modeled in a computational experiment. The test is based on artificially creating CPE while complying with the requirements of the theorem. Hence, an analytical expression of the absorbed dose can be obtained and compared to the simulated dose of the MC algorithm. The deviation of the simulated absorbed dose from the theoretical value is then used to assess the accuracy and stability of the MC algorithm. Therefore, the self-consistency of the transport algorithm is evaluated within its own cross sections. Certainly, this test does not provide any information about the accuracy of the differential cross section models, which are typically based on phenomenological approximations on top of MSC theories in CH MC algorithms. This approach, known as the *Fano cavity test*, has been extensively exploited for charged particles (electrons and protons) as theoretical benchmark and was also used in ionization chamber dose response simulations to determine an optimal set of simulation parameters [6, 25, 26, 27, 28, 29, 30, 31, 32]. It was shown that most MC transport codes could pass the Fano test within 0.1% for ionization chamber geometries.

Die approbierte gedruckte Originalversion dieser Diplomarbeit ist an der TU Wien Bibliothek verfügbar
The approved original version of this thesis is available in print at TU Wien Bibliothek.
TU Bibliothek Your knowledge hub WIEN

2.6.1 Conditions in external electromagnetic fields

H. Bouchard et al. [18] demonstrated that the (classical) Fano theorem does not hold in the presence of external electromagnetic fields. Assuming CPE, the time-dependent BTE (2.27) reduces to:

$$\rho(S+I) - q\left(\frac{\boldsymbol{E}}{\beta c} + \boldsymbol{u}\times\boldsymbol{B}\right)\cdot\nabla_{\boldsymbol{p}}\Phi + \frac{q}{\gamma^3\beta^2 m_0 c^2}(\boldsymbol{E}\cdot\boldsymbol{u})\Phi \overset{CPE}{=} 0 \tag{2.30}$$

The Fano theorem would be valid if the electric field and magnetic field is proportional to the mass density of the medium. However, since $\boldsymbol{E}$ and $\boldsymbol{B}$ do in general not scale with the density, the particle fluence cannot be assumed to be independent of the density of the medium.

The same group proposed two separate additional conditions, based on fundamental proofs, in order to comply with the classical Fano theorem in the presence of magnetic fields [33]. The first condition is a constraint on the source and can be intuitively understood. The magnetic field affects only the direction of a charged particle due to the Lorentz force. Hence, an isotropic particle distribution in equilibrium state should not be perturbed by the presence of the magnetic field. A rigorous proof of this condition is presented in [33]. In fact, the condition of charged particle isotropy allows the BTE to reduce to the field-free case, independently of the magnetic field strength or direction. The second condition is directly based on Eq. (2.30) and requires a uniform magnetic field scaled proportionally to the local mass density, i.e., $\boldsymbol{B} \propto \rho\boldsymbol{B}$. While the first condition does not constrain the magnetic field, allowing non-uniform fields, the latter one explicitly requires a magnetic field of fixed direction and proportional to the mass density. This is a disadvantage, since it does not allow to verify arbitrary (realistic) magnetic fields. Furthermore, interpolation methods in magnetic vector field maps are commonly used to determine field values in between two points. This can be an issue at volume interfaces with high density variations which typically exists in the simulation of ionization chambers.

Pooter et al. confirmed the first condition presenting an alternative proof [34]. Furthermore, they performed a Fano cavity test and demonstrated that charged particle isotropy is essential in the execution of the test in the presence of magnetic fields. The particle transport inside magnetic fields of several MC codes (EGSnrc, Geant4, MCNP and PENELOPE) have been validated using the adapted Fano test based on the first condition [34, 35, 36, 37, 38, 39]. A comprehensive overview of previous studies is summarized in the recently published review paper by Pooter et al. [40]. To the extend of our knowledge, no Fano cavity test has been performed using the Geant4 application GATE.

It remains open, whether a Fano test can be performed in the presence of an external electric field and how it can be implemented. Although equation (2.30) indicates that a density scaled electric field complies with the theorem, the electric field accelerates the particles and changes the kinetic energy. So far, no studies had been performed yet addressing this.

Die approbierte gedruckte Originalversion dieser Diplomarbeit ist an der TU Wien Bibliothek verfügbar
The approved original version of this thesis is available in print at TU Wien Bibliothek.
TU Bibliothek Your knowledge hub WIEN

3 Materials and Methods

3.1 Software frameworks

All Monte Carlo simulations within this study were conducted using the open-source software framework GATE [41, 42, 43]. GATE (Geant4 Application for Tomographic Emission) is dedicated to numerical simulations in medical imaging and radiotherapy. It is developed and maintained by the international OpenGATE collaboration. As the name implies, GATE is an application built on top of Geant4 [44, 45, 46]. Geant4 (GEometry ANd Tracking) is a C++ based software platform which uses the MC method for the simulation of particles traversing matter. Data output handling in GATE relies on ROOT [47], an open-source data analysis framework developed by CERN and specifically designed for particle physics applications. Being a Geant4 application, GATE acts as a C++ wrapper and provides an user friendly interface to create standardized and reproducible MC simulations using simple macro commands. However, if necessary, the source code can be extended to a user defined level, retaining the full capabilities of Geant4. Throughout this project, the development branch of GATE v9.0 compiled with Geant4 v10.06 patch-01 and ROOT v6.20.02 was used.

3.2 Parallelization

Monte Carlo simulations require extensive computational resources in order to obtain a sufficient level of accuracy. Although GATE v9.0 does not support message-passing standards like Message Passing Interface (MPI) or Open Multi-Processing (OpenMP), simulations can be distributed on different cores or nodes of a cluster. Since GATE simulates particles subsequently and independently from each other, there is no need for communication between those parallel sub-tasks or for their results.

A custom Python script (Python Software Foundation[1], version 3.8.3) was used to split the N-particle GATE simulation (task) in k independent sub-tasks. Thus, effectively simulating $\frac{N}{k}$ particles per sub-task. The engine seed of the random number generator was set to automatic to ensure that k independent streams were produced. In order to distribute the sub-tasks simultaneously on different CPU cores, GNU parallel [48] was used. After job execution, the data output of each sub-task was merged using a custom post-processing script.

For the Fano cavity test, only the energy deposition ε and its relative statistical uncertainty σ was scored. The total energy deposition ε_{tot} of the N-particle simulation was calculated as the sum of the individual energy depositions ε_j of each sub-task j:

[1] https://www.python.org

Die approbierte gedruckte Originalversion dieser Diplomarbeit ist an der TU Wien Bibliothek verfügbar
The approved original version of this thesis is available in print at TU Wien Bibliothek.
TU Bibliothek Your knowledge hub WIEN

$$\varepsilon_{tot} = \sum_{j=1}^{k} \varepsilon_j \tag{3.1}$$

considering that the energy deposition of each particle inside a volume was scored independently.

In order to calculate the total uncertainty σ_{tot}, the sum of the squared energy deposition and the total number of hits n in the volume of each sub-task were taken into account. The total uncertainty was then calculated as:

$$\sigma_{tot} = \sqrt{\frac{1}{n-1} \cdot \left[\sum_{i=1}^{n} \frac{\varepsilon_i^2}{n} - \left(\sum_{i=1}^{n} \frac{\varepsilon_i}{n} \right)^2 \right]} \cdot \sum_{i=1}^{n} \frac{n}{\varepsilon_i} \tag{3.2}$$

In the initial phase of this project, simulations were performed on a dedicated machine with 20 Intel(R) Xeon(R) Gold 6136 CPU @ 3.00GHz cores and at a later stage on the MoccaMed (Monte Carlo Calculations in Medicine) cluster of the Medical University of Vienna [49]. The MoccaMed cluster is as a local computing grid and uses HTCondor [50] as job distributing system. Simulations were performed inside Docker (Docker, Inc., Palo Alto, California, USA) containers in order to circumvent any dependencies on the operating system or locally installed software versions.

Die approbierte gedruckte Originalversion dieser Diplomarbeit ist an der TU Wien Bibliothek verfügbar
The approved original version of this thesis is available in print at TU Wien Bibliothek.
TU Bibliothek Your knowledge hub WIEN

4 Proton beam transport inside electromagnetic fields

4.1 Electromagnetic fields in Geant4 and GATE

In the following section, a brief introduction will be presented of how charged particles are propagated inside electromagnetic fields in Geant4 and GATE. The introduction will highlight some crucial aspects of the methods used in order to provide a documentation of the software implementation. The Book For Application Developers [51] of Geant4 is recommended for a comprehensive explanation of the stepping algorithm and its parameters.

4.1.1 Overview

Geant4 is capable of describing and propagating charged particles in a variety of fields including electric, magnetic and electromagnetic fields. In general, these fields can be uniform, non-uniform, time varying or time independent. The propagation of tracks inside the fields can be performed to a user-defined accuracy.

To propagate a particle track inside an electromagnetic field, the equation of motion of the particle in that field is integrated. In general, this is done using numerical methods for ordinary differential equations, defined as *steppers*. Geant4 provides several *steppers*, suitable for different conditions. Those include the *classical Runge-Kutta 4*, *simple Runge-Kutta*, *implicit Euler*, *explicit Euler* and *simple Heum*. However, if an analytical solution is known for a specific problem, such as for uniform fields, it can be utilized instead.

Using a particular *stepper*, particle tracks in electromagnetic fields are calculated by approximating the curved trajectories into a set of *linear chord segments*. The *chords* are also used in the determination of whether the track has crossed a volume boundary. Geant4 provides several *precision parameters* that adjust the accuracy and performance of the integration and the subsequent interrogation of the geometry [51]. The *miss distance* is used to define the level of accuracy to which the *chords* approximate the real curved trajectory. Geometrically it corresponds to the maximum distance between the real curve and the linear approximated *chord* (see Fig. 4.1).

Die approbierte gedruckte Originalversion dieser Diplomarbeit ist an der TU Wien Bibliothek verfügbar
The approved original version of this thesis is available in print at TU Wien Bibliothek.
TU Bibliothek Your knowledge hub WIEN

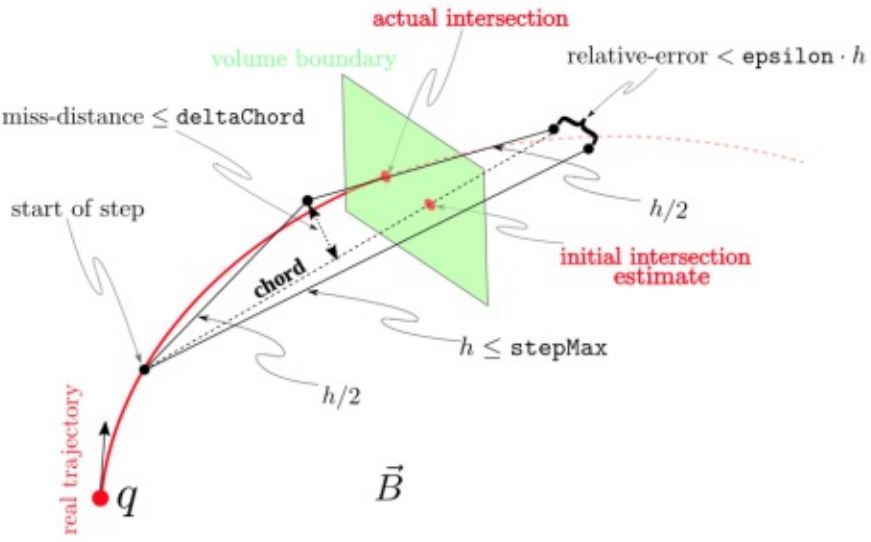

Figure 4.1: Geometrical representation of a *tracking step* inside an (electro-) magnetic field using a *Runge-Kutta 4* method . The real trajectory is approximated by *linear chords* controlled by the parameter *miss distance*. The step length h is proposed by a physics process. Figure taken from [52].

The *delta intersection* parameter restricts the maximum accuracy of the calculation of an intersection with a volume boundary. This parameter correlates with potential systematic errors in the momentum of reconstructed tracks because it affects the Geant4 boundary crossing algorithm. As it is described in [51], this algorithm is used to determine the intersection with a volume boundary. This is done by using a *chord* between two points of the curved trajectory. Hence, the intersection point is always inside the curve. If a potential boundary intersection point is estimated with a better precision than this parameter, it gets accepted, otherwise a new candidate will be calculated. Therefore, it can be understood as a position error or bias.

The numerical integration error is handled by three parameters. The *delta one step* parameter is a distance and can be understood as a positional error which is acceptable in an ordinary (without boundary crossing) integration step. It defines the accuracy of the end points of *chord segments*. Similar to that, the two parameters *epsilon min* and *epsilon max* determine the minimum and maximum relative positional error of the proposed *tracking step*. The *step minimum* is the minimum length of a step for the integration.

Up to now, GATE v9.0 provides two methods to apply electric or magnetic fields. The first method allows to create a uniform field across the whole simulation geometry. However, it is not possible to attach the field to a single logical volume. The second method allows to generate a vector field map with three components from a custom look-up table. This facilitates the usage of even non-uniform fields as for example simulated by external programs. The uniform field method is based on the predefined Geant4 field

Die approbierte gedruckte Originalversion dieser Diplomarbeit ist an der TU Wien Bibliothek verfügbar
The approved original version of this thesis is available in print at TU Wien Bibliothek.
TU Bibliothek Your knowledge hub WIEN

classes *G4UniformElectricField* and *G4UniformMagField*, which propagate the particle track using the analytical solution of the equation of motion. The vector field method is based on the user-defined field classes *GateElectricTabulatedField3D* and *GateMagTabulatedField3D*, recently implemented in GATE [53]. They solve the equation of motion numerically using the classical *Runge-Kutta 4* method as the default option.

To provide a new method for particle transport in a custom electromagnetic field, a new class was introduced and extended based on the existing class *GateMagTabulatedField3D*, which is based on the official Geant4 *Purging Magnet* [54] example.

4.1.2 Implementation

The new class *GateElectMagTabulatedField3D* was implemented in the development branch of GATE v9.0 to generate an electromagnetic field from a custom look-up table containing the spatial positions $\boldsymbol{r} = (x, y, z)^\top$ cm and their associated electric and magnetic field strengths $\boldsymbol{E} = (E_x, E_y, E_z)^\top$ V m^{-1} and $\boldsymbol{B} = (B_x, B_y, B_z)^\top$ T. The 3D field grid is read in and interpolated to the entire simulation geometry determined by the minimum and maximum value of the grid using a simple linear interpolation method.

The structure of the input file (`.txt` recommended) is shown in Figure 4.2 for an arbitrary field configuration. The coordinates specified in the input file are assumed to be absolute Cartesian coordinates. The grid size can be either an integer or a floating point number. The first line of the file must be the number of values per coordinate. In the *example* shown in Figure 4.2, the arbitrarily chosen field ranges from $-5\,\text{cm} \leq \boldsymbol{r} \leq 5\,\text{cm}$ and has a grid size of 1 cm, so the number of values per coordinate is 11. The permittivity and permeability of various materials are assumed to be already taken into account in the field strength.

```
1 #x y z Ex Ey Ez Bx By Bz
2 11 11 11
3 -5.00 -5.00 -5.00 0 0 0 0 3 0
4 -4.00 -5.00 -5.00 0 0 0 0 3 0
5 -3.00 -5.00 -5.00 0 0 0 0 3 0
6 -2.00 -5.00 -5.00 0 0 0 0 3 0
7 -1.00 -5.00 -5.00 0 0 0 0 3 0
8 0.00 -5.00 -5.00 0 0 0 0 3 0
9 1.00 -5.00 -5.00 0 0 0 0 3 0
10 2.00 -5.00 -5.00 0 0 0 0 3 0
11 3.00 -5.00 -5.00 0 0 0 0 3 0
12 4.00 -5.00 -5.00 0 0 0 0 3 0
13 5.00 -5.00 -5.00 0 0 0 0 3 0
14 -5.00 -4.00 -5.00 0 0 0 0 3 0
15 -4.00 -4.00 -5.00 0 0 0 0 3 0
16 -3.00 -4.00 -5.00 0 0 0 0 3 0
17 -2.00 -4.00 -5.00 0 0 0 0 3 0
18 -1.00 -4.00 -5.00 0 0 0 0 3 0
19 0.00 -4.00 -5.00 0 0 0 0 3 0
20 1.00 -4.00 -5.00 0 0 0 0 3 0
21 2.00 -4.00 -5.00 0 0 0 0 3 0
22 3.00 -4.00 -5.00 0 0 0 0 3 0
23 4.00 -4.00 -5.00 0 0 0 0 3 0
24 5.00 -4.00 -5.00 0 0 0 0 3 0
25 .
26 .
27 .
```

Figure 4.2: *Example* of a GATE input file for electromagnetic vector field maps.

Die approbierte gedruckte Originalversion dieser Diplomarbeit ist an der TU Wien Bibliothek verfügbar
The approved original version of this thesis is available in print at TU Wien Bibliothek.
TU Bibliothek Your knowledge hub WIEN

The field is created and declared in the *GateDetectorConstruction* class. For the propagation of the particle tracks inside the field, *G4EqMagElectricField* is integrated. In the declaration, the *classical Runge-Kutta 4*, *simple Runge-Kutta*, *implicit Euler*, *explicit Euler* and *simple Heum* as well as the *precision parameters* discussed above were made accessible to adjust the accuracy of the propagation if needed by the user. The GATE commands:

```
/gate/geometry/setElectMagTabulateField3D
/gate/geometry/setElectMagTabulateField3D/setStepMinimum
/gate/geometry/setElectMagTabulateField3D/setMissDistance
/gate/geometry/setElectMagTabulateField3D/setDeltaIntersection
/gate/geometry/setElectMagTabulateField3D/setDeltaOneStep
/gate/geometry/setElectMagTabulateField3D/setMinimumEpsilonStep
/gate/geometry/setElectMagTabulateField3D/setMaximumEpsilonStep
/gate/geometry/setElectMagTabulateField3D/setIntegratorStepper
```

were defined in the *GateDetectorMessenger* class in order to apply the electromagnetic field in a GATE simulation. Apart from the electromagnetic field, no functional changes between the base class *GateMagTabulatedField3D* and the new class *GateElectMagTabulatedField3D* were implemented.

F. Padilla-Cabal et al. [53] evaluated the simulation performance in terms of accuracy and calculation times for different *steppers*, *stepper orders* and *precision parameters* for magnetic fields in GATE. The results are shown in Table 4.1 for the deflection of proton beams inside a magnetic field in air. The classical *Runge-Kutta 4* was the fastest method and decreasing the *precision parameters* did not improve the accuracy, it only resulted in slower calculation times by a factor of 2.4. Based on the previous findings for particle transport in magnetic fields, the *classical Runge-Kutta 4* and the recommended Geant4 values were set as the default option for electromagnetic fields in GATE.

However, it is recommended to adapt the transport parameters according to the specific simulation problem. Recommendations and general considerations are given in the Book For Application Developers of Geant4 [51].

It is emphasized that the methods used for the implementation of the electromagnetic field are for the most part the same as for magnetic fields. Therefore, it could be also used for the simulation of pure magnetic fields while setting the electric field components to zero.

Die approbierte gedruckte Originalversion dieser Diplomarbeit ist an der TU Wien Bibliothek verfügbar
The approved original version of this thesis is available in print at TU Wien Bibliothek.
TU Bibliothek Your knowledge hub WIEN

Parameter	Geant4 recommended value	GATE tested value	Calculation times ratio
Integrator stepper	ClassicalRK4	ClassicalRK4	1
		SimpleRunge	5.3
		ImplicitEuler	5.4
		ExplicitEuler	12.9
		SimpleHeum	2.0
Delta chord	250 µm	1 µm - 250 µm	
Delta intersection	$\leq$ 1 µm	1 nm - 1 µm	
Delta one step	$\leq$ 10 µm	1 nm - 10 µm	2.4
Epsilon min	$5 \cdot 10^{-5}$	10^{-10} - $5 \cdot 10^{-5}$	
Epsilon max	10^{-3}	10^{-11} - 10^{-3}	
Step minimum	10 µm	1 µm - 10 µm	

Table 4.1: Overview of the implemented precision parameters and integration *steppers* in GATE. The ratio between the calculation times using the lowest tested values in GATE over the recommended Geant4 values is presented. Based on reference [53].

4.2 Verification

Simple tests and integrity checks in vacuum were performed to assess the accuracy and correctness of the implemented methods for particle transport within electromagnetic fields in GATE. Simulated particle trajectories were compared with independent calculations using numerical methods. Due to the highly object-oriented structure of GATE and Geant4, simple tests were done to verify the basic functionalities of newly added features, especially with regard to physical principles. Furthermore, it served as a verification procedure for the correct configuration and integration within the MC framework.

4.2.1 GATE simulation

A mono-energetic parallel proton beam inside a $400 \times 400 \times 400\text{mm}^3$ vacuum box was simulated. The lateral beam profile was modelled to be Gaussian shaped with a spot size of $\sigma_x = \sigma_y = 3\,\text{mm}$. Two configurations with regard to the beam energy, electric field strength and the direction of the electric and magnetic field were used.

First, a $E_0 = 1\,\text{MeV}$ proton beam was generated along the y-axis at $y = 0\,\text{mm}$ in the center of the lateral surface of the box. A uniform electric and magnetic field, both oriented in the z-direction, was applied to the entire system with a field strength of $E_z = 40\,\text{kV}\,\text{m}^{-1}, 80\,\text{kV}\,\text{m}^{-1}$ and $B_z = 1.5\,\text{T}$ (c.f. Fig. 4.3). These field strengths are typically used in dosimetric applications using ionization chambers ($\approx$ 200-400 V inside a 2 mm cavity) and MRI scanners.

Die approbierte gedruckte Originalversion dieser Diplomarbeit ist an der TU Wien Bibliothek verfügbar
The approved original version of this thesis is available in print at TU Wien Bibliothek.
TU Bibliothek Your knowledge hub WIEN

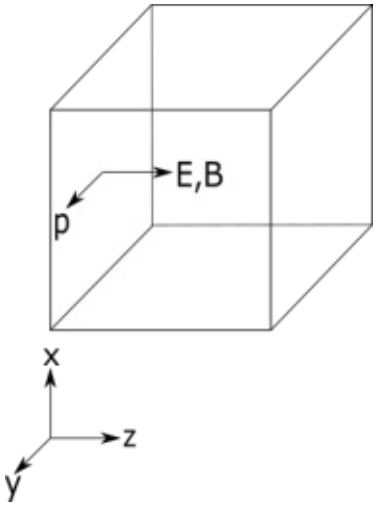

Figure 4.3: Electromagnetic field configuration 1: $\vec{p} = p\,\vec{e}_y$, $\vec{E} = E\,\vec{e}_z$, $\vec{B} = B\,\vec{e}_z$.

A second run was conducted using a field configuration which is typically used for ionization chamber dose response measurements. A proton beam with an initial kinetic energy of $E_0 = 60\,\mathrm{MeV}$ was generated along the z-axis at $z = 0\,\mathrm{mm}$ in the center of the lateral surface of the box. A uniform magnetic field of $B_y = 1.5\,\mathrm{T}$ encompassed the entire geometry in y-direction. The protons were accelerated by a uniform electric field of $E_z = 40\,\mathrm{kV\,m^{-1}}$ and $E_z = 80\,\mathrm{kV\,m^{-1}}$ in parallel to the beam direction (c.f. Fig 4.4).

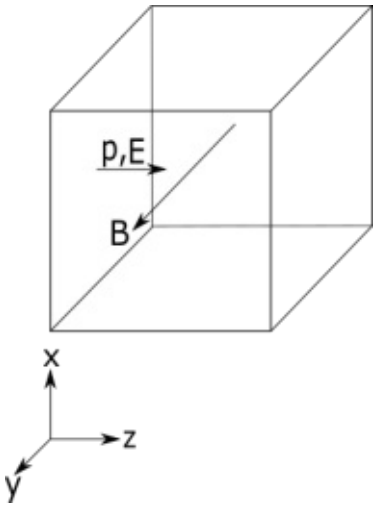

Figure 4.4: Electromagnetic field configuration 2: $\vec{p} = p\,\vec{e}_z$, $\vec{E} = E\,\vec{e}_z$, $\vec{B} = B\,\vec{e}_y$.

An overview of the simulation settings is presented in Table 4.2. The custom electromagnetic vector field maps were generated in Python with an arbitrary grid size of 1 cm.

Die approbierte gedruckte Originalversion dieser Diplomarbeit ist an der TU Wien Bibliothek verfügbar
The approved original version of this thesis is available in print at TU Wien Bibliothek.
TU Bibliothek Your knowledge hub WIEN

Simulation settings		
Density	Vacuum	$1\,\mathrm{ng\,cm^{-3}}$
Production cuts (γ, e^-, e^+)	World	1 mm
	Box	0.1 mm
Maximum step size	World	1 mm
	Box	0.1 mm
Electromagnetic field	Integrator stepper	ClassicalRK4
	Delta chord	1 µm
	Delta intersection	1 nm
	Delta one step	1 nm
	Epsilon min	10^{-11}
	Epsilon max	10^{-10}
	Step minimum	1 µm
Physics list	QGSP BERT EMZ	

Table 4.2: GATE simulation settings used for the verification of the electromagnetic field maps.

Two dimensional dose distributions in the transverse plane (xz- and yz-projection) were scored at $\Delta z = 0.1\,\mathrm{mm}$ (first configuration) and $\Delta z = 1\,\mathrm{mm}$ (second configuration) distances. The deflection curve of the particle beam was obtained by extracting the dose maximum, i.e., the center of the beam, at each scored penetration depth from the Gaussian fit of the correspondent transverse dose profiles. The kinetic energy was scored using the phase space actor of GATE. This actor can be attached to a volume and allows to store phase space information of the particles entering and leaving the volume such as the kinetic energy. The simulations were performed with 100 primary particles.

4.2.2 Numerical solution

A numerical solution of the particle transport inside an electromagnetic field was implemented in Python. The spatial positions of a single charged particle were calculated directly from the equation of motion. The motion of a relativistic particle with charge q in an electromagnetic field $\boldsymbol{E}, \boldsymbol{B}$ is described by a system of *ordinary differential equations* (ODEs):

$$\frac{d\boldsymbol{p}}{dt} = q(\boldsymbol{E} + \boldsymbol{v} \times \boldsymbol{B}) \tag{4.1}$$

with the Lorentz force on the right hand side. The momentum of the particle with rest mass m_0 and velocity $\boldsymbol{v}$ is given by:

$$\boldsymbol{p} = \gamma(\boldsymbol{v}) m_0 \boldsymbol{v} \tag{4.2}$$

with the Lorentz factor $\gamma = 1/\sqrt{(1 - \boldsymbol{v}^2/c^2)}$ and $c = 299\,792\,458\,\mathrm{m\,s^{-1}}$ the speed of light. Using the expression of the momentum of the particle, equation (4.1) can be

Die approbierte gedruckte Originalversion dieser Diplomarbeit ist an der TU Wien Bibliothek verfügbar
The approved original version of this thesis is available in print at TU Wien Bibliothek.
TU Bibliothek Your knowledge hub WIEN

rewritten as:

$$\frac{d\boldsymbol{v}}{dt} = \frac{q}{\gamma m_0}(\boldsymbol{E} + \boldsymbol{v} \times \boldsymbol{B}) - \frac{\boldsymbol{v}}{\gamma}\frac{d\gamma(\boldsymbol{v})}{dt} \tag{4.3}$$

The derivative of the Lorentz factor is:

$$\frac{d\gamma(\boldsymbol{v})}{dt} = \left(1 - \frac{\boldsymbol{v}^2}{c^2}\right)^{-\frac{3}{2}} \cdot \frac{\boldsymbol{v} \cdot \boldsymbol{a}}{c^2} = \gamma^3 \cdot \frac{\boldsymbol{v} \cdot \boldsymbol{a}}{c^2} \tag{4.4}$$

and the acceleration $\boldsymbol{a} = \dot{\boldsymbol{v}}$ of the charged particle can be expressed as:

$$\frac{d\boldsymbol{v}}{dt} = \frac{q}{\gamma m_0}(\boldsymbol{E} + \boldsymbol{v} \times \boldsymbol{B}) - \frac{\gamma^2}{c^2}(\boldsymbol{v} \cdot \boldsymbol{a})\,\boldsymbol{v} \tag{4.5}$$

This second order differential equation ($\boldsymbol{a} = \ddot{\boldsymbol{r}}$) can be expressed as a system of 2 first order differential equations:

$$\frac{d}{dt}\begin{pmatrix}\boldsymbol{r}\\ \boldsymbol{v}\end{pmatrix} = \begin{pmatrix}\boldsymbol{v}\\ \frac{q}{\gamma m_0}(\boldsymbol{E} + \boldsymbol{v} \times \boldsymbol{B}) - \frac{\gamma^2}{c^2}(\boldsymbol{v} \cdot \boldsymbol{a})\,\boldsymbol{v}\end{pmatrix} \tag{4.6}$$

and numerically solved using the *Runge-Kutta 4* method. The acceleration on the right hand side in equation (4.6) was approximated by numerically differentiating the velocity using finite differences:

$$\boldsymbol{a}(t) \approx \frac{\boldsymbol{v}(t + \Delta t) - \boldsymbol{v}(t)}{\Delta t} \tag{4.7}$$

The *Runge-Kutta 4* is an iterative numerical integration method used for solving ODEs:

$$\frac{d}{dt}\boldsymbol{u}(t) = \boldsymbol{f}(t, \boldsymbol{u}(t)), \quad \boldsymbol{u}(t_0) = \boldsymbol{u}_0 \tag{4.8}$$

where

$$\boldsymbol{u} = \begin{pmatrix} x\\ y\\ z\\ v_x\\ v_y\\ v_z\end{pmatrix} \tag{4.9}$$

The differential equation in (4.8) is numerically solved at each step $t_{n+1} = t_n + \Delta t$ for $n = 0, 1, 2, ...$ in an iterative manner. The *Runge-Kutta 4* (RK4) approximation of $\boldsymbol{u}(t_{n+1})$ is:

$$\boldsymbol{u}(t_{n+1}) = \boldsymbol{u}(t_n) + \frac{1}{6}\Delta t \cdot (\boldsymbol{k_1} + 2\boldsymbol{k_2} + 2\boldsymbol{k_3} + \boldsymbol{k_4}) \tag{4.10}$$

with

Die approbierte gedruckte Originalversion dieser Diplomarbeit ist an der TU Wien Bibliothek verfügbar
The approved original version of this thesis is available in print at TU Wien Bibliothek.
TU Bibliothek Your knowledge hub WIEN

$$\boldsymbol{k_1} = \boldsymbol{f}(t_n, \boldsymbol{u}(t_n)) \tag{4.11}$$

$$\boldsymbol{k_2} = \boldsymbol{f}(t_n + \frac{\Delta t}{2}, \boldsymbol{u}(t_n) + \frac{\Delta t}{2}\boldsymbol{k_1}) \tag{4.12}$$

$$\boldsymbol{k_3} = \boldsymbol{f}(t_n + \frac{\Delta t}{2}, \boldsymbol{u}(t_n) + \frac{\Delta t}{2}\boldsymbol{k_2}) \tag{4.13}$$

$$\boldsymbol{k_4} = \boldsymbol{f}(t_n + \Delta t, \boldsymbol{u}(t_n) + \Delta t\, \boldsymbol{k_3}) \tag{4.14}$$

The initial condition of the velocity $\boldsymbol{v}_0$ was calculated from the beam energy E_0:

$$v = \sqrt{1 - \left(\frac{m_0 c^2}{E_0 + m_0 c^2}\right)^2} \cdot c \tag{4.15}$$

4.2.3 Results

The trajectory of a 1 MeV proton beam ($v = 0.05c$) in y-direction and perpendicular to a parallel electric and magnetic field in z-direction is shown in Figure 4.5a and Figure 4.5b for GATE and the RK4 ODE solver. A deflection in both x- and y-direction was observed with a resulting motion in z-direction. The maximum deflection in GATE was $\Delta x = 192.9\,\text{mm}$ in x-direction. A relative difference of 1.5% between the positive $\Delta y = 95.6\,\text{mm}$ and negative $\Delta y = -97.1\,\text{mm}$ maximum deflection in y-direction was encountered. A maximum deviation of less than 0.4% was observed for the maximum deflection between the two methods. The results for two different electric field strengths show that the electric field does not affect the transverse deflection as the amplitudes in both figures remain constant for $40\,\text{kV}\,\text{m}^{-1}$ and $80\,\text{kV}\,\text{m}^{-1}$, respectively. In fact, as depicted in both figures, the electric field does only affect the particles pitch, i.e., the linear distance travelled after one rotation.

The results of a 60 MeV proton beam ($v = 0.34c$) parallel to an electric field in z-direction and perpendicular to a magnetic field in y-direction is presented in Figure 4.6. A transverse deflection of $\Delta x = -114.3\,\text{mm}$ was observed for both solvers and independent of the electric field strength. In accordance with the Lorentz force, no deflection was observed in y-direction.

For this configuration, no effect of the electric field on the transverse particle trajectory was expected. Due to the acceleration of the electric field in z-direction, a rise of the kinetic energy was observed. The kinetic energy increased to 60.016 MeV for $40\,\text{kV}\,\text{m}^{-1}$ and 60.032 MeV for $80\,\text{kV}\,\text{m}^{-1}$ at $z = 400\,\text{mm}$ and was identical for both methods.

Die approbierte gedruckte Originalversion dieser Diplomarbeit ist an der TU Wien Bibliothek verfügbar
The approved original version of this thesis is available in print at TU Wien Bibliothek.
TU Bibliothek Your knowledge hub WIEN

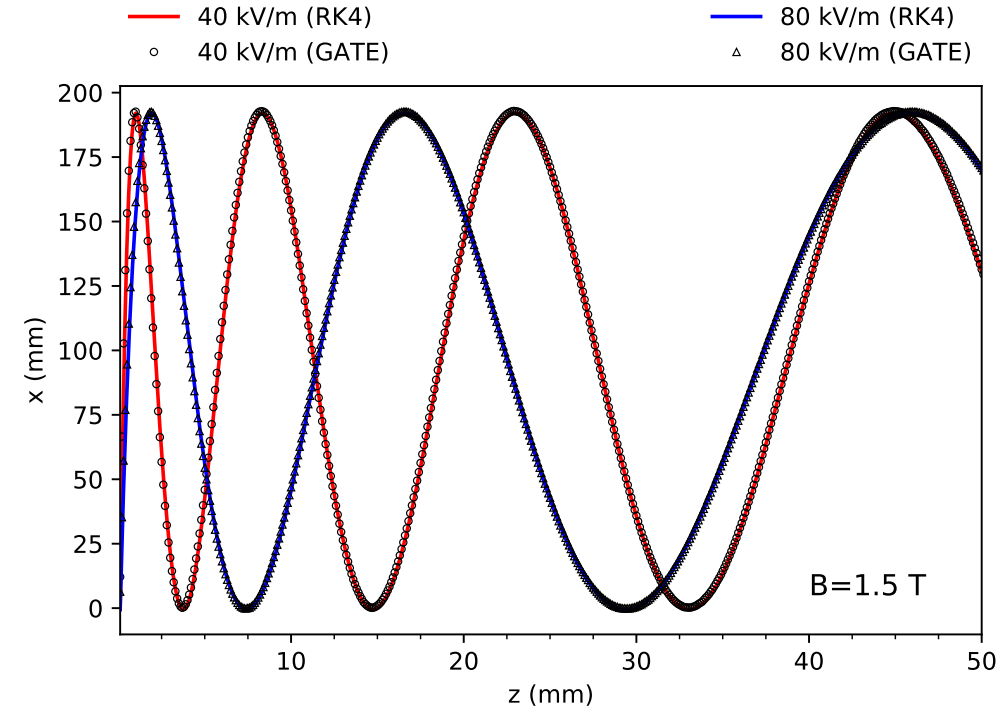

(a)

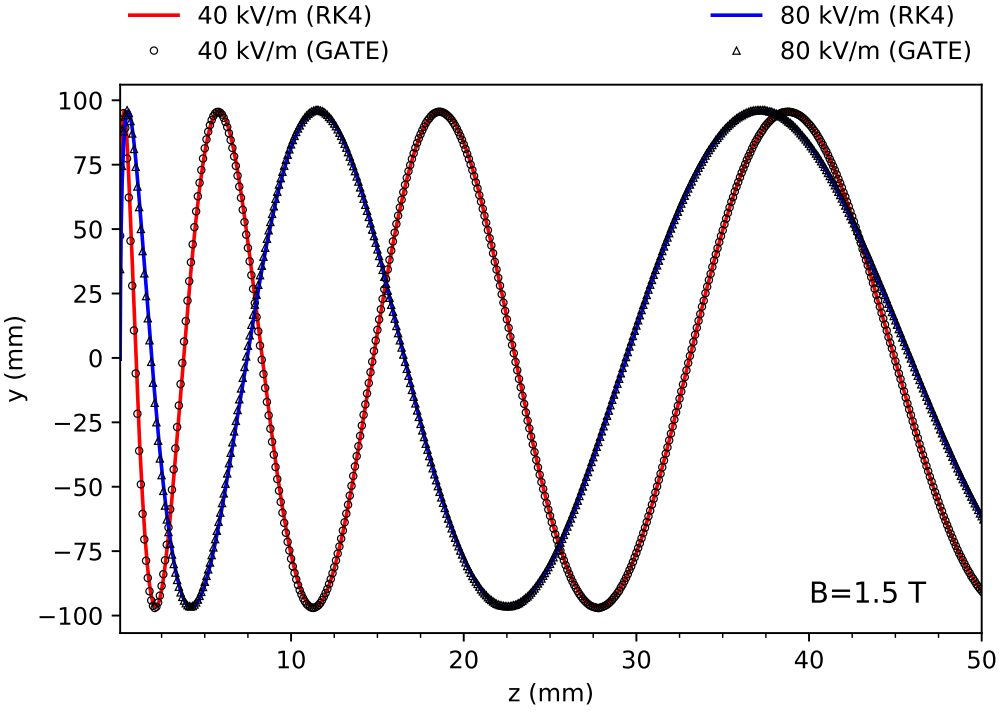

(b)

Figure 4.5: Beam deflection in x- and y-direction.

Die approbierte gedruckte Originalversion dieser Diplomarbeit ist an der TU Wien Bibliothek verfügbar
The approved original version of this thesis is available in print at TU Wien Bibliothek.

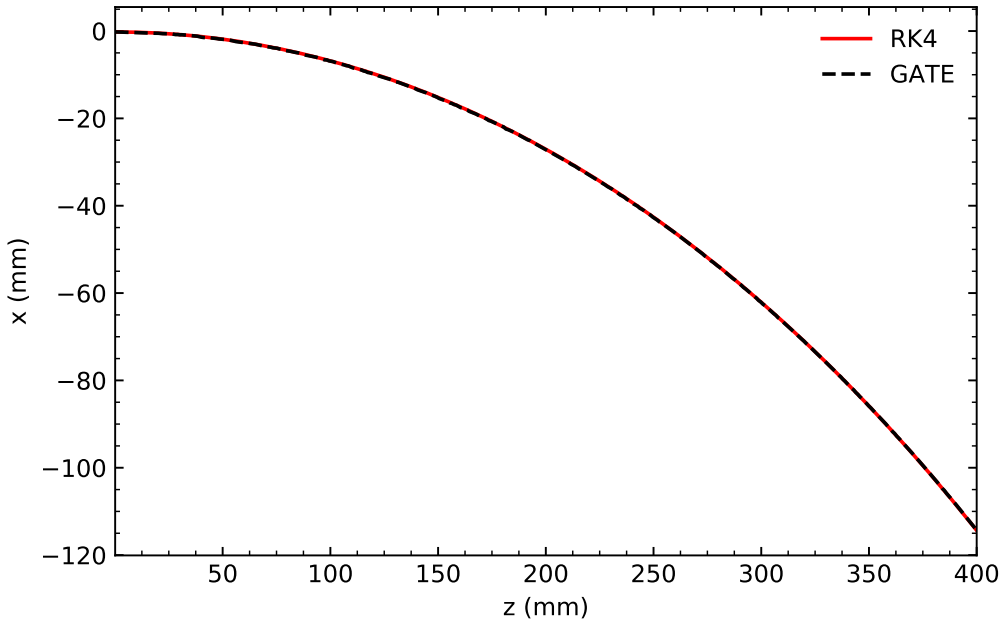

Figure 4.6: Transverse deflection of a 60 MeV proton beam in z-direction inside an electromagnetic field of $E_z = 40\,\mathrm{kV\,m^{-1}}$ and $B_y = 1.5\,\mathrm{T}$. The same deflection curve was obtained for $80\,\mathrm{kV\,m^{-1}}$.

4.2.4 Discussion

The resulting motion of 1 MeV protons perpendicular to a parallel electric and magnetic field can be explained as follows: The magnetic force is perpendicular to the velocity and forces the particles on circular paths in the xy-plane similar to a centripetal force. The electric field accelerates the particles in z-direction. Hence, the velocity of the protons increases and the distance travelled after one rotation changes. The resulting motion is a helical motion in z-direction with an increasing pitch.

In case of the higher energetic 60 MeV proton beam, the magnetic force bends the particle beam in the direction perpendicular to the initial beam axis and the magnetic field, while the applied electric field, parallel to the beam incidence direction, changes the kinetic energy of the particle.

The results of both scenarios agreed with the theoretical expectation of the Lorentz force. Although the two methods differed in their numerical implementation, the results between GATE and the RK4 ODE solver were consistent. Deviations were observed which are most likely attributed to the fitting procedure of the dose maps or numerical artifacts such as round-off errors. The RK4 ODE solver is based on single particle dynamics where the electromagnetic field is implemented as a constant value throughout the whole integration (c.f. Eq. 4.6). Hence, the deflection curves and the kinetic

Die approbierte gedruckte Originalversion dieser Diplomarbeit ist an der TU Wien Bibliothek verfügbar
The approved original version of this thesis is available in print at TU Wien Bibliothek.
TU Bibliothek Your knowledge hub WIEN

energy were directly calculated from the equation of motion. In contrast, GATE uses an electromagnetic vector field map in order to propagate particles inside the field by means of the *GetFieldValue* function, called at each integration step. It takes the spatial positions and values from an external input file, and outputs the corresponding (interpolated) field strengths over the whole custom volume. The deflection curves obtained from GATE were calculated from particle beams and are based on the energy deposition in a voxelized phantom (box). The results demonstrated that the deflection curve of a particle beam can be described by a single particle dynamics approach. Furthermore, in the non-relativistic limit both methods agreed as well.

From these results, two important conclusions can be made: (*i*) the theoretically expected physical principles are valid in our model implementation and (*ii*) the software integration in GATE is in harmony with the existing complex MC algorithm and other features.

Die approbierte gedruckte Originalversion dieser Diplomarbeit ist an der TU Wien Bibliothek verfügbar
The approved original version of this thesis is available in print at TU Wien Bibliothek.
TU Bibliothek Your knowledge hub WIEN

5 Fano cavity test

5.1 Fano cavity setup

The setup for the Fano cavity test was implemented in GATE for electrons and protons in the presence of magnetic fields. The implementation was based on the *fanoCavity2* [55] example for electrons, officially distributed with the Geant4 release v10.06.p01. However, this version does not include magnetic fields, which require additional conditions in order to ensure CPE.

5.1.1 Detector geometry

The chamber was described as a cylinder that contains a cavity inside it (see Fig. 5.1). The material of the cylinder was set to water with a density of $1\,\mathrm{g\,cm^{-3}}$. A cavity of 2 mm thickness was filled with a fictitious material, in the following referred to as gas. The gas had the same atomic composition and differential cross sections of water but a mass density of $1\,\mathrm{mg\,cm^{-3}}$. This intended to represent a real ionization chamber with a fill gas of ambient air while satisfying the conditions of CPE. The mean excitation energy of both materials were set to 78 eV. The cavity was delimited by two parallel planes that act as the wall interfaces.

A uniform magnetic field was applied to the effective simulation geometry in parallel to the central axis of the chamber using the previously implemented vector field method in GATE.

5.1.2 Reciprocity theorem and particle source

The reciprocity theorem was applied, serving as a *variance reduction technique*. It states that the absorbed dose in the detector, normalized to the number of emitted particles, is the same when a small detector is used inside a broad beam or a large detector is used inside a small beam [27]. Therefore, a uniform line source per unit mass along the central axis of the chamber was implemented. In order to comply with the Fano theorem in presence of uniform magnetic fields, all generated primary particles were emitted isotropically at every point of the line source. By choosing a chamber radius larger than the maximum range of the charged particles, the theorem holds and the geometry is identical to a plane-parallel chamber being irradiated by a laterally extended beam.

Die approbierte gedruckte Originalversion dieser Diplomarbeit ist an der TU Wien Bibliothek verfügbar
The approved original version of this thesis is available in print at TU Wien Bibliothek.
TU Bibliothek Your knowledge hub WIEN

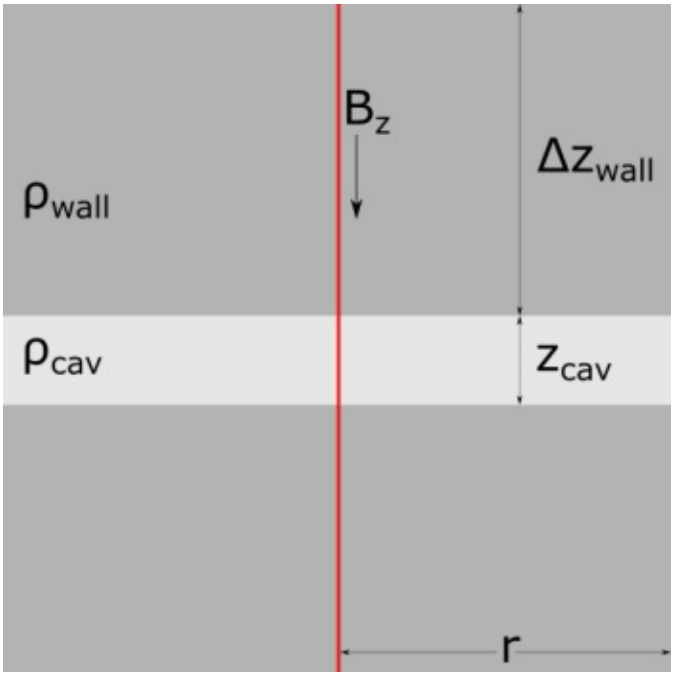

Figure 5.1: Slab geometry of an ionization chamber used for the Fano test (not to scale). The red line represents an uniform and isotropic distributed particle beam.

5.1.3 Range rejection

In addition to the reciprocal geometry, range rejection for the primary particles was applied. Thus, all particles with a negligible probability of reaching the cavity were discarded. This was achieved by defining an effective wall thickness Δz_{wall} such that no particles were generated beyond this limit:

$$\Delta z_{wall} = 1.2 \cdot R_{wall}(E_0) \tag{5.1}$$

where $R_{wall}(E_0)$ is the range of the charged particle at initial kinetic energy E_0 in the continuous slowing down approximation (CSDA). The factor of 1.2 was used to take into account the possibility that a charged particle may travel a distance beyond its CSDA range because of range straggling. Although this factor varies in literature [39, 38, 35], J. Sempau et al. [27] motivated their choice of 1.2 for electron energies higher than 0.01 MeV with the determination from depth-dose curves in graphite. They found out that only 0.1% contribute to the energy imparted beyond the corresponding extended range. Although they used graphite as a material and only electrons with energies below 20 MeV, the same value was used within this project as a rough approximation for electrons and protons in water.

The same approach was used for the calculation of the chamber radius r in order to ensure that the reciprocity theorem holds:

$$r \geq 1.2 \cdot R_{cav}(E_0) \tag{5.2}$$

Die approbierte gedruckte Originalversion dieser Diplomarbeit ist an der TU Wien Bibliothek verfügbar
The approved original version of this thesis is available in print at TU Wien Bibliothek.

where R_{cav} is the CSDA range in the cavity material.

Since this method is based on the CSDA, it was important to set the production cut values of secondary particles to infinity, thereby preventing, e.g., the explicit generation of delta rays or bremsstrahlung.

5.1.4 Density correction term

The Fano theorem requires the same stopping power in the walls and the cavity. But due to the different densities, this will not be the case, since the density correction term (c.f. Eq. 2.13) in the mean energy loss calculation (c.f. Subsec. 2.4.2) is density dependent. Therefore, the density correction term was removed from the Geant4 class *G4MollerBhabhaModel*, where the calculation of the energy loss is performed. As shown in Figure 5.2, this step can be omitted when using lower electron energies, because the density effect is a pure relativistic correction and hence becomes important only in the relativistic energy spectrum.

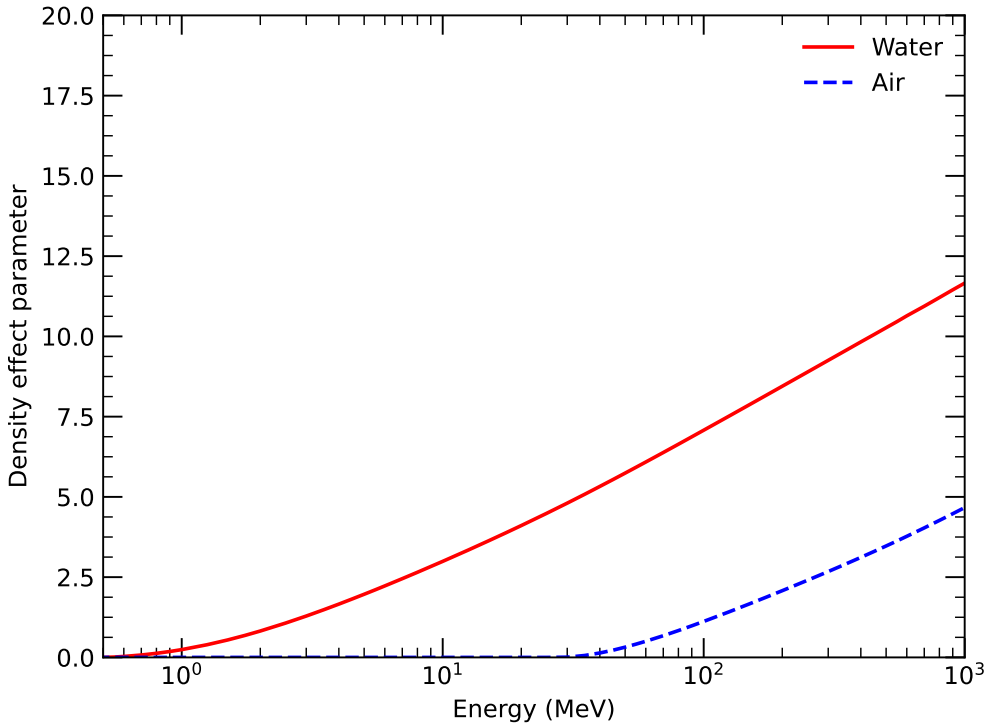

Figure 5.2: Density effect parameter for different electron energies in water and air. Numerical values were obtained from the NIST-ESTAR database [21].

The correct implementation was verified by comparing the mass stopping power in

Die approbierte gedruckte Originalversion dieser Diplomarbeit ist an der TU Wien Bibliothek verfügbar
The approved original version of this thesis is available in print at TU Wien Bibliothek.
TU Bibliothek Your knowledge hub WIEN

the walls and the cavity, expecting equal numerical values. The mass stopping power of both materials was calculated using the *EmCalculatorActor* of GATE. This actor is based on the *G4EmCalculator* class using the *ComputeElectronicDEDX* method. The calculated mass stopping power of the wall material (water) with an energy cut off value of $E_{cut} = 10\,\text{km}$ is listed in Table 5.1. The presented numerical values of the wall were identical to the mass stopping power of the cavity (air) after canceling the density correction term in the *G4MollerBhabhaModel* class.

Energy [MeV]		ρ^{-1} **dE/dx** [MeV cm^2 g^{-1}]
Electrons	0.05	6.6
	0.1	4.1
	0.5	2.0
	1	1.9
	3	2.0
	6	2.2
	20	2.8

Table 5.1: Mass stopping power for electrons (without density correction) in water.

For protons in water and air, it was not necessary to cancel the density correction term in the Bethe-Bloch formula because due to the proton's higher mass it applies only for very high energies ($E_0 \geq$ GeV) [56].

5.1.5 Electromagnetic physics constructor

In Geant4, physical processes are simulated utilizing different physics models. The user is required to build and compile his own set of models dedicated to his particular simulation problem. In newer versions, Geant4 provides pre-built validated and tested physics configurations [45]. Those configurations are summarized in *physics lists* and are developed and maintained by the Geant4 working group. Numerous physics lists exist and the application of a particular configuration may depend on the problem. Furthermore, there are many different alternative physics models (e.g. MSC can be described by different theories) available, differing in simulation performance in terms of computation time and precision.

Dedicated electromagnetic physics constructors exist for an accurate simulation of electromagnetic physical processes [46, 57, 58]. The default electromagnetic physics list is referred to as *option 0*. On top of that, different alternative physics models are implemented as required by the particular problem.

For the Fano test for electrons, primarily *option 3* and *option 4* of the electromagnetic physics constructor were used. While *option 3* represents a trade-off between accuracy and computation time, *option 4* has its focus on the best possible physics using the best set of models selected from the low energy and standard packages [59]. In the context of the Fano test, the most relevant difference between the two options is the utilization of

Die approbierte gedruckte Originalversion dieser Diplomarbeit ist an der TU Wien Bibliothek verfügbar
The approved original version of this thesis is available in print at TU Wien Bibliothek.
TU Bibliothek Your knowledge hub WIEN

different MSC models along with its step size restricting parameters. An overview of the used scattering models is presented in Table 5.2.

Model	Particle	Energy limit	Specifics and applicability
Urban	any	-	MSC Lewis theory [16] Parameterized to HEP (LHC data)
Goudsmit-Saunderson	e^+, e^-	$\leq 1\,\mathrm{GeV}$	MSC Goudsmit-Saunderson theory [60] Dedicated to electron transport
Coulomb-Scattering	any	-	Single scattering model Wentzel theory [9] Proposed to apply in low-density media (e.g., vacuum, gas)
WentzelVI	any	-	MSC for small angles Single scattering for large angles Wentzel theory [9] Focused on muons and hadrons

Table 5.2: Overview of the scattering models used within this project. Based on Geant4 v10.06 patch-01. Adapted from Geant4 working group. [61]

Option 3 (CH scheme) uses only the multiple scattering model by *Urban* [15] for all charged particles and energies, whereas *option 4* employs different models according to the particle type and energy range. Furthermore, it uses both multiple and single Coulomb scattering. For electron energies below 100 MeV, the *Goudsmit-Saunderson* MSC model (CH scheme) [61] is used and for higher energies the *WentzelVI* model (mixed scheme) [8, 9, 61] which uses a single scattering model [61] for large angle scattering (controlled by a threshold angle). The scattering of protons is performed by the *WentzelVI* model.

In some older releases of Geant4 (10.4 and older) [62], it is explicitly stated that *option 3* is designed for any applications of charged particle tracking *without* magnetic fields. However, this statement could not be found in recent releases (greater Geant4 10.5).

A comprehensive explanation of the electromagnetic physics constructor is presented in the Guide For Physics Lists and Physics Reference Manual by Geant4 [7, 59].

5.1.6 Calculation of absorbed dose

Absorbed dose D was calculated by integrating the energy deposition ε at each step in the cavity and dividing by the mass of the cavity m_{cav}:

$$D = \frac{\varepsilon}{m_{cav}} = \frac{\varepsilon}{z_{cav} \cdot \rho_{cav}} \tag{5.3}$$

where z_{cav} is the cavity thickness and ρ_{cav} the density of the cavity material.

Die approbierte gedruckte Originalversion dieser Diplomarbeit ist an der TU Wien Bibliothek verfügbar
The approved original version of this thesis is available in print at TU Wien Bibliothek.
TU Bibliothek Your knowledge hub WIEN

Furthermore, an analytical expression for the dose can be given since Fano's conditions are met. The constant number of particles per unit mass $\mathcal{I}$ is given by:

$$\mathcal{I} = \frac{N}{m_{total}} = \frac{N}{m_{cav} + m_{wall}} = \frac{N}{z_{cav} \cdot \rho_{cav} + 2 \cdot \Delta z_{wall} \cdot \rho_{wall}} \tag{5.4}$$

If the primary particles are all generated with an initial energy E_0, the conservation of energy implies:

$$D = \mathcal{I} \cdot E_0 \tag{5.5}$$

which is equivalent to the beam energy fluence. The ratio of the simulated dose and the theoretical value $D_{simulated}/D_{theory}$ was used to assess the accuracy of the MC particle transport in GATE. Hence, a numerical value of 1 for the ratio indicates a valid Fano response with a 100% transport accuracy, while deviations from 1 indicated inaccuracies of the transport algorithm.

5.1.7 Data evaluation and statistical testing

We were aiming for a Fano test in GATE, valid for all incident particle energies and magnetic field strengths, and with no significant dependency on neither of these magnitudes. Statistical analysis and tests with regard to the beam energy and the field strength were performed using Libre Office[1] (The Document Foundation, Berlin, Germany).

The *root mean square error* (RMSE) was used to quantify the deviation from the predicted value and the observed value. Statistical errors, here defined as the differences between the predicted value of 1 and the observed values, were calculated as:

$$\Delta x = x_{predicted} - x_{observed} = 1 - \frac{D_{simulated}}{D_{theory}} \tag{5.6}$$

Since the ratio of $D_{simulated}/D_{theory}$ can be either smaller or greater 1, it was practical to use the squared errors for quantification. By calculating the squared errors of each data point, i.e., for each incident beam energy and field strength, the RMSE was determined by taking the square root of the arithmetic mean of the squared errors for N beam energies or field strengths:

$$x_{RMS} = \sqrt{\frac{1}{N}\left[(\Delta x_1)^2 + (\Delta x_2)^2 + ... + (\Delta x_N)^2\right]} \tag{5.7}$$

The RMSE was used because it takes into account that negative values do not cancel the positive ones while averaging the data. Therefore, it represents an absolute measure of the magnitude of the error and can be understood as a distance between the predicted and the observed quantity.

One-way *analysis of variance* (ANOVA) was used to assess differences between different beam energies and field strengths, providing a statistical test for the quantification of the energy and magnetic field dependence on the outcome of the Fano test. ANOVA

[1] https://www.libreoffice.org

Die approbierte gedruckte Originalversion dieser Diplomarbeit ist an der TU Wien Bibliothek verfügbar
The approved original version of this thesis is available in print at TU Wien Bibliothek.

is statistical test used to determine if multiple groups statistically differ from each other (induced by systematic factors) or not (induced by random factors). ANOVA was calculated from the squared errors of each data point where the one independent variable was either the beam energy or the magnetic field strength. It assumes normally distributed data, homogeneity of variance (approximately equal variances among the groups) and independent observations. These assumptions were considered and ensured prior to statistical testing.

5.2 Fano test for electrons

Secondary electrons are one of the main contributors to the total dose deposition in ion beam therapy. It was shown [63, 64], that a magnetic field can cause significant dose deposition modifications in homogeneous materials, as well as at the boundaries between two materials with varying densities which is known as the *electron return effect*. To account and compensate for these dosimetric effects, a reliable MC electron transport code inside a magnetic field is required.

In this chapter, the results of the Fano test for electrons in the presence of a magnetic field are presented. In Subsection 5.2.1, an overview of the MC model is given and simulation details are described. Thereafter, the results for different electromagnetic physics lists and step sizes are presented. The results of the simulations are discussed and compared to literature in Subsection 5.2.3.

5.2.1 Simulation

Electrons with initial kinetic energies of E_0 = 0.05, 0.1, 0.5, 1, 3, 6 and 20 MeV were simulated. The energy range is based on the secondary electron energy spectrum for clinically relevant photon and proton beams. In a first step, the CSDA ranges of the electrons were calculated using the *G4EmCalculator* class and its *GetCSDARange* method. Since the density of the gas is 0.001 times the density of water, the range in the cavity could be easily calculated by multiplying the range in the wall with 1000. The calculated ranges are shown in Table 5.3.

Energy [MeV]	**Range wall** [cm]	**Range cavity** [cm]
0.05	4.35×10^{-3}	4.35
0.1	1.44×10^{-2}	14.4
0.5	1.78×10^{-1}	178
1	4.39×10^{-1}	439
3	1.50	1500
6	2.97	2970
20	9.15	9150

Table 5.3: Calculated CSDA ranges of the primary electrons in water and gas.

Die approbierte gedruckte Originalversion dieser Diplomarbeit ist an der TU Wien Bibliothek verfügbar
The approved original version of this thesis is available in print at TU Wien Bibliothek.
TU Bibliothek Your knowledge hub WIEN

From the CSDA ranges in the wall and cavity, the dimensions of the effective simulation geometry, displayed in Table 5.4, were further calculated. The dimension of the world was set to 2 times the chamber radius r in all directions. A uniform magnetic field of $B = 0.35,\ 0.5,\ 1,\ 1.5$ and $3\,\mathrm{T}$ was applied to the effective simulation geometry using custom vector field maps generated in Python. These field strengths are typically used in conventional MR scanners for routine clinical use. Since the grid size of the vector field does not affect the linear interpolation between to points (uniform field), it was chosen to be feasible in terms of reading time and file size.

Energy [MeV]	**Chamber radius** [cm]	**Wall thickness** [cm]	**Cavity thickness** [cm]
0.05	5.22	5.22×10^{-3}	0.2
0.1	17.30	1.73×10^{-2}	0.2
0.5	213	2.13×10^{-1}	0.2
1	527	5.27×10^{-1}	0.2
3	1790	1.79	0.2
6	3570	3.57	0.2
20	10980	10.98	0.2

Table 5.4: Physical dimensions of the ionization chamber for different electron energies.

Electromagnetic physical processes were simulated using *option 3* and *option 4* of the physics constructors of Geant4. A summary of the used settings for the Fano test for electrons is presented in Table 5.5. In order to prevent the explicit generation of secondary particles and bremsstrahlung, the tracking cutoff for electrons, positrons and gammas was set to 10 km, ensuring that their energies are deposited locally.

The energy deposition in the cavity was scored using GATE's *DoseActor* with an isotropic resolution of 1 voxel and stored randomly distributed along the line of each step. Phase space actors were applied to both sides of the cavity to retrieve information about the particles entering and leaving the volume. The kinetic energy and production volume of each particle was saved in phase space files. The phase space file of the entrance was parsed as follows: all particles produced in wall 1 were scored as particles entering the cavity and the energy spectrum of those particles was integrated to obtain the total incoming energy flux. The phase space file of the outgoing particles was parsed in a similar way: particles produced in wall 1 or the cavity were scored. Furthermore, all particles produced only in the cavity were scored. The number of particles entering and leaving the cavity as well as the energy flux were compared to analyze the condition of CPE. Deviations of those values would indicate CPE violations.

Die approbierte gedruckte Originalversion dieser Diplomarbeit ist an der TU Wien Bibliothek verfügbar
The approved original version of this thesis is available in print at TU Wien Bibliothek.
TU Bibliothek Your knowledge hub WIEN

Simulation settings		
Mean excitation energy	Water	78 eV
	Water gas	78 eV
Density	Water	$1\,\mathrm{g\,cm^{-3}}$
	Water gas	$1\,\mathrm{mg\,cm^{-3}}$
Production cuts (γ, e^-, e^+)	World	10 km
	Wall	10 km
	Cavity	10 km
Maximum step size	World	1 mm
	Wall	0.1 mm
	Cavity	0.1 mm
Magnetic field	Integrator stepper	ClassicalRK4
	Delta chord	1 µm
	Delta intersection	1 nm
	Delta one step	1 nm
	Epsilon min	10^{-11}
	Epsilon max	10^{-10}
	Step minimum	1 µm
Physics list	option 3	
	option 4	

Table 5.5: GATE simulation settings used for the Fano test.

The electron source must be homogeneous, meaning that the number of particles per unit mass is uniform. Hence, the generation of electrons in each region of the chamber was weighted by its correspondent density. Using several sources, GATE provides a functionality to define the priorities of the added sources. An intensity can be applied to each source which is taken into account before a source is randomly selected at each event. The intensities were calculated from the ratio of the mass densities. The source intensities for 0.05 and 0.1 MeV were $wall : cavity = 10 : 0.2$ and 10:0.1 respectively, with negligible differences for higher energies.

The Mersenne Twister pseudo random number generator was used. The engine seed was set to automatic ensuring that a new seed was automatically generated each time a new run is started in GATE. The total number of primary particles was set to 10^8 electrons, unless otherwise explicitly stated.

5.2.2 Results

In the following figures, unless otherwise explicitly mentioned, the error bars represent a 1σ relative statistical uncertainty, based on the number of electrons entering the cavity. The light red shaded area represents a 0.1% deviation from the expected theoretical result, depicted as a continuous red line in all following figures.

Figure 5.3a shows the results of the Fano cavity test for electrons using *option 3*.

Die approbierte gedruckte Originalversion dieser Diplomarbeit ist an der TU Wien Bibliothek verfügbar
The approved original version of this thesis is available in print at TU Wien Bibliothek.

The ratio of the absorbed dose in the cavity and the theoretical value was calculated for different magnetic field strengths and initial energies within an uncertainty of less than 0.4%. For 0.5 and 1 MeV electrons, differences up to 3.9 % ($B = 0\,\mathrm{T}$) and 4.1% ($B > 0\,\mathrm{T}$) were observed. Even higher deviations were obtained for electrons with 0.05 and 0.1 MeV. The maximum difference for those beam energies were 5.8% for $B \geq 0\,\mathrm{T}$. Smaller deviations were observed towards higher beam energies. Electrons with 20 MeV achieved less than 1% deviation, except for $B = 0\,\mathrm{T}$ (1.2%). Throughout all energies and field strengths, no simulation passed the Fano test with less than 0.5% difference.

The results of the Fano test utilizing *option 4* are shown in Figure 5.3b with an uncertainty of less than 0.4%. The maximum relative difference for electrons with 0.05 and 0.1 MeV was 4.8% ($B = 0\,\mathrm{T}$) 4.9% ($B > 0\,\mathrm{T}$). Electrons within 0.5-20 MeV showed deviations less than 0.3% ($B = 0\,\mathrm{T}$) and 0.6% ($B > 0\,\mathrm{T}$).

The RMSE are presented in Table 5.6 for both physics lists. The outcome of the ANOVA was $p = 0$ (*option 3*) and $p = 0.38$ (*option 4*) for energies above 0.1 MeV at a 5% significance level ($\alpha = 0.05$). The energies 0.05 MeV and 0.1 MeV were excluded in the ANOVA, because the homogeneity of the variance could not be longer assumed. The squared errors for those energies were significantly higher compared to the rest of the energies as one can see in Figure 5.3a and 5.3b or in the RMSE in Table 5.6. The p-value with regard to the magnetic field strengths was for both physics lists $p = 1$ at a 5% significance level.

Die approbierte gedruckte Originalversion dieser Diplomarbeit ist an der TU Wien Bibliothek verfügbar
The approved original version of this thesis is available in print at TU Wien Bibliothek.
TU Bibliothek Your knowledge hub WIEN

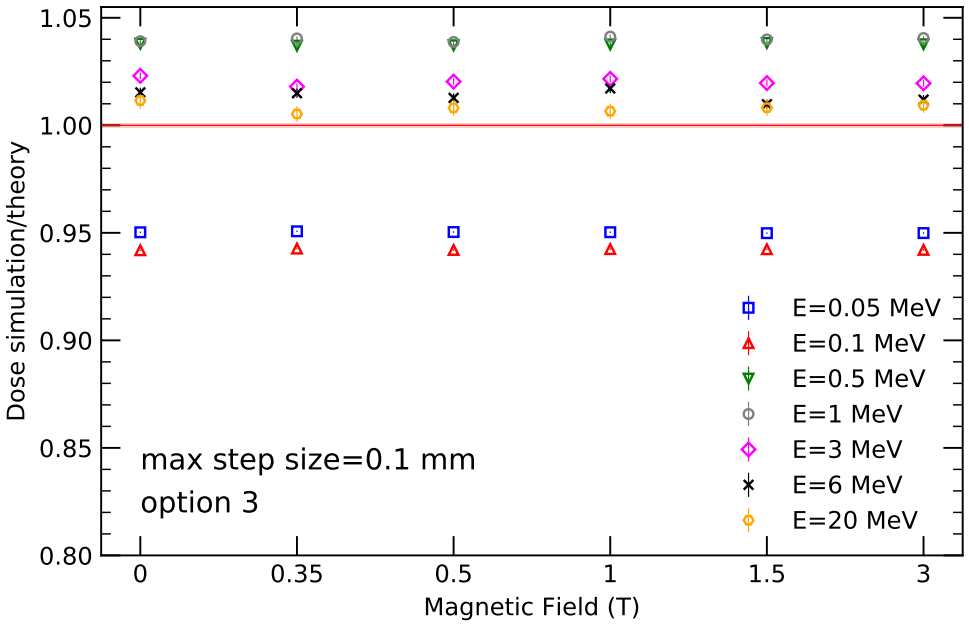

(a) Urban MSC model (*option 3*). Numerical values are listed in Appendix Table A.1.

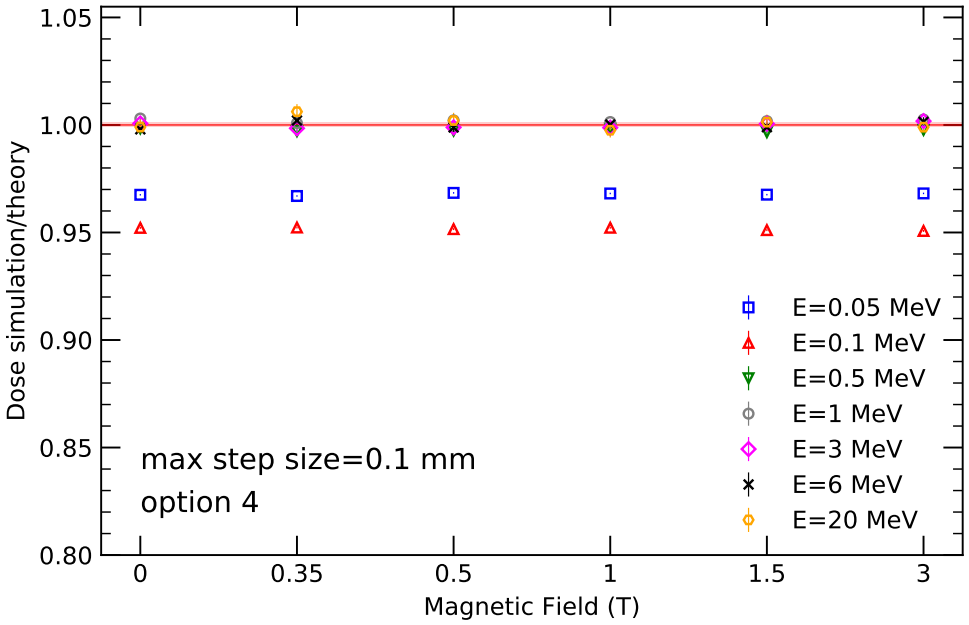

(b) Goudsmit-Saunderson MSC model (*option 4*). Numerical values are listed in Appendix Table A.2.

Figure 5.3: Comparison of electromagnetic physics lists with a *step size* of 0.1 mm.

Die approbierte gedruckte Originalversion dieser Diplomarbeit ist an der TU Wien Bibliothek verfügbar
The approved original version of this thesis is available in print at TU Wien Bibliothek.
TU Bibliothek Your knowledge hub WIEN

Root mean square error		option 3	option 4
Magnetic Field [T]	0	3.73×10^{-2}	2.61×10^{-2}
	0.35	3.64×10^{-2}	2.61×10^{-2}
	0.5	3.65×10^{-2}	2.61×10^{-2}
	1	3.72×10^{-2}	2.59×10^{-2}
	1.5	3.67×10^{-2}	2.65×10^{-2}
	3	3.69×10^{-2}	2.65×10^{-2}
Energy [MeV]	0.05	4.98×10^{-2}	3.22×10^{-2}
	0.1	5.77×10^{-2}	4.83×10^{-2}
	0.5	3.76×10^{-2}	2.50×10^{-3}
	1	4.00×10^{-2}	2.10×10^{-3}
	3	2.04×10^{-2}	1.20×10^{-3}
	6	1.38×10^{-2}	1.50×10^{-3}
	20	8.40×10^{-3}	3.00×10^{-3}

Table 5.6: RMSE calculated from the means of the squared errors for different electron energies and magnetic field strengths.

Step size restrictions

The dependency of the Fano cavity test with the step size was investigated by limiting the transport parameter maximum *step size* to smaller values. The results are shown in Figure 5.4a and 5.4b for lower energy electrons (0.05 and 0.1 MeV) and two physics lists (*option 3*, *option 4*). The implementation of a 0.1 µm maximum *step size* led to a relative difference from the theoretical value of 3.1% (*option 3*) and 2.1% (*option 4*) for 0.05 MeV electrons. Using *option 3*, the relative differences increased towards smaller *step sizes* reaching its maximum at 0.01 mm and decreased beyond that limit. A similar behaviour for *option 4* was observed, whereas the deviation did not decreased, but rather stayed constant until 0.01 mm. Similar results were obtained for 0.1 MeV electrons. Deviations higher than 4% and almost constant were noticed with decreasing maximum *step sizes*.

Die approbierte gedruckte Originalversion dieser Diplomarbeit ist an der TU Wien Bibliothek verfügbar
The approved original version of this thesis is available in print at TU Wien Bibliothek.
TU Bibliothek Your knowledge hub WIEN

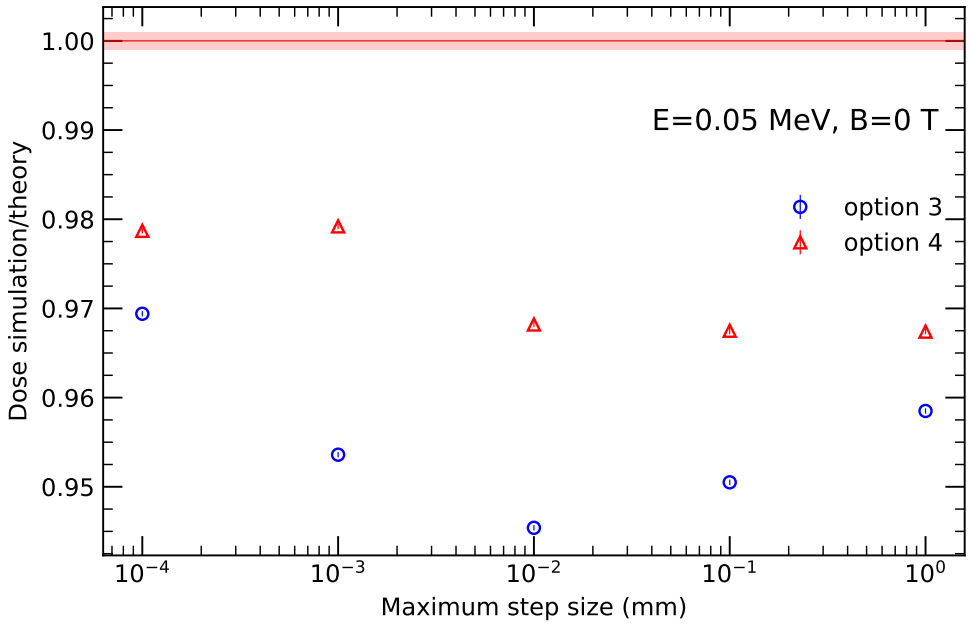

(a) $E_0 = 0.05\,\mathrm{MeV}$

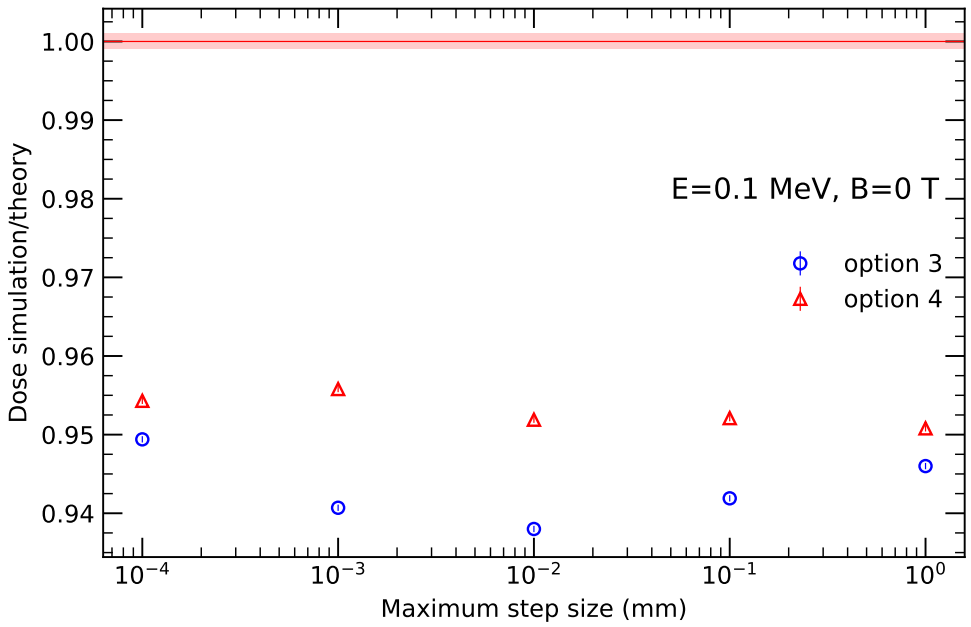

(b) $E_0 = 0.1\,\mathrm{MeV}$

Figure 5.4: Simulated dose per energy fluence of an electron beam for different *step sizes* utilizing *option 3* and *option 4*. Numerical values are listed in Appendix D.

Die approbierte gedruckte Originalversion dieser Diplomarbeit ist an der TU Wien Bibliothek verfügbar
The approved original version of this thesis is available in print at TU Wien Bibliothek.
TU Bibliothek Your knowledge hub WIEN

Further *step size* decreasing down to 1 nm and two more physics lists were applied to cross validate the low energy results against other models. The *em Low EP* and *em SS* (single scattering, c.f. Tab. 5.2) physics lists were additionally employed. The *em Low EP* is a dedicated low energy model on top of the Livermore physics for electron transport [7, 59]. Due to the remarkable increase in calculation time, the number of primary particles was adjusted to 10^6 and all runs were performed for 0.05 MeV and $B = 0$ T only. The results are summarized in Table 5.7. No significant improvements were obtained compared to the baseline simulation with a *step size* of 0.1 mm and *option 4*.

	option 4	**em SS**	**em Low EP**
10 nm	0.9772 (0.0033)	0.9748 (0.0033)	0.9744 (0.0033)
1 nm	0.9668 (0.0033)	0.9684 (0.0032)	0.9654 (0.0033)

Table 5.7: Fano cavity response of an 0.05 MeV electron beam for step lengths in the nanometer range. Conducted with 10^6 primary particles.

Different *step sizes* for 1 MeV electrons were applied in order to investigate if the results obtained with *option 3* and a *step size* of 0.1 mm (see Fig. 5.3a) could be improved. The results are shown in Figure 5.5 for the Fano cavity response. The deviation from the theoretical value significantly decreased with smaller *step sizes*. Results within a 0.1% deviation were obtained for a maximum *step size* of 1 µm and $B = 0$, 1, 3 T.

Die approbierte gedruckte Originalversion dieser Diplomarbeit ist an der TU Wien Bibliothek verfügbar
The approved original version of this thesis is available in print at TU Wien Bibliothek.
TU Bibliothek Your knowledge hub WIEN

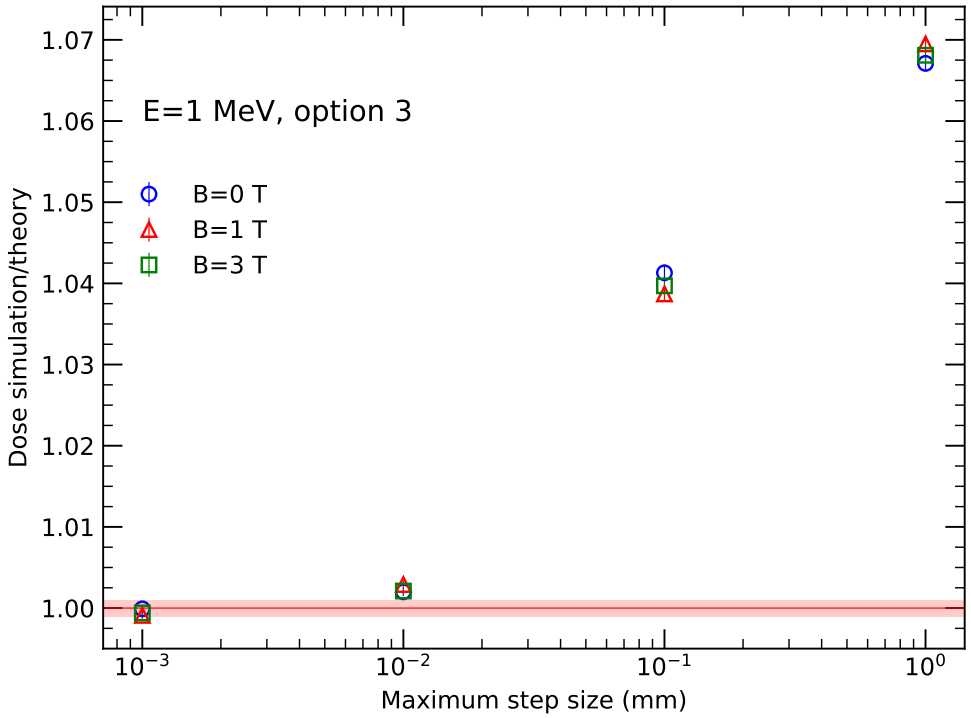

Figure 5.5: Simulated dose per energy fluence of an 1 MeV electron beam for different *step sizes* employing *option 3*. Numerical values are listed in Appendix D.

Based on the results for 1 MeV electrons, a subsequent run for 0.5, 3 and 6 MeV was conducted using a maximum *step size* of 1 µm and *option 3*. Since the previous results showed no dependence on the magnetic field strength, the simulations were performed for one configuration only. The magnetic field was set to zero, thus accelerating the already time-consuming simulations. The results are depicted in Figure 5.6. The significant *step size* reduction resulted in 0.1% deviations for energies above 1 MeV. The computation time increased by a factor of 44 (0.5 MeV), 53 (1 MeV), 63 (3 MeV) and 66 (6 MeV). Hence, no run for 20 MeV electrons was performed.

Die approbierte gedruckte Originalversion dieser Diplomarbeit ist an der TU Wien Bibliothek verfügbar
The approved original version of this thesis is available in print at TU Wien Bibliothek.
TU Bibliothek Your knowledge hub WIEN

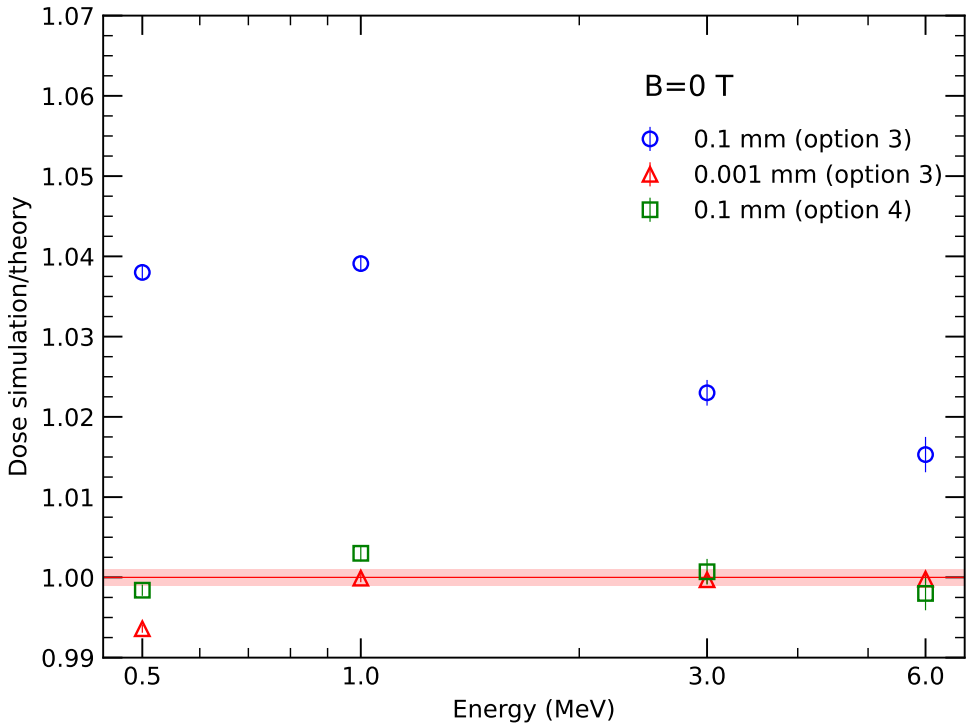

Figure 5.6: Comparison of *option 3* and *option 4* utilizing different *step sizes*. Comparable Fano responses for *option 3* were only obtained for a 100 times smaller *step size* and at the cost of increased calculation time. Numerical values are listed in Appendix D.

Figure 5.6 shows that comparable accuracies between *option 3* and *option 4* could only be achieved by reducing the *step size* from 0.1 mm to 0.001 mm. A drawback of decreasing the *step size* in our calculations is the resulting increased calculation time. Figure 5.7 shows the calculation times of Figure 5.4a, 5.4b and 5.5 as a function of the *step size* for *option 3*. An exponential increase of the calculation time with decreasing *step sizes* was observed, independent of the magnetic field strength. The rate of increase depended on the incident energy of the electrons. The same exponential relationship was observed for 0.05 MeV and 0.1 MeV electrons using *option 4*.

Die approbierte gedruckte Originalversion dieser Diplomarbeit ist an der TU Wien Bibliothek verfügbar
The approved original version of this thesis is available in print at TU Wien Bibliothek.
TU Bibliothek Your knowledge hub WIEN

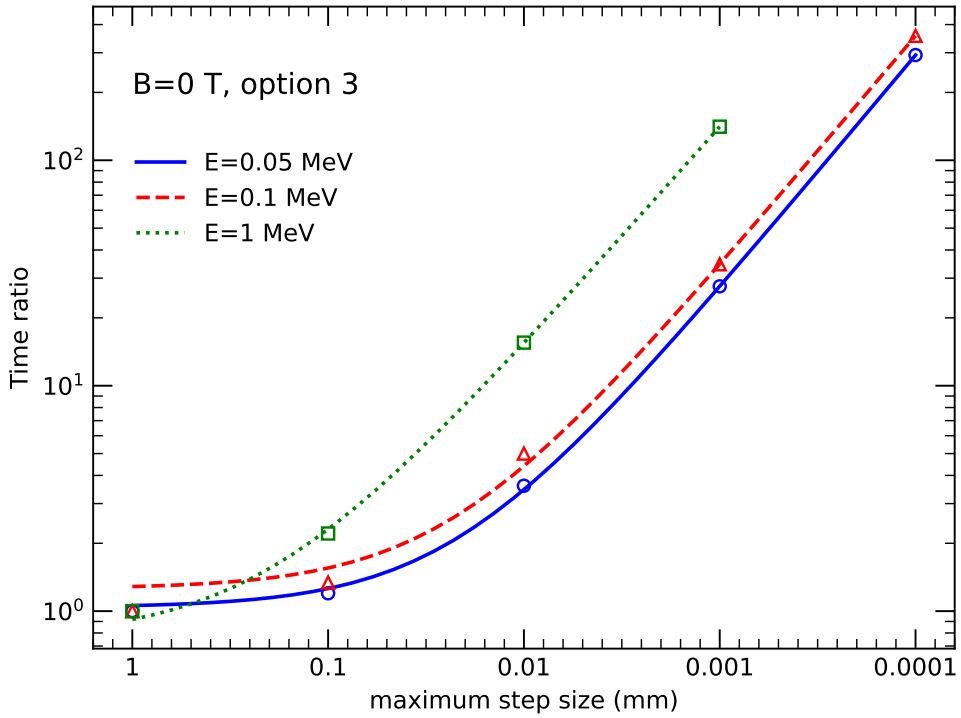

Figure 5.7: The computation time increased exponentially with smaller *step sizes*. The time ratio is based on the calculation time with 1 mm.

5.2.3 Discussion

Differences in the accuracy of the electron transport algorithm were observed using different physics lists in GATE. Calculations using the *Urban* MSC model (*option 3*) were not capable of passing the Fano test with an acceptable accuracy for a maximum *step size* of 0.1 mm. Moreover, the model showed a strong dependence of the Fano cavity test on the energies of the particle beam. Deviations from the expected theoretical value increased considerably towards lower energies. The best result (less than 1% deviation) with this configuration was obtained for 20 MeV electrons. This is in accordance with previous results from the Geant4 working group [61], who achieved a simulation precision of 1% in their dedicated validation experiments, i.e., MC production for LHC experiments.

The implementation of strict *step size* limitations in GATE (≤ 0.01 mm) yielded more accurate results but at the cost of increased computation time. The Fano test for electron energies between 1-6 MeV passed within 0.1% precision for a maximum *step size* of 1 µm.

The *Goudsmit-Saunderson* model of *option 4* showed overall better agreement with theory. For electron energies higher than 0.05 MeV, the Fano cavity response was within 0.6% and less. For those energies, no energy dependence of the model was found using

Die approbierte gedruckte Originalversion dieser Diplomarbeit ist an der TU Wien Bibliothek verfügbar
The approved original version of this thesis is available in print at TU Wien Bibliothek.
TU Bibliothek Your knowledge hub WIEN

a statistical test, which was not the case for *option 3*. However, both models exhibit a lack of convergence and accuracy in the low energy ($\leq 100\,\mathrm{keV}$) electron transport, even for strict *step size* limitations (down to 1 nm).

In general, the calculation time was depending on the electron energy and the magnetic field strength when using a fixed *step size*. Within our calculations, negligible differences in the calculation times were observed between *option 3* and *option 4*. However, it must be considered that for the Fano test production cuts were set to infinity and therefore no secondary particles were produced. This is affecting the calculation time since no secondaries must be further tracked within in the geometry. A crucial difference in the calculation time for both models will most likely be observed in a properly configured MC simulation. V. Ivanchenko et al. discussed the trade of precision versus performance of both models but with focus on LHC detector simulations, i.e., high energies, and reported an increase of calculation time by a factor of about 2 using *option 4* [61].

To our knowledge, the Fano test for electrons in the presence of a magnetic field was conducted for the first time in GATE. However, since GATE is a Geant4 application using the same transportation process and MSC models, the results can be compared with studies of the Fano test in Geant4. In general, previous studies revealed that for an accurate electron transport severely restrictions of transport parameters were necessary which can be cumbersome and time intensive [36, 38, 39, 65]. Those include the step function, magnetic field and MSC model. This is consistent with the results obtained in this work. However, only minor adjustments of user-accessible transport parameters within GATE were applied. *Step size* control in GATE is handled by a single parameter (maximum *step size*) and magnetic field parameters can be easily changed using the macro commands mentioned in Chapter 4.1.2. This reduces the complexity of the simulation process and allows user-friendly adjustments for higher accuracy.

In this study, the influence of the magnetic field strength on the Fano cavity response was found to be negligible. The charged particle propagation inside custom electromagnetic vector field maps were implemented in GATE within this project. The correctness of the implementation is confirmed by the independence of the Fano test with the magnetic field strength.

Based on the results of this work, the electromagnetic standard *option 4* is more suitable for simulating ionization chamber responses in GATE. The simulation accuracy is considerably higher compared to *option 3* using the same *step size*. The *Goudsmit-Saunderson* MSC model is supposed to perform on accuracy levels of dedicated well established models from PENELOPE and EGSnrc and is based on the same theory [61].

For the low electron energy spectrum, it is not useful to further reduce the maximum *step size* in GATE. The results of this work showed no significant improvement in the detector response but an exponential growth in calculation time. J. Lee et al. [39] and Simiele et al. [38] achieved results for 0.01 and 0.1 MeV electrons of 1.7% and 0.2% deviation from the theoretical Fano response for their particular setup using Geant4. However, they did major parameter adjustments in the step function and the boundary crossing algorithm of the MSC models. It should be analyzed if GATE is capable of passing the Fano test for comparable low energies by only using the dedicated parameters mentioned before, i.e., maximum *step size* and magnetic field parameters. Otherwise, it

Die approbierte gedruckte Originalversion dieser Diplomarbeit ist an der TU Wien Bibliothek verfügbar
The approved original version of this thesis is available in print at TU Wien Bibliothek.
TU Bibliothek Your knowledge hub WIEN

will be necessary to extend GATE to make the parameters of, e.g., the MSC model, user accessible. Nevertheless, it should be kept in mind that (*i*) the calculation time drastically increases and (*ii*) that too short step lengths might affect the MSC approximations.

5.3 Fano test for protons

These days, particle therapy facilities primarily use proton beams for patient treatment. The main advantage of protons is their improved physical selectivity compared to electrons or photons while having similar radiobiological characteristics. This chapter investigates the proton MC transport algorithm inside a magnetic field. The employed simulation model is mostly the same as for electrons in Section 5.2. However, clinical protons have significant higher ranges in water compared with secondary electrons, which requires different dimensions of the chamber geometry in order to fulfil Fano's conditions. Similar to the previous chapter, first the necessary calculations and simulation details are described. Then, the simulation results are presented and discussed.

5.3.1 Simulation

Protons in the clinically relevant energy range of 60-250 MeV were simulated in GATE. The same magnetic field strengths were used as for electrons. The CSDA ranges for protons in water and gas are listed in Table 5.8.

Energy [MeV]	**Range wall** [cm]	**Range cavity** [cm]
60	3.11	3.11×10^3
90	6.43	6.43×10^3
120	10.71	10.71×10^3
150	15.85	15.85×10^3
180	21.75	21.75×10^3
220	30.69	30.69×10^3
250	38.1	38.1×10^3

Table 5.8: Calculated CSDA ranges of the primary protons in water and gas.

The effective chamber geometry was further calculated from the ranges of the protons and are shown in Table 5.9. The magnetic vector field maps were adapted to the new geometry. In general, the same simulation settings were used as for electrons, displayed in Table 5.5. However, all simulations were performed using the electromagnetic physics list *option 4*, because it showed better agreement in the results for electrons compared to *option 3*. Moreover, as it was shown in [61], the performance is competitive with *option 3* and the mixed scheme of the *WentzelVI* model describes better the tail of the MSC distribution compared to the *Urban* MSC model of *option 3*.

Die approbierte gedruckte Originalversion dieser Diplomarbeit ist an der TU Wien Bibliothek verfügbar
The approved original version of this thesis is available in print at TU Wien Bibliothek.
TU Bibliothek Your knowledge hub WIEN

Energy [MeV]	**Chamber radius** [cm]	**Wall thickness** [cm]	**Cavity thickness** [cm]
60	3.73×10^3	3.73	0.2
90	7.71×10^3	7.71	0.2
120	12.85×10^3	12.85	0.2
150	19.02×10^3	19.02	0.2
180	26.1×10^3	26.1	0.2
220	36.82×10^3	36.82	0.2
250	45.72×10^3	45.72	0.2

Table 5.9: Physical dimensions of the ionization chamber for different proton energies.

Since the mass of the wall and the cavity depends on the CSDA range of the particles, the source intensities were also calculated for protons, but it was found that the mass and source intensity differences were negligible in that energy range.

If not explicitly mentioned, all simulations were performed with 10^8 particles using the Mersenne Twister random number generator.

5.3.2 Results

Similar to Subsection 5.2.2, the error bars represent a 1σ relative statistical uncertainty based on the number of protons entering the cavity. The red shaded area indicates a 0.1% deviation from the expected theoretical value in all following figures.

The ratios of the simulated absorbed dose in the cavity and the theoretical value for seven beam energies and six magnetic field strengths are presented in Figure 5.8 with statistical uncertainties of less than 0.1%. Relative differences were smaller than 0.2% ($B = 0\,\mathrm{T}$) and 0.3% ($B > 0\,\mathrm{T}$). Higher deviations up to 0.3% were only observed for 60 MeV protons.

Die approbierte gedruckte Originalversion dieser Diplomarbeit ist an der TU Wien Bibliothek verfügbar
The approved original version of this thesis is available in print at TU Wien Bibliothek.
TU Bibliothek Your knowledge hub WIEN

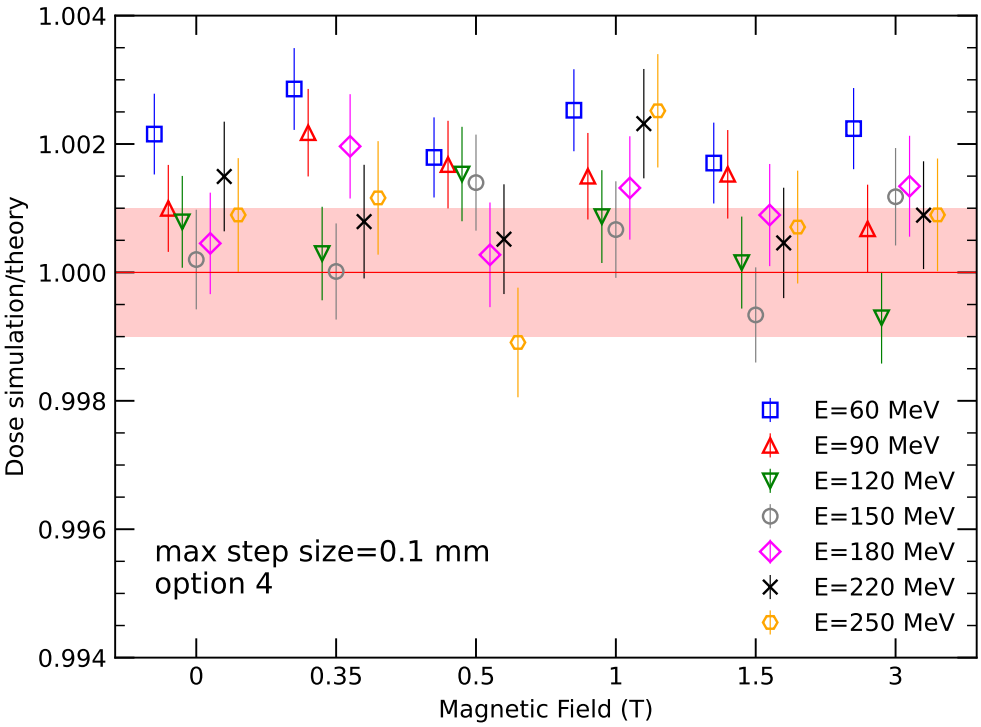

Figure 5.8: Simulated dose per energy fluence of a proton beam for different magnetic field strengths utilizing *option 4* with a step size of 0.1 mm. The data points for each magnetic field strength were shifted for a better distinguishability. Numerical values are listed in Appendix Table B.1.

Using a similar statistical analysis, as previously presented for electrons, results from the RMSE for different energies and field strengths are shown in Table 5.10. The maximum RMSE was obtained for protons with 60 MeV. The outcome of the ANOVA with regard to the beam energy was $p = 0$ at the 5% significance level and respectively $p = 0.27$ with regard to the magnetic field strength. Excluding the 60 MeV protons from the ANOVA, resulted in $p = 0.46$ at a 5% significance level for the group means of the beam energies.

For the lowest energy protons (60 MeV), a subsequent simulation with a restricted maximum *step size* of 0.01 mm and $B = 0$ T resulted in a cavity response of 1.0011 (0.0006), corresponding to a deviation of 0.1% from the expected theoretical value.

Die approbierte gedruckte Originalversion dieser Diplomarbeit ist an der TU Wien Bibliothek verfügbar
The approved original version of this thesis is available in print at TU Wien Bibliothek.
TU Bibliothek Your knowledge hub WIEN

Root mean square error		option 4
Magnetic Field [T]	0	1.2×10^{-3}
	0.35	1.7×10^{-3}
	0.5	1.3×10^{-3}
	1	1.8×10^{-3}
	1.5	1.0×10^{-3}
	3	1.2×10^{-3}
Energy [MeV]	60	2.3×10^{-3}
	90	1.5×10^{-3}
	120	8.0×10^{-4}
	150	9.0×10^{-4}
	180	1.2×10^{-3}
	220	1.3×10^{-3}
	250	1.4×10^{-3}

Table 5.10: RMSE calculated from the means of the squared errors for different proton energies and magnetic field strengths.

Remaining range in water

Lower proton energies and $B = 0\,\mathrm{T}$ were simulated to compare the Fano cavity response of protons with electrons using the remaining range in water as common axis. The results are depicted in Figure 5.9. The detector response is within 0.1% deviation from the theoretical value for protons with 20-90 MeV, while the relative deviation increases for 3 MeV and 12.5 MeV to 0.5% and 0.6% respectively. As expected, highest deviations up to 7.7% from the theoretical values were obtained for lowest energy protons.

The restriction to a maximum *step size* of 10 nm and the employment of a single scattering model (*em SS*) and the *Urban* MSC model (*option 3*) did not improve the Fano cavity response. The results are listed in Table 5.11.

	option 4	**option 3**	**em SS**
10 nm	0.9207 (0.0029)	0.9174 (0.0029)	0.9153 (0.0029)

Table 5.11: Fano cavity response of a 1.5 MeV proton beam using different physics lists with a 10 nm *step size*. Conducted with 10^6 primary particles.

Die approbierte gedruckte Originalversion dieser Diplomarbeit ist an der TU Wien Bibliothek verfügbar
The approved original version of this thesis is available in print at TU Wien Bibliothek.
TU Bibliothek Your knowledge hub WIEN

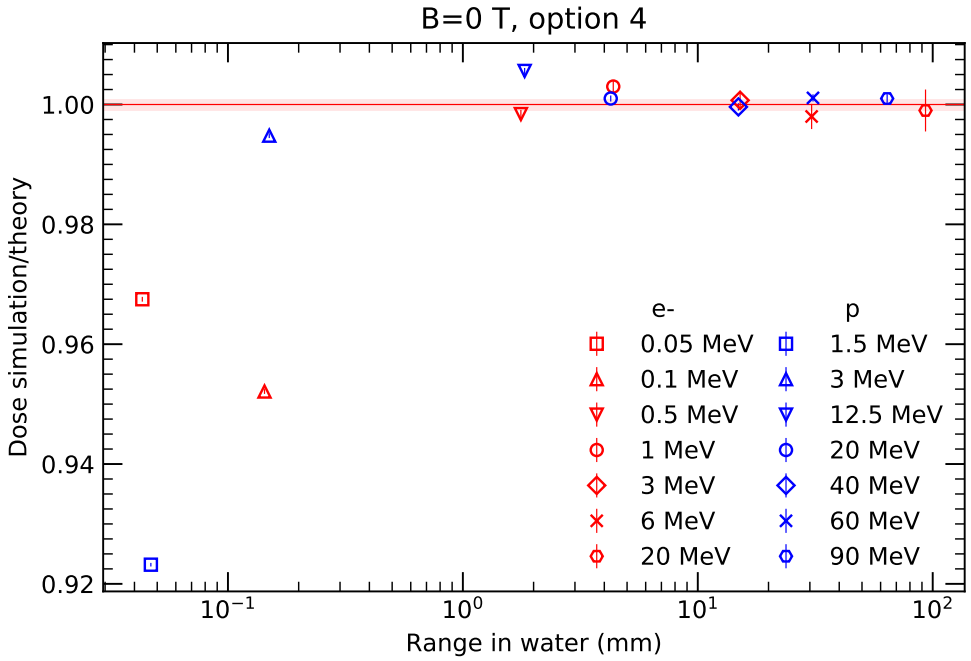

Figure 5.9: Comparison of Fano cavity responses for electrons and protons utilizing *option 4*. Simulations were performed with a maximum *step size* of 0.1 mm for all electron energies and protons with 90 MeV, and 0.01 mm for protons with 1.5-60 MeV. Numerical values are listed in Appendix Table C.1 (electrons) and Table C.2 (protons).

5.3.3 Discussion

Higher discrepancies between the simulated dose and the analytical dose value were observed towards lower proton energies indicating considerable differences in the accuracy of the proton transport algorithm. Protons with an initial kinetic energy of 60 MeV did not pass the 0.1% level of accuracy in neither of the simulations using a *step size* of 0.1 mm. A reduction of the maximum *step size* from 0.1 mm to 0.01 mm led to an improvement in the accuracy by a factor of 2, but the calculation time was about 9 times higher.

The minimum RMSE was obtained for 120 and 150 MeV. The RMSE increases slightly for higher energies. This can be explained by the higher statistical uncertainties obtained for the transport of higher energy protons. The p-value of the ANOVA and the RMSE indicated no significant differences of the Fano cavity test with the magnetic field strength.

Overall, our results show good agreement with theoretical values. Similar results were obtained by J. Wulff et al. [31] using the TOPAS MC code, also based on Geant4. In their simulations they used almost the same Fano cavity setup and physics models (*option 4* with user-defined settings), but no magnetic fields. An agreement within 0.1%

Die approbierte gedruckte Originalversion dieser Diplomarbeit ist an der TU Wien Bibliothek verfügbar
The approved original version of this thesis is available in print at TU Wien Bibliothek.
TU Bibliothek Your knowledge hub WIEN

was only obtained for strict parameter restrictions in the step function of Geant4, which were considered as impractical due to the enormously increased calculation time. For reasonable calculation times, a set of transport parameters was proposed to reach 0.2% deviations for the Fano cavity test. Similar to the results of this study, better agreement towards higher energies was found.

Based on our results, for 90-250 MeV protons a maximum *step size* of 0.1 mm and the electromagnetic standard *option 4* should be used for ionization chamber dose response simulations. For protons with an energy less than 60 MeV, a reduction of the *step size* to 0.01 mm is recommended. Protons with 1.5 MeV did not pass the Fano test with an acceptable level of accuracy. The transport of protons in *option 4* is described by the *WentzelVI* model, which is the default model for all charged particles [7]. Geant4, being a high energy particle physics simulation platform, does currently not provide a dedicated model for the transport of low energy protons. Since the *WentzelVI* model does cover all particle types and energy ranges, its parametrization might not be accurate enough for lower energies. Moreover, differential cross sections are highly energy dependent resulting in different electromagnetic physics processes. In a first step, it should investigated if low energy proton transport using the *WentzelVI* model can be improved by adapting the transport parameters in the MSC model or the stepping function of Geant4. Therefore, it will be necessary to extend GATE in order to make the parameters user accessible. If the fine tuning of transport parameters does not improve the Fano response, a new physics list/MSC model must be developed specifically for low energy proton transport. This should be investigated in future releases of GATE/Geant4.

Die approbierte gedruckte Originalversion dieser Diplomarbeit ist an der TU Wien Bibliothek verfügbar
The approved original version of this thesis is available in print at TU Wien Bibliothek.
TU Bibliothek Your knowledge hub WIEN

6 Summary and Outlook

This work examined the accuracy of GATE for the transport of charged particles in electromagnetic fields. It consisted of two work packages, i.e., the implementation of particle transport within custom three-dimensional electromagnetic vector field maps (see Chap. 4) and the design and implementation of a Fano cavity test (see Chap. 5) in GATE.

The implementation of electromagnetic vector field maps in GATE is the basis of detailed simulations of ionization chambers and allows to use custom and realistic electromagnetic fields based on finite element models generated from external field modelling software. In fact, this will be a crucial step in the early research phase of MR guided proton therapy, since the interaction of the MR system and the particle beam line has to be studied in great detail before the technical realization. Therefore, GATE was extended to simulate particle transport in custom electromagnetic fields. The close agreement between proton beam trajectories, simulated in GATE and calculated using a numerical method, demonstrated the accuracy of our implemented model in GATE.

The accuracy of GATE for dosimetric applications within external magnetic fields was tested using a Fano cavity setup. Based on Fano's theorem, an analytical value for the absorbed dose within the cavity could be calculated and compared to the absorbed dose simulated with GATE. The ratio of the analytical (theoretical) and the simulated value was used to asses the accuracy of the MC transport algorithm. To best of our knowledge, the Fano cavity test for electrons and protons was implemented and conducted for the first time in GATE. This test was also performed in the presence of external magnetic fields ($B = 0.35$-$3\,\mathrm{T}$). The results of the Fano test were overall consistent with theory, but an acceptable level of accuracy could only be achieved with kinetic energies greater or equal than 3 MeV (protons) and 0.5 MeV (electrons). A clear trend towards higher deviations was observed when using a fixed maximum *step size* and decreasing particle beam energies. The outcome of the Fano test showed considerable differences in the accuracy of the particle transport utilizing different physics lists. Moreover, a distinct dependence on the *step size* was found. A statistical test (ANOVA) indicated independence of the Fano cavity response with the magnetic field strength, emphasizing the correctness of the field implementation model in GATE.

Based on the results, the electromagnetic physics list *option 4* showed better agreement with theory and should therefore be used for detector response modelling of ionization chambers, independent of the magnetic field strength. A maximum *step size* of 0.1 mm is suitable for electron beam energies between 0.5-20 MeV and proton beam energies between 90-250 MeV. A reduction of the *step size* from 0.1 mm to 0.01 mm is recommended for proton energies between 3-60 MeV. For lower electron and proton energies ($\leq 1.5\,\mathrm{MeV}$) it is not worth to further reduce the *step size* in GATE.

Die approbierte gedruckte Originalversion dieser Diplomarbeit ist an der TU Wien Bibliothek verfügbar
The approved original version of this thesis is available in print at TU Wien Bibliothek.
TU Bibliothek Your knowledge hub WIEN

In conclusion, GATE is capable of passing the Fano cavity test for energies above 1.5 MeV with a level of accuracy which is acceptable for many applications. However, a clear limitation has been revealed for charged particles in the low energy regime. The accuracy of low energy particle transport might be improved by investigating the parameterization of the underlying MSC models in Geant4. This should be further investigated in future releases of GATE. The results of this study provide essential benchmark data for future simulations of ionization chambers and serve as a reference for the selection of important transport parameters such as the physics list and the maximum *step size*.

Die approbierte gedruckte Originalversion dieser Diplomarbeit ist an der TU Wien Bibliothek verfügbar
The approved original version of this thesis is available in print at TU Wien Bibliothek.
TU Bibliothek Your knowledge hub WIEN

Appendix A: Fano cavity response for electrons

A.1 Numerical values

The numerical values of the Fano cavity response for electrons are shown in Table A.1 and Table A.2. The values represent the ratio of the simulated absorbed dose and the analytical (theoretical) absorbed dose:

$$ratio = \frac{D_{simulated}}{D_{theory}} \tag{A.1}$$

The relative statistical uncertainty (1σ) on the Fano response values are based on the number of electrons entering the cavity and are shown in the parentheses.

	0 T	**0.35 T**	**0.5 T**
0.05 MeV	0.9503 (0.0003)	0.9507 (0.0003)	0.9504 (0.0003)
0.1 MeV	0.9419 (0.0004)	0.9427 (0.0004)	0.9420 (0.0004)
0.5 MeV	1.0380 (0.0008)	1.0370 (0.0008)	1.0372 (0.0008)
1 MeV	1.0391 (0.0010)	1.0404 (0.0010)	1.0387 (0.0010)
3 MeV	1.0230 (0.0016)	1.0180 (0.0016)	1.0203 (0.0016)
6 MeV	1.0153 (0.0022)	1.0149 (0.0021)	1.0128 (0.0021)
20 MeV	1.0115 (0.0037)	1.0053 (0.0035)	1.0081 (0.0036)
	1 T	**1.5 T**	**3 T**
0.05 MeV	0.9503 (0.0003)	0.9498 (0.0003)	0.9499 (0.0003)
0.1 MeV	0.9425 (0.0004)	0.9424 (0.0004)	0.9421 (0.0004)
0.5 MeV	1.0376 (0.0008)	1.0383 (0.0008)	1.0377 (0.0008)
1 MeV	1.0412 (0.0010)	1.0399 (0.0010)	1.0406 (0.0010)
3 MeV	1.0216 (0.0016)	1.0196 (0.0016)	1.0195 (0.0016)
6 MeV	1.0171 (0.0022)	1.0098 (0.0021)	1.0119 (0.0021)
20 MeV	1.0065 (0.0036)	1.0082 (0.0037)	1.0094 (0.0035)

Table A.1: Fano cavity response for electrons utilizing *option 3* with a maximum *step size* of 0.1 mm.

Die approbierte gedruckte Originalversion dieser Diplomarbeit ist an der TU Wien Bibliothek verfügbar
The approved original version of this thesis is available in print at TU Wien Bibliothek.
TU Bibliothek Your knowledge hub WIEN

	0 T	0.35 T	0.5 T
0.05 MeV	0.9675 (0.0004)	0.9670 (0.0004)	0.9684 (0.0004)
0.1 MeV	0.9521 (0.0004)	0.9523 (0.0004)	0.9516 (0.0004)
0.5 MeV	0.9984 (0.0007)	0.9971 (0.0007)	0.9974 (0.0007)
1 MeV	1.0030 (0.0010)	1.0009 (0.0010)	1.0022 (0.0010)
3 MeV	1.0007 (0.0016)	0.9985 (0.0015)	0.9989 (0.0016)
6 MeV	0.9980 (0.0021)	1.0021 (0.0022)	0.9988 (0.0020)
20 MeV	0.9990 (0.0035)	1.0062 (0.0035)	1.0020 (0.0036)
	1 T	**1.5 T**	**3 T**
0.05 MeV	0.9681 (0.0004)	0.9676 (0.0004)	0.9682 (0.0004)
0.1 MeV	0.9522 (0.0004)	0.9511 (0.0004)	0.9507 (0.0004)
0.5 MeV	0.9983 (0.0007)	0.9966 (0.0007)	0.9977 (0.0007)
1 MeV	1.0014 (0.0010)	1.0018 (0.0010)	1.0025 (0.0010)
3 MeV	0.9987 (0.0015)	1.0005 (0.0016)	1.0018 (0.0016)
6 MeV	1.0002 (0.0021)	0.9990 (0.0021)	1.0014 (0.0021)
20 MeV	0.9975 (0.0034)	1.0013 (0.0035)	0.9990 (0.0034)

Table A.2: Fano cavity response for electrons utilizing *option 4* with a maximum *step size* of 0.1 mm.

Die approbierte gedruckte Originalversion dieser Diplomarbeit ist an der TU Wien Bibliothek verfügbar
The approved original version of this thesis is available in print at TU Wien Bibliothek.

Appendix B: Fano cavity response for protons

B.1 Numerical values

The numerical values of the Fano cavity response for protons are shown in Table B.1. The values represent the ratio of the simulated absorbed dose and the analytical (theoretical) absorbed dose:

$$ratio = \frac{D_{simulated}}{D_{theory}} \tag{B.1}$$

The relative statistical uncertainty (1σ) on the Fano response values are based on the number of protons entering the cavity and are shown in the parentheses.

	0 T	**0.35 T**	**0.5 T**
60 MeV	1.0022 (0.0006)	1.0029 (0.0006)	1.0018 (0.0006)
90 MeV	1.0010 (0.0007)	1.0022 (0.0007)	1.0017 (0.0007)
120 MeV	1.0008 (0.0007)	1.0003 (0.0007)	1.0015 (0.0007)
150 MeV	1.0002 (0.0008)	1.0000 (0.0007)	1.0014 (0.0007)
180 MeV	1.0005 (0.0008)	1.0020 (0.0008)	1.0003 (0.0008)
220 MeV	1.0015 (0.0009)	1.0008 (0.0009)	1.0005 (0.0009)
250 MeV	1.0009 (0.0009)	1.0012 (0.0009)	0.9989 (0.0009)
	1 T	**1.5 T**	**3 T**
60 MeV	1.0025 (0.0006)	1.0017 (0.0006)	1.0022 (0.0006)
90 MeV	1.0015 (0.0007)	1.0015 (0.0007)	1.0007 (0.0007)
120 MeV	1.0009 (0.0007)	1.0002 (0.0007)	0.9993 (0.0007)
150 MeV	1.0007 (0.0008)	0.9993 (0.0007)	1.0012 (0.0008)
180 MeV	1.0013 (0.0008)	1.0009 (0.0008)	1.0013 (0.0008)
220 MeV	1.0023 (0.0009)	1.0005 (0.0009)	1.0009 (0.0008)
250 MeV	1.0025 (0.0009)	1.0007 (0.0009)	1.0009 (0.0009)

Table B.1: Fano cavity response for protons utilizing *option 4* with a maximum *step size* of 0.1 mm.

Die approbierte gedruckte Originalversion dieser Diplomarbeit ist an der TU Wien Bibliothek verfügbar
The approved original version of this thesis is available in print at TU Wien Bibliothek.
TU Bibliothek Your knowledge hub WIEN

Appendix C: Fano cavity response vs. remaining range in water

C.1 Numerical values

The numerical values of the remaining range in water and the Fano cavity response for electrons and protons are shown in Table C.1 and Table C.2 respictively. Relative differences are calculated as:

$$Rel.\,diff.(\%) = 100 \times \left| 1 - \frac{D_{simulated}}{D_{theory}} \right| \tag{C.1}$$

Energy (MeV)	Range (mm)	Fano response	Rel. difference (%)
0.05	4.32×10^{-2}	0.9675 (0.0004)	3.25
0.1	1.43×10^{-1}	0.9521 (0.0004)	4.79
0.5	1.77	0.9984 (0.0007)	0.16
1	4.37	1.0030 (0.0010)	0.30
3	15.14	1.0007 (0.0016)	0.07
6	30.52	0.9980 (0.0021)	0.20
20	93.20	0.9990 (0.0035)	0.10

Table C.1: Fano cavity response for electrons utilizing *option 4* with a maximum *step size* of 0.1 mm.

Energy (MeV)	Range (mm)	Fano response	Rel. difference (%)
1.5	4.7×10^{-2}	0.9232 (0.0003)	7.68
3	1.5×10^{-1}	0.9948 (0.0004)	0.52
12.5	1.83	1.0056 (0.0005)	0.56
20	4.26	1.0010 (0.0005)	0.10
40	14.89	0.9996 (0.0006)	0.04
60	30.93	1.0011 (0.0006)	0.11
90	63.98	1.0010 (0.0007)	0.10

Table C.2: Fano cavity response for protons utilizing *option 4* with a maximum *step size* of 0.01 mm (1.5-60 MeV) and 0.1 mm (90 MeV).

Die approbierte gedruckte Originalversion dieser Diplomarbeit ist an der TU Wien Bibliothek verfügbar
The approved original version of this thesis is available in print at TU Wien Bibliothek.
TU Bibliothek Your knowledge hub WIEN

Appendix D: Fano cavity response - Overview for B=0T

D.1 Numerical values

A summary of the numerical results for electrons and protons with $B = 0\,\mathrm{T}$ is listed in the table on the next page. The values represent the ratio of the simulated absorbed dose and the analytical (theoretical) absorbed dose:

$$ratio = \frac{D_{simulated}}{D_{theory}} \tag{D.1}$$

The relative statistical uncertainty (1σ) on the Fano response values are shown in the parentheses. Numerical values in bold were obtained with 10^6 primary particles instead of 10^8.

Die approbierte gedruckte Originalversion dieser Diplomarbeit ist an der TU Wien Bibliothek verfügbar
The approved original version of this thesis is available in print at TU Wien Bibliothek.
TU Bibliothek Your knowledge hub WIEN

	Energy (MeV)	Step size (mm)	option 3	option 4	em SS	em Low EP
Electrons	0.05	1	0.9585 (0.0003)	0.9674 (0.0003)		
		1e-1	0.9505 (0.0003)	0.9675 (0.0004)	**0.9737 (0.0034)**	**0.2113 (0.0015)**
		1e-2	0.9454 (0.0003)	0.9682 (0.0003)		
		1e-3	0.9536 (0.0003)	0.9792 (0.0003)		
		1e-4	0.9694 (0.0003)	0.9787 (0.0003)		
		1e-5		**0.9772 (0.0033)**	**0.9748 (0.0033)**	**0.9744 (0.0033)**
		1e-6		**0.9668 (0.0033)**	**0.9684 (0.0032)**	**0.9654 (0.0033)**
	0.1	1	0.9460 (0.0004)	0.9508 (0.0004)		
		1e-1	0.9419 (0.0004)	0.9521 (0.0004)		
		1e-2	0.9380 (0.0004)	0.9519 (0.0004)		
		1e-3	0.9407 (0.0004)	0.9558 (0.0004)		
		1e-4	0.9494 (0.0004)	0.9543 (0.0004)		
	0.5	1e-1	1.0380 (0.0008)	0.9984 (0.0007)		
		1e-3	0.9936 (0.0005)			
	1	1	1.0671 (0.0010)			
		1e-1	1.0413 (0.0010)	1.0030 (0.0010)		
		1e-2	1.0020 (0.0005)			
		1e-3	0.9999 (0.0005)	1.0015 (0.0005)		
	3	1e-1	1.0230 (0.0016)	1.0007 (0.0016)		
		1e-3	0.9997 (0.0005)			
	6	1e-1	1.0153 (0.0022)	0.9980 (0.0021)		
		1e-3	0.9998 (0.0005)			
	20	1e-1	1.0115 (0.0037)	0.9990 (0.0035)		
Protons	1.5	1e-2		0.9232 (0.0003)		
		1e-5	**0.9174 (0.0029)**	**0.9207 (0.0029)**	**0.9153 (0.0029)**	
	3	1e-2		0.9948 (0.0004)		
		1e-3		0.9932 (0.0004)		
		1e-4		0.9919 (0.0004)		
	12.5	1e-2		1.0056 (0.0005)		
		1e-3		1.0036 (0.0005)		
		1e-4		1.0027 (0.0005)		
	20	1e-2		1.0010 (0.0005)		
	40	1e-2		0.9996 (0.0006)		
	60	1e-1		1.0022 (0.0006)		
		1e-2		1.0011 (0.0006)		
	90	1e-1		1.0010 (0.0007)		
	120	1e-1		1.0008 (0.0007)		
	150	1e-1		1.0002 (0.0008)		
	180	1e-1		1.0005 (0.0008)		
	220	1e-1		1.0015 (0.0009)		
	250	1e-1		1.0009 (0.0009)		

Die approbierte gedruckte Originalversion dieser Diplomarbeit ist an der TU Wien Bibliothek verfügbar
The approved original version of this thesis is available in print at TU Wien Bibliothek.
TU Bibliothek Your knowledge hub WIEN

Appendix E: GATE macro file

E.1 Simulation setup

The following GATE macro commands (`main.mac`) simulate a mono-energetic electron beam with an initial kinetic energy of $E = 0.05\,\text{MeV}$ traversing an ionization chamber in the presence of a magnetic field ($B = 1\,\text{T}$) based on Fano's theorem.

The GATE macro requires the following files as input:

1. `alias.mac`: This file contains aliases of the `main.mac` macro file. This was done for automation and parallelization purposes only.

2. `vis_G4.mac`: This file was used to visualize the geometry using QT and OPENGL (refer to Geant4 installation guide). This particular visualization file is officially distributed with the Geant4 release v10.06.p01 and can be found in the git repository of reference [55].

3. `GateMaterials.db`: This file contains information (e.g., density and state) about the used materials. For the Fano test, a fictitious material *Water_gas* was manually added (see Subsec. 5.1.1).

4. `Bz_1T.txt`: Magnetic vector field map (lookup table). The coordinates of the vector field were based on the chamber geometry, which again depended on the incident energy (see Subsec. 5.1.3). The vector field maps were generated with a custom Python script and had the form of Figure 4.2.

The output of the simulation are the following text files:

1. `stat.txt`: Stores important simulation statistics such as the number of events, tracks, steps and the elapsed time (calculation time).

2. Several files associated to the *Dose Actor* `doseInZ-*.txt`: Stores the energy deposition (Edep), squared energy deposition (Edep-Squared) and number of hits (NbOfHits). The energy deposition was used to calculate the absorbed dose in the cavity (see Eq. 5.3). The squared energy deposition and the number of hits were used in the calculation of the total statistical uncertainty in case of job parallelization (see Eq. 3.2).

Please note that for a correct implementation and execution of the Fano cavity test, the density correction term in the Geant4 class *G4MollerBhabhaModel*:

Die approbierte gedruckte Originalversion dieser Diplomarbeit ist an der TU Wien Bibliothek verfügbar
The approved original version of this thesis is available in print at TU Wien Bibliothek.
TU Bibliothek Your knowledge hub WIEN

geant4/geant4.10.06.p01/source/processes/electromagnetic/standard/src/G4MollerBhabhaModel.cc

must be removed and GATE recompiled as it is described in Subsection 5.1.4 and in reference [55].

```
G4double G4MollerBhabhaModel::ComputeDEDXPerVolume(
                                          const G4Material* material,
                                          const G4ParticleDefinition* p,
                                                G4double kineticEnergy,
                                                G4double cut)
{
  if(nullptr == particle) { SetParticle(p); }
  // calculate the dE/dx due to the ionization by Seltzer-Berger formula
  // check low-energy limit

  G4double electronDensity = material->GetElectronDensity();
  G4double Zeff  = electronDensity/material->GetTotNbOfAtomsPerVolume();
  G4double th    = 0.25*sqrt(Zeff)*keV;
  G4double tkin = kineticEnergy;
  G4bool   lowEnergy = false;
  if (kineticEnergy < th) {
    tkin = th;
    lowEnergy = true;
  }
  G4double tau   = tkin/electron_mass_c2;
  G4double gam   = tau + 1.0;
  G4double gamma2= gam*gam;
  G4double beta2 = 1. - 1./gamma2;

  G4double eexc  = material->GetIonisation()->GetMeanExcitationEnergy();
  eexc          /= electron_mass_c2;
  G4double eexc2 = eexc*eexc;

  G4double d = min(cut, MaxSecondaryEnergy(p, tkin))/electron_mass_c2;
  G4double dedx;

  // electron
  if (isElectron) {

    dedx = G4Log(2.0*(tau + 2.0)/eexc2) - 1.0 - beta2
         + G4Log((tau-d)*d) + tau/(tau-d)
         + (0.5*d*d + (2.0*tau + 1.)*G4Log(1. - d/tau))/gamma2;

  //positron
  } else {

    G4double d2 = d*d*0.5;
    G4double d3 = d2*d/1.5;
    G4double d4 = d3*d*0.75;
    G4double y  = 1.0/(1.0 + gam);
    dedx = G4Log(2.0*(tau + 2.0)/eexc2) + G4Log(tau*d)
         - beta2*(tau + 2.0*d - y*(3.0*d2
         + y*(d - d3 + y*(d2 - tau*d3 + d4))))/tau;
```


Die approbierte gedruckte Originalversion dieser Diplomarbeit ist an der TU Wien Bibliothek verfügbar
The approved original version of this thesis is available in print at TU Wien Bibliothek.
TU Bibliothek Your knowledge hub WIEN

```
  }

  // now you can compute the total ionization loss
  dedx *= twopi_mc2_rcl2*electronDensity/beta2;
  if (dedx < 0.0) { dedx = 0.0; }

  // lowenergy extrapolation
  if (lowEnergy) {

    if (kineticEnergy >= lowLimit) dedx *= sqrt(tkin/kineticEnergy);
    else                           dedx *= sqrt(tkin*kineticEnergy)/
    lowLimit;

  }
  return dedx;
}
```

Listing E.1: *ComputeDEDXPerVolume* function in G4MollerBhabhaModel.cc without the density correction term.

In the following, comments are denoted with a hash (#). Several command blocks are commented out such as the visualization commands, electromagnetic properties actor (see Subsec. 5.1.4) and the phase space actor (see Subsec. 5.2.1). Those commands were used for analysis purposes only and were not applied in the actual test execution.

```
#=====================================================
# Fano cavity test for e- in the presence of magnetic
# fields
#=====================================================

#=====================================================
# ALIAS
#=====================================================
/control/execute alias.mac

#=====================================================
# VISUALIZATION
#=====================================================
#/control/execute vis_G4.mac

#=====================================================
# MATERIAL
#=====================================================
/gate/geometry/setMaterialDatabase data/GateMaterials.db

/gate/geometry/setIonisationPotential Water 78 eV
/gate/geometry/setIonisationPotential Water_gas 78 eV

#=====================================================
# GEOMETRY
#=====================================================
# World
/gate/world/geometry/setXLength {world_radius}
/gate/world/geometry/setYLength {world_radius}
```


Die approbierte gedruckte Originalversion dieser Diplomarbeit ist an der TU Wien Bibliothek verfügbar
The approved original version of this thesis is available in print at TU Wien Bibliothek.
TU Bibliothek Your knowledge hub WIEN

```
/gate/world/geometry/setZLength {world_radius}
/gate/world/setMaterial Water
#/gate/world/vis/setVisible 0

# Main Volume
/gate/world/daughters/name mainVolume
/gate/world/daughters/insert cylinder
/gate/mainVolume/geometry/setRmin 0 m
/gate/mainVolume/geometry/setRmax {cylinder_radius}
/gate/mainVolume/geometry/setHeight {cylinder_height}
/gate/mainVolume/placement/setTranslation 0 0 0 cm
/gate/mainVolume/setMaterial Water
#/gate/mainVolume/vis/setVisible 0
#/gate/mainVolume/vis/setColor green
#/gate/mainVolume/vis/forceWireframe

# Cavity
/gate/mainVolume/daughters/name cavity
/gate/mainVolume/daughters/insert cylinder
/gate/cavity/geometry/setRmin 0 m
/gate/cavity/geometry/setRmax {cylinder_radius}
/gate/cavity/geometry/setHeight 0.2 cm
/gate/cavity/placement/setTranslation 0 0 0 cm
/gate/cavity/setMaterial Water_gas
#/gate/cavity/vis/setVisible 1
#/gate/cavity/vis/setColor white
#/gate/cavity/vis/forceWireframe

# Wall1
/gate/mainVolume/daughters/name wall1
/gate/mainVolume/daughters/insert cylinder
/gate/wall1/geometry/setRmin 0 m
/gate/wall1/geometry/setRmax {cylinder_radius}
/gate/wall1/geometry/setHeight {wall_thickness}
/gate/wall1/placement/setTranslation {wall1_placement}
/gate/wall1/setMaterial Water
#/gate/wall1/vis/setVisible 1
#/gate/wall1/vis/setColor white
#/gate/wall1/vis/forceWireframe

# Wall2
/gate/mainVolume/daughters/name wall2
/gate/mainVolume/daughters/insert cylinder
/gate/wall2/geometry/setRmin 0 m
/gate/wall2/geometry/setRmax {cylinder_radius}
/gate/wall2/geometry/setHeight {wall_thickness}
/gate/wall2/placement/setTranslation {wall2_placement}
/gate/wall2/setMaterial Water
#/gate/wall2/vis/setVisible 1
#/gate/wall2/vis/setColor white
#/gate/wall2/vis/forceWireframe

# Magnetic Field
/gate/geometry/setMagTabulateField3D {B_LUT}
```


Die approbierte gedruckte Originalversion dieser Diplomarbeit ist an der TU Wien Bibliothek verfügbar
The approved original version of this thesis is available in print at TU Wien Bibliothek.
TU Bibliothek Your knowledge hub WIEN

```
84
85 #=====================================================
86 # PHYSICS
87 #=====================================================
88 # Builder
89 /gate/physics/addPhysicsList {physics_list}
90
91 # Cuts in world
92 /gate/physics/Gamma/SetCutInRegion world 10 km
93 /gate/physics/Electron/SetCutInRegion world 10 km
94 /gate/physics/Positron/SetCutInRegion world 10 km
95
96 # Step limiter in world
97 /gate/physics/SetMaxStepSizeInRegion world 1 mm
98 /gate/physics/ActivateStepLimiter e-
99
100 # Cuts in main volume
101 /gate/physics/Gamma/SetCutInRegion mainVolume 10 km
102 /gate/physics/Electron/SetCutInRegion mainVolume 10 km
103 /gate/physics/Positron/SetCutInRegion mainVolume 10 km
104
105 # Step limiter in main volume
106 /gate/physics/SetMaxStepSizeInRegion mainVolume 0.1 mm
107 /gate/physics/ActivateStepLimiter e-
108
109 #=====================================================
110 # ACTORS
111 #=====================================================
112 # Simulation statistic
113 /gate/actor/addActor SimulationStatisticActor stat
114 /gate/actor/stat/save output/stat.txt
115 /gate/actor/stat/saveEveryNSeconds 60
116
117 # Phase space ingoing
118 #/gate/actor/addActor PhaseSpaceActor MyActor
119 #/gate/actor/MyActor/save output/phsp_in.npy
120 #/gate/actor/MyActor/attachTo cavity
121 #/gate/actor/MyActor/storeOutgoingParticles false
122 #/gate/actor/MyActor/enableXPosition false
123 #/gate/actor/MyActor/enableYPosition false
124 #/gate/actor/MyActor/enableZPosition false
125 #/gate/actor/MyActor/enableWeight false
126 #/gate/actor/MyActor/enableXDirection false
127 #/gate/actor/MyActor/enableYDirection false
128 #/gate/actor/MyActor/enableZDirection false
129 #/gate/actor/MyActor/enableParticleName false
130 #/gate/actor/MyActor/enableWeight false
131
132 # Phase space outgoing
133 #/gate/actor/addActor PhaseSpaceActor MyActor1
134 #/gate/actor/MyActor1/save output/phsp_out.npy
135 #/gate/actor/MyActor1/attachTo cavity
136 #/gate/actor/MyActor1/storeOutgoingParticles true
137 #/gate/actor/MyActor1/enableXPosition false
```


Die approbierte gedruckte Originalversion dieser Diplomarbeit ist an der TU Wien Bibliothek verfügbar
The approved original version of this thesis is available in print at TU Wien Bibliothek.
TU Bibliothek Your knowledge hub WIEN

```
#/gate/actor/MyActor1/enableYPosition false
#/gate/actor/MyActor1/enableZPosition false
#/gate/actor/MyActor1/enableWeight false
#/gate/actor/MyActor1/enableXDirection false
#/gate/actor/MyActor1/enableYDirection false
#/gate/actor/MyActor1/enableZDirection false
#/gate/actor/MyActor1/enableParticleName false
#/gate/actor/MyActor1/enableWeight false

# EM properties
#/gate/actor/addActor EmCalculatorActor MyActor2
#/gate/actor/MyActor2/attachTo cavity
#/gate/actor/MyActor2/setParticleName e-
#/gate/actor/MyActor2/setEnergy {E}
#/gate/actor/MyActor2/save output/emproperties.txt

# 1D Dose actor - Energy deposition
/gate/actor/addActor DoseActor doseInZ
/gate/actor/doseInZ/save output/doseInZ.txt
/gate/actor/doseInZ/attachTo cavity
/gate/actor/doseInZ/stepHitType random
/gate/actor/doseInZ/setPosition 0 0 0 cm
/gate/actor/doseInZ/setResolution 1 1 1
/gate/actor/doseInZ/enableEdep true
/gate/actor/doseInZ/enableUncertaintyEdep false
/gate/actor/doseInZ/enableSquaredEdep true
/gate/actor/doseInZ/enableNumberOfHits true
/gate/actor/doseInZ/enableDose false

#=====================================================
# INITIALIZATION
#=====================================================
/gate/run/initialize

#=====================================================
# SOURCE
#=====================================================
# Cavity
/gate/source/addSource sourceCavity
/gate/source/sourceCavity/gps/pos/type Volume
/gate/source/sourceCavity/gps/pos/shape Cylinder
/gate/source/sourceCavity/gps/pos/radius 1 fm
/gate/source/sourceCavity/gps/pos/halfz 0.1 cm
/gate/source/sourceCavity/gps/particle e-
/gate/source/sourceCavity/setIntensity {cavity_intensity}
/gate/source/sourceCavity/attachTo cavity
/gate/source/sourceCavity/gps/ene/mono {E}
/gate/source/sourceCavity/gps/direction 0 0 1
/gate/source/sourceCavity/gps/ang/type iso
/gate/source/sourceCavity/gps/ang/mintheta 0. deg
/gate/source/sourceCavity/gps/ang/maxtheta 180. deg
/gate/source/sourceCavity/gps/ang/minphi 0. deg
/gate/source/sourceCavity/gps/ang/maxphi 360. deg

```


Die approbierte gedruckte Originalversion dieser Diplomarbeit ist an der TU Wien Bibliothek verfügbar
The approved original version of this thesis is available in print at TU Wien Bibliothek.
TU Bibliothek Your knowledge hub WIEN

```
# Wall 1
/gate/source/addSource sourceWall1
/gate/source/sourceWall1/gps/pos/type Volume
/gate/source/sourceWall1/gps/pos/shape Cylinder
/gate/source/sourceWall1/gps/pos/radius 1 fm
/gate/source/sourceWall1/gps/pos/halfz {half_z}
/gate/source/sourceWall1/gps/particle e-
/gate/source/sourceWall1/setIntensity {wall_intensity}
/gate/source/sourceWall1/attachTo wall1
/gate/source/sourceWall1/gps/ene/mono {E}
/gate/source/sourceWall1/gps/direction 0 0 1
/gate/source/sourceWall1/gps/pos/centre {source_wall1_placement}
/gate/source/sourceWall1/gps/ang/type iso
/gate/source/sourceWall1/gps/ang/mintheta 0. deg
/gate/source/sourceWall1/gps/ang/maxtheta 180. deg
/gate/source/sourceWall1/gps/ang/minphi 0. deg
/gate/source/sourceWall1/gps/ang/maxphi 360. deg

# Wall 2
/gate/source/addSource sourceWall2
/gate/source/sourceWall2/gps/pos/type Volume
/gate/source/sourceWall2/gps/pos/shape Cylinder
/gate/source/sourceWall2/gps/pos/radius 1 fm
/gate/source/sourceWall2/gps/pos/halfz {half_z}
/gate/source/sourceWall2/gps/particle e-
/gate/source/sourceWall2/setIntensity {wall_intensity}
/gate/source/sourceWall2/attachTo wall2
/gate/source/sourceWall2/gps/ene/mono {E}
/gate/source/sourceWall2/gps/direction 0 0 1
/gate/source/sourceWall2/gps/pos/centre {source_wall2_placement}
/gate/source/sourceWall2/gps/ang/type iso
/gate/source/sourceWall2/gps/ang/mintheta 0. deg
/gate/source/sourceWall2/gps/ang/maxtheta 180. deg
/gate/source/sourceWall2/gps/ang/minphi 0. deg
/gate/source/sourceWall2/gps/ang/maxphi 360. deg


# Visualize source
#/gate/source/sourceCavity/visualize 10 yellow 5
#/gate/source/sourceWall1/visualize 10 yellow 5
#/gate/source/sourceWall2/visualize 10 yellow 5

#=====================================================
# START SIMULATION
#=====================================================
/gate/random/setEngineName MersenneTwister
/gate/random/setEngineSeed auto
/gate/application/setTotalNumberOfPrimaries 100000000
/gate/application/start

exit
```

Listing E.2: main.mac

Die approbierte gedruckte Originalversion dieser Diplomarbeit ist an der TU Wien Bibliothek verfügbar
The approved original version of this thesis is available in print at TU Wien Bibliothek.
TU Bibliothek Your knowledge hub WIEN

```
#=====================================================
# Parameters for the Fano cavity test for e- in  the
# presence of magnetic fields
#=====================================================

#=====================================================
# WORLD RADIUS
#=====================================================
/control/alias world_radius "12 cm"

#=====================================================
# CYLINDER
#=====================================================
/control/alias cylinder_radius "6 cm"
/control/alias cylinder_height "2.2 cm"

#=====================================================
# WALLS
#=====================================================
/control/alias wall_thickness "1 cm"
/control/alias wall1_placement "0 0 -0.6 cm"
/control/alias wall2_placement "0 0 0.6 cm"

#=====================================================
# MAGNETIC FIELD
#=====================================================
/control/alias B_LUT "data/Bz_1T.txt"

#=====================================================
# SOURCE PLACEMENT
#=====================================================
/control/alias source_wall1_placement "0. 0. 0.49738928 cm"
/control/alias source_wall2_placement "0. 0. -0.49738928 cm"
/control/alias half_z "0.00261072 cm"

#=====================================================
# SOURCE INTENSITY
#=====================================================
/control/alias wall_intensity "100000"
/control/alias cavity_intensity "1879"

#=====================================================
# PHYSICS LIST
#=====================================================
/control/alias physics_list "emstandard_opt4"

#=====================================================
# ENERGY
#=====================================================
/control/alias E "0.05 MeV"
```

Listing E.3: alias.mac

```
#
```


Die approbierte gedruckte Originalversion dieser Diplomarbeit ist an der TU Wien Bibliothek verfügbar
The approved original version of this thesis is available in print at TU Wien Bibliothek.
TU Bibliothek Your knowledge hub WIEN

```
# Macro file for the initialization phase of "TestEm6.cc"
#
# Sets some default verbose
# and initializes the graphic.
#
/control/verbose 2
/run/verbose 2
#
/run/initialize
#
# Use this open statement to create an OpenGL view:
/vis/open OGL 600x600-0+0
#
# Use this open statement to create a .prim file suitable for
# viewing in DAWN:
#/vis/open DAWNFILE
#
# Use this open statement to create a .heprep file suitable for
# viewing in HepRApp:
#/vis/open HepRepFile
#
# Use this open statement to create a .wrl file suitable for
# viewing in a VRML viewer:
#/vis/open VRML2FILE
#
# Disable auto refresh and quieten vis messages whilst scene and
# trajectories are established:
/vis/viewer/set/autoRefresh false
/vis/verbose errors
#
# Draw geometry:
/vis/drawVolume
#
# Specify view angle:
/vis/viewer/set/viewpointThetaPhi 90. 180.
#
# Specify zoom value:
/vis/viewer/zoom 1.4
#
# Specify style (surface or wireframe):
#/vis/viewer/set/style wireframe
#
# Draw coordinate axes:
#/vis/scene/add/axes 0 0 0 1 m
#
# Draw smooth trajectories at end of event, showing trajectory points
# as markers 2 pixels wide:
/vis/scene/add/trajectories smooth
/vis/modeling/trajectories/create/drawByCharge
/vis/modeling/trajectories/drawByCharge-0/default/setDrawStepPts true
/vis/modeling/trajectories/drawByCharge-0/default/setStepPtsSize 1
# (if too many tracks cause core dump => /tracking/storeTrajectory 0)
#
# Draw hits at end of event:
```


Die approbierte gedruckte Originalversion dieser Diplomarbeit ist an der TU Wien Bibliothek verfügbar
The approved original version of this thesis is available in print at TU Wien Bibliothek.
TU Bibliothek Your knowledge hub WIEN

```
#/vis/scene/add/hits
#
# To draw only gammas:
#/vis/filtering/trajectories/create/particleFilter
#/vis/filtering/trajectories/particleFilter-0/add gamma
#
# To invert the above, drawing all particles except gammas,
# keep the above two lines but also add:
#/vis/filtering/trajectories/particleFilter-0/invert true
#
# Many other options are available with /vis/modeling and /vis/filtering.
# For example, to select colour by particle ID:
#/vis/modeling/trajectories/create/drawByParticleID
#/vis/modeling/trajectories/drawByParticleID-0/set e- blue
#
# To superimpose all of the events from a given run:
/vis/scene/endOfEventAction accumulate
#
# Re-establish auto refreshing and verbosity:
/vis/viewer/set/autoRefresh true
/vis/verbose warnings
#
# For file-based drivers, use this to create an empty detector view:
#/vis/viewer/flush
```

Listing E.4: vis_G4.mac

```
[Elements]
Hydrogen:    S= H    ; Z=  1. ; A=   1.01   g/mole
Oxygen:      S= O    ; Z=  8. ; A=  16.00   g/mole

[Materials]
Vacuum: d=0.000001 mg/cm3 ; n=1
  +el: name=Hydrogen ; n=1

Water: d=1.00 g/cm3; n=2 ; state=liquid
  +el: name=Hydrogen ; n=2
  +el: name=Oxygen; n=1

Water_gas: d=1.00 mg/cm3; n=2 ; state=liquid
  +el: name=Hydrogen ; n=2
  +el: name=Oxygen; n=1
```

Listing E.5: GateMaterials.db

Die approbierte gedruckte Originalversion dieser Diplomarbeit ist an der TU Wien Bibliothek verfügbar
The approved original version of this thesis is available in print at TU Wien Bibliothek.

Bibliography

[1] Hermann Fuchs et al. "MR-guided proton therapy: Impact of magnetic fields on the detector response". In: *Medical Physics* (2020). ISSN: 0094-2405. DOI: 10.1002/mp.14660.

[2] Aswin Hoffmann et al. *MR-guided proton therapy: A review and a preview*. 2020. DOI: 10.1186/s13014-020-01571-x.

[3] F. Salvat et al. *Practical aspects of Monte Carlo simulation of charged particle transport: Mixed algorithms and variance reduction techniques*. 1999. DOI: 10.1007/s004110050133.

[4] Joao Seco and Frank Verhaegen. *Monte Carlo Techniques in Radiation Therapy, Imaging in medical diagnosis and therapy Series*. 2013. ISBN: 9781138199903.

[5] MJ. Berger. "Monte Carlo calculation of the penetration and diffusion of fast charged particles". In: *Methods in Computational Physics* (1963).

[6] Vere G. Smyth. "Interface effects in the Monte Carlo simulation of electron tracks". In: *Medical Physics* (1986). ISSN: 00942405. DOI: 10.1118/1.595896.

[7] Geant4 Collaboration. *Physics Reference Manual Release 10.6*. 2020. URL: https://geant4.web.cern.ch/support/user%7B%5C_%7Ddocumentation.

[8] J. M. Fernández-Varea et al. "On the theory and simulation of multiple elastic scattering of electrons". In: *Nuclear Inst. and Methods in Physics Research, B* (1993). ISSN: 0168583X. DOI: 10.1016/0168-583X(93)95827-R.

[9] G. Wentzel. "Zwei Bemerkungen über die Zerstreuung korpuskularer Strahlen als Beugungserscheinung". In: *Zeitschrift für Physik* (1926). ISSN: 14346001. DOI: 10.1007/BF01390457.

[10] Bernard Gottschalk. *Radiotherapy Proton Interactions in Matter*. 2018. arXiv: 1804.00022.

[11] Gert Moliere. "Theorie der Streuung schneller geladener Teilchen II Mehrfach-und Vielfachstreuung1". In: *Zeitschrift fur Naturforschung - Section A Journal of Physical Sciences* (1948). ISSN: 18657109. DOI: 10.1515/zna-1948-0203.

[12] H. A. Bethe. "Molière's theory of multiple scattering". In: *Physical Review* (1953). ISSN: 0031899X. DOI: 10.1103/PhysRev.89.1256.

[13] A. O. Hanson et al. "Measurement of multiple scattering of 15.7-Mev electrons". In: *Physical Review* (1951). ISSN: 0031899X. DOI: 10.1103/PhysRev.84.634.

Die approbierte gedruckte Originalversion dieser Diplomarbeit ist an der TU Wien Bibliothek verfügbar
The approved original version of this thesis is available in print at TU Wien Bibliothek.
TU Bibliothek Your knowledge hub WIEN

[14] Virgil L. Highland. "Some practical remarks on multiple scattering". In: *Nuclear Instruments and Methods* (1975). ISSN: 0029554X. DOI: 10.1016/0029-554X(75)90743-0.

[15] László Urban. "A model for multiple scattering in geant4". In: *Monte Carlo 2005 Topical Meeting*. 2005.

[16] H. W. Lewis. "Multiple scattering in an infinite medium". In: *Physical Review* (1950). ISSN: 0031899X. DOI: 10.1103/PhysRev.78.526.

[17] Gerald R. Lynch and Orin I. Dahl. "Approximations to multiple Coulomb scattering". In: *Nuclear Inst. and Methods in Physics Research, B* (1991). ISSN: 0168583X. DOI: 10.1016/0168-583X(91)95671-Y.

[18] Hugo Bouchard and Alex Bielajew. "Lorentz force correction to the Boltzmann radiation transport equation and its implications for Monte Carlo algorithms". In: *Physics in Medicine and Biology* (2015). ISSN: 13616560. DOI: 10.1088/0031-9155/60/13/4963.

[19] D. E. Groom et al. "Review of particle physics". In: *European Physical Journal C* 15.1-4 (Aug. 2000), pp. 1–878. ISSN: 14346044. DOI: 10.1093/ptep/ptaa104. URL: https://academic.oup.com/ptep/article/doi/10.1093/ptep/ptaa104/5891211.

[20] Enrico Fermi. "The ionization loss of energy in gases and in condensed materials". In: *Physical Review* (1940). ISSN: 0031899X. DOI: 10.1103/PhysRev.57.485.

[21] M.J. Berger et al. "Stopping-Power & Range Tables for Electrons, Protons, and Helium Ions". In: *Nistir* (2017). DOI: 10.18434/T4NC7P.

[22] Bruno Rossi and William B. Fretter. "High-Energy Particles". In: *American Journal of Physics* (1953). ISSN: 0002-9505. DOI: 10.1119/1.1933408.

[23] James L. Bedford. *Calculation of absorbed dose in radiotherapy by solution of the linear Boltzmann transport equations*. 2019. DOI: 10.1088/1361-6560/aaf0e2.

[24] U. FANO. "Note on the Bragg-Gray cavity principle for measuring energy dissipation." In: *Radiation research* (1954). ISSN: 00337587. DOI: 10.2307/3570368.

[25] I. Kawrakow. "Accurate condensed history Monte Carlo simulation of electron transport. I. EGSnrc, the new EGS4 version". In: *Medical Physics* (2000). ISSN: 00942405. DOI: 10.1118/1.598917.

[26] Emily Poon, Jan Seuntjens, and Frank Verhaegen. "Consistency test of the electron transport algorithm in the GEANT4 Monte Carlo code". In: *Physics in Medicine and Biology* (2005). ISSN: 00319155. DOI: 10.1088/0031-9155/50/4/008.

[27] J. Sempau and P. Andreo. "Configuration of the electron transport algorithm of PENELOPE to simulate ion chambers". In: *Physics in Medicine and Biology* (2006). ISSN: 00319155. DOI: 10.1088/0031-9155/51/14/017.

[28] Chul Young Yi, Suck Ho Hah, and Min Sun Yeom. "Monte Carlo calculation of the ionization chamber response to 60Co beam using PENELOPE". In: *Medical Physics* (2006). ISSN: 00942405. DOI: 10.1118/1.2188822.

Die approbierte gedruckte Originalversion dieser Diplomarbeit ist an der TU Wien Bibliothek verfügbar
The approved original version of this thesis is available in print at TU Wien Bibliothek.
TU Bibliothek Your knowledge hub WIEN

[29] S. Elles et al. "Geant4 and Fano cavity test: Where are we?" In: *Journal of Physics: Conference Series* 102.1 (2008). ISSN: 17426596. DOI: 10.1088/1742-6596/102/1/012009.

[30] Edmond Sterpin et al. "A Fano cavity test for Monte Carlo proton transport algorithms". In: *Medical Physics* (2014). ISSN: 00942405. DOI: 10.1118/1.4835475.

[31] Jörg Wulff et al. "TOPAS/Geant4 configuration for ionization chamber calculations in proton beams". In: *Physics in Medicine and Biology* (2018). ISSN: 13616560. DOI: 10.1088/1361-6560/aac30e.

[32] Ana Lourenço et al. "The influence of nuclear interactions on ionization chamber perturbation factors in proton beams: FLUKA simulations supported by a Fano test". In: *Medical Physics* (2019). ISSN: 00942405. DOI: 10.1002/mp.13281.

[33] Hugo Bouchard et al. "Reference dosimetry in the presence of magnetic fields: Conditions to validate Monte Carlo simulations". In: *Physics in Medicine and Biology* (2015). ISSN: 13616560. DOI: 10.1088/0031-9155/60/17/6639.

[34] J. A. De Pooter, L. A. De Prez, and H. Bouchard. "Application of an adapted Fano cavity test for Monte Carlo simulations in the presence of B-fields". In: *Physics in Medicine and Biology* (2015). ISSN: 13616560. DOI: 10.1088/0031-9155/60/24/9313.

[35] V. N. Malkov and D. W.O. Rogers. "Charged particle transport in magnetic fields in EGSnrc". In: *Medical Physics* (2016). ISSN: 00942405. DOI: 10.1118/1.4954318.

[36] D. J. O'Brien et al. "Reference dosimetry in magnetic fields: formalism and ionization chamber correction factors". In: *Medical Physics* (2016). ISSN: 00942405. DOI: 10.1118/1.4959785.

[37] Michael Reynolds, Satyapal Rathee, and B. Gino Fallone. "Technical Note: Ion chamber angular dependence in a magnetic field: Ion". In: *Medical Physics* (2017). ISSN: 00942405. DOI: 10.1002/mp.12405.

[38] E. Simiele and L. Dewerd. "On the accuracy and efficiency of condensed history transport in magnetic fields in GEANT4". In: *Physics in Medicine and Biology* (2018). ISSN: 13616560. DOI: 10.1088/1361-6560/aaedc9.

[39] Jaegi Lee et al. "Fano cavity test for electron Monte Carlo transport algorithms in magnetic fields: Comparison between EGSnrc, PENELOPE, MCNP6 and Geant4". In: *Physics in Medicine and Biology* (2018). ISSN: 13616560. DOI: 10.1088/1361-6560/aadf29.

[40] Jacco A de Pooter et al. "Reference dosimetry in MRI-linacs: evaluation of available protocols and data to establish a code of practice". In: *Physics in Medicine & Biology* (2020). ISSN: 0031-9155. DOI: 10.1088/1361-6560/ab9efe.

[41] S. Jan et al. "GATE: A simulation toolkit for PET and SPECT". In: *Physics in Medicine and Biology* (2004). ISSN: 00319155. DOI: 10.1088/0031-9155/49/19/007. arXiv: 0408109 [physics].

Die approbierte gedruckte Originalversion dieser Diplomarbeit ist an der TU Wien Bibliothek verfügbar
The approved original version of this thesis is available in print at TU Wien Bibliothek.
TU Bibliothek Your knowledge hub WIEN

[42] S. Jan et al. "GATE V6: A major enhancement of the GATE simulation platform enabling modelling of CT and radiotherapy". In: *Physics in Medicine and Biology* (2011). ISSN: 13616560. DOI: 10.1088/0031-9155/56/4/001.

[43] David Sarrut et al. *A review of the use and potential of the GATE Monte Carlo simulation code for radiation therapy and dosimetry applications*. 2014. DOI: 10.1118/1.4871617.

[44] S. Agostinelli et al. "GEANT4 - A simulation toolkit". In: *Nuclear Instruments and Methods in Physics Research, Section A: Accelerators, Spectrometers, Detectors and Associated Equipment* (2003). ISSN: 01689002. DOI: 10.1016/S0168-9002(03)01368-8.

[45] J. Allison et al. "Geant4 developments and applications". In: *IEEE Transactions on Nuclear Science* (2006). ISSN: 00189499. DOI: 10.1109/TNS.2006.869826.

[46] J. Allison et al. "Recent developments in GEANT4". In: *Nuclear Instruments and Methods in Physics Research, Section A: Accelerators, Spectrometers, Detectors and Associated Equipment* (2016). ISSN: 01689002. DOI: 10.1016/j.nima.2016.06.125.

[47] I. Antcheva et al. "ROOT - A C++ framework for petabyte data storage, statistical analysis and visualization". In: *Computer Physics Communications* (2009). ISSN: 00104655. DOI: 10.1016/j.cpc.2009.08.005. arXiv: 1508.07749.

[48] Ole Tange. "GNU Parallel: the command-line power tool". In: *;login: The USENIX Magazine* (2011). DOI: 10.5281/zenodo.16303.

[49] Hermann Fuchs. *MOCCAMED*. URL: https://www.meduniwien.ac.at/hp/moccamed/ (visited on 11/26/2020).

[50] Douglas Thain, Todd Tannenbaum, and Miron Livny. "Distributed computing in practice: the Condor experience". In: *Concurrency and Computation: Practice and Experience* 17.2-4 (Feb. 2005), pp. 323–356. ISSN: 1532-0626. DOI: 10.1002/cpe.938. URL: http://doi.wiley.com/10.1002/cpe.938.

[51] Geant4 Collaboration. *Book For Application Developers Release 10.6*. 2020. URL: https://geant4.web.cern.ch/support/user%7B%5C_%7Ddocumentation.

[52] Lucio Santi et al. "GQLink: An implementation of Quantized State Systems (QSS) methods in Geant4". In: *Journal of Physics: Conference Series*. 2018. DOI: 10.1088/1742-6596/1085/5/052015.

[53] Fatima Padilla-Cabal et al. "Benchmarking a GATE/Geant4 Monte Carlo model for proton beams in magnetic fields". In: *Medical Physics* (2020). ISSN: 00942405. DOI: 10.1002/mp.13883.

[54] S. Larsson. *purging magnet*. 2004. URL: https://gitlab.cern.ch/geant4/geant4/-/tree/v10.6.1/examples/advanced/purging%7B%5C_%7Dmagnet (visited on 11/26/2020).

[55] Collaboration Geant4. *fanoCavity2*. URL: https://gitlab.cern.ch/geant4/geant4/-/tree/v10.6.1/examples/extended/medical/fanoCavity2 (visited on 11/26/2020).

TU Bibliothek Your knowledge hub WIEN
Die approbierte gedruckte Originalversion dieser Diplomarbeit ist an der TU Wien Bibliothek verfügbar
The approved original version of this thesis is available in print at TU Wien Bibliothek.

[56] R. M. Sternheimer, M. J. Berger, and S. M. Seltzer. *Density effect for the ionization loss of charged particles in various substances*. 1984. DOI: 10.1016/0092-640X(84)90002-0.

[57] J. Apostolakis et al. "Geometry and physics of the Geant4 toolkit for high and medium energy applications". In: *Radiation Physics and Chemistry* (2009). ISSN: 0969806X. DOI: 10.1016/j.radphyschem.2009.04.026.

[58] Vladimir IVANCHENKO et al. "Recent Improvements in Geant4 Electromagnetic Physics Models and Interfaces". In: *Progress in Nuclear Science and Technology* (2011). ISSN: 2185-4823. DOI: 10.15669/pnst.2.898.

[59] Geant4 Collaboration. *Guide For Physics Lists Release 10.6*. 2020. URL: https://geant4.web.cern.ch/support/user%7B%5C_%7Ddocumentation.

[60] S. Goudsmit and J. L. Saunderson. "Multiple scattering of electrons". In: *Physical Review* (1940). ISSN: 0031899X. DOI: 10.1103/PhysRev.57.24.

[61] V. N. Ivanchenko. "Geant4 models for simulation of multiple scattering". In: *Journal of Physics: Conference Series*. 2010. DOI: 10.1088/1742-6596/219/3/032045. URL: https://indico.cern.ch/event/35523/contributions/839637/attachments/704983/967809/msc.pdf.

[62] Collaboration Geant4. *Physics Lists EM constructors in Geant4 10.4*. URL: https://geant4.web.cern.ch/node/1731 (visited on 11/26/2020).

[63] Philipp Moser. *Effects on particle beams in the presence of a magnetic field during radiation therapy*. Wien, 2015.

[64] Hermann Fuchs et al. "Magnetic field effects on particle beams and their implications for dose calculation in MR-guided particle therapy". In: *Medical physics* (2017). ISSN: 24734209. DOI: 10.1002/mp.12105.

[65] Emily Poon, Jan Seuntjens, and Frank Verhaegen. "Consistency test of the electron transport algorithm in the GEANT4 Monte Carlo code". In: *Physics in Medicine and Biology* (2005). ISSN: 00319155. DOI: 10.1088/0031-9155/50/4/008.

Die approbierte gedruckte Originalversion dieser Diplomarbeit ist an der TU Wien Bibliothek verfügbar
The approved original version of this thesis is available in print at TU Wien Bibliothek.
TU Bibliothek Your knowledge hub WIEN